



Universiteit
Leiden
The Netherlands

Understanding functional dynamics and conformational stability of beta-glycosidases

Ben Bdira, F.

Citation

Ben Bdira, F. (2018, February 20). *Understanding functional dynamics and conformational stability of beta-glycosidases*. Retrieved from <https://hdl.handle.net/1887/61148>

Version: Not Applicable (or Unknown)

License: [Licence agreement concerning inclusion of doctoral thesis in the Institutional Repository of the University of Leiden](#)

Downloaded from: <https://hdl.handle.net/1887/61148>

Note: To cite this publication please use the final published version (if applicable).

Cover Page



Universiteit Leiden



The following handle holds various files of this Leiden University dissertation:
<http://hdl.handle.net/1887/61148>

Author: Ben Bdira, F.

Title: Understanding functional dynamics and conformational stability of beta-glycosidases

Issue Date: 2018-02-20

Understanding functional dynamics and conformational stability of β -glycosidases

Proefschrift

ter verkrijging van
de graad van Doctor aan de Universiteit Leiden,
op gezag van Rector Magnificus prof.mr. C.J.J.M. Stolker,
volgens besluit van het College voor Promoties
te verdedigen op dinsdag 20 februari 2018
klokke 10:00 uur

door

Fredj Ben Bdira

Geboren te Sousse, Tunesië in 1982

Understanding functional dynamics and conformational stability of β -glycosidases

Fredj Ben Bdira

Doctoral thesis, Leiden University, 2018

Cover image: The olive tree

ISBN number: 978-94-028-0927-5

©2018, Fredj Ben Bdira

Printed by IPSK printing, the Netherlands

Promotor: Prof. Dr. M. Ubbink
Second promotor: Prof. Dr. J.M.F.G. Aerts

Promotiecommissie: Prof. Dr. H.S. Overkleeft (chair)
Prof. Dr. M.H.M. Noteborn (secretary)
Prof. Dr. L.P. McIntosh (University of British Columbia,
Canada)
Prof. Dr. W.J.H. van Berkel (Wageningen University &
Research)
Prof. Dr. M.M.A.E. Claessens (University of Twente)

The research described in this thesis was performed in the Macromolecular Biochemistry Department of the Leiden Institute of Chemistry, Leiden, the Netherlands.
This work was supported by the Netherlands Organization for Scientific Research, the Netherlands Research School of Chemical Biology (NRSCB), grant number 022.004.027.

عَلَى قَدْرِ أَهْلِ الْعَزْمِ تَأْتِي الْعَزَائِمُ

Strong resolves come in proportion to men of determination

وَتَأْتِي عَلَى قَدْرِ الْكِرَامِ الْمَكَارِمُ

And noble deeds come in proportion to magnanimous men

وَتَعْتَظُمُ فِي عَيْنِ الصَّغِيرِ صِبَاغُهَا

Little things are deemed great by little minds

وَتَصْغُرُ فِي عَيْنِ الْعَظِيمِ الْعِظَائِمُ

While grave challenges pale into insignificance in the eyes of the great

Al-Mutanabbi

To my father the olive grower (1936-2015)

TABLE OF CONTENTS

	List of abbreviations	6
Chapter 1	Retaining β -glycosidases GH5, GH30 and GH11: Folds, Dynamics, Stability and Inhibition	7
	Thesis Outline	29
Chapter 2	Hydrophobic Interactions Contribute to Conformational Stabilization of Endoglycoceramidase II by Mechanism-Based Probes	31
Chapter 3	Stabilization of Glucocerebrosidase by Active Site Occupancy	57
Chapter 4	Exploring the Conformational Landscape and the Dynamics of GH11 xylanases During Catalysis	83
Chapter 5	General Conclusion & Perspectives	119
	Appendices	128
	English summary	132
	Nederlandse samenvatting	134
	List of publications	136
	Curriculum vitae	137

LIST OF ABBREVIATIONS

4MU-Glc: 4-methylumbelliferone β -D-glucose
4MU-Lac: 4-methylumbelliferone β -D-lactopyranoside
4MU-X2: 4-methylumbelliferone β -D-xylobiose
ABPs: Activity Based Probes
ANSA: 8-anilino-1-naphthalenesulfonic acid
BCX: xylanase from *Bacillus circulans*
CD: Circular Dichroism
COSY: Correlation Spectroscopy
CPMG-RD: Carr-Purcell- Meiboom-Gill Relaxation Dispersion
CSP: Chemical Shift Perturbations
EGCII: Endoglycoceramidase II (EGCII) from *Rhodococcus* sp.
endo-ABP: endo-glycosidases Activity Based Probe
Fluoro 3: 2-deoxy-2-fluoro- β -D-glucopyranosyl-N-phenyltrifluoroacetimidate
GBA: Glucocerebrosidase
GH: Glycosyl Hydrolases
HSQC: Heteronuclear Single Quantum Correlation Spectroscopy
IFG: Isofagomine
MeCN: Acetonitrile
NMR: Nuclear Magnetic Resonance Spectroscopy
NN-DNJ: N-nonyldeoxynojirimycin
PABP: paramagnetic NMR Activity Based Probe
PBS: Phosphate Buffered Saline
PCS: Pseudocontactshifts
pNMR: paramagnetic NMR
PRE: Paramagnetic Relaxation Enhancement
RDC: Residual Dipolar Coupling
rGBA: recombinant Glucocerebrosidase
RMSD: Root Mean Square Deviation
RT: Room Temperature
SAHS: Solvent-Accessible Hydrophobic Surface
SBS: Secondary Binding Site
SEC-MALLS: Size Exclusion Chromatography and Multiangle Laser Light Scattering
TLC: Thin-Layer Chromatography
 T_m : Melting temperature
TMS: Tetramethylsilane
TROSY: Transverse Relaxation Optimized Spectroscopy

CHAPTER 1

Retaining β -glycosidases GH5, GH30 and GH11: Folds, Dynamics, Stability and Inhibition

Abstract

Retaining β -glycosidases are a ubiquitous family of enzymes found in all kingdoms of life. They are produced by living organisms to catalyze the hydrolysis of carbohydrates β -glycosidic links in a highly sophisticated manner, thus they are involved in a plethora of biological processes. In fungi and bacteria, they are used to process organic biomass as source of energy and also to metabolize carbohydrate conjugates for structural and host infection purposes. In mankind, their functions or dysfunctions are correlated with multiple metabolic disorders, such as lysosomal storage disorders and lactose intolerance. Among the largest families of retaining β -glycosidases are GH5, GH30 and GH11. These hydrolase families include most of the known β -glycosidases in nature with different substrate specificities and structural topologies. GH5 and GH30 belong to Clan A hydrolases with a $(\beta/\alpha)_8$ TIM barrel catalytic domain, while GH11 belongs to Clan C with a β -jelly roll fold. All of the three families have found multiple biotechnological applications and the quest for discovering new inhibitors against them has been an intense research area. In this introduction, the aim is to discuss the general characteristics of GH5, GH30 and GH11 fold topologies and classification, in addition to the dynamics and stability of their catalytic domains. Besides, it is aimed to introduce the most important inhibitors and discuss their applications in fundamental research, biotechnology and therapeutic fields.

Introduction

Carbohydrates in their diverse forms in conjunction to their glycoconjugates are cornerstone components of life in all organisms. Besides their structural and energy storage roles, they are involved in a myriad of biological processes, including -but not limited to- cell communication, host-pathogen interactions¹, signal transduction, inflammation², intracellular trafficking and multiple diseases³. In nature, plant cell walls represents the largest reservoir of carbohydrates, forming about 75% of the biomass on earth⁴. The functional and structural diversity of carbohydrates is a consequence of the astronomic number of possible combinations of their monosaccharides building blocks⁵, therefore it is not surprising that the genomes of most organism include about 1-3% genes that code for carbohydrate-active enzymes⁶. Polysaccharides are very stable compounds in nature; their spontaneous hydrolysis occurs at a rate in the range of 10^{-15} s⁻¹, corresponding to a half-life of 4.7 million years⁷. Organisms have evolved to produce highly efficient catalysts that hydrolyze carbohydrate glycosidic bonds and enhance the hydrolysis rate by a factor of more than 10^{17} ⁷. This superfamily of sophisticated enzymes is called glycoside hydrolases (GHs), and its members exert their function in a specific manner on various glycosidic bonds depending on the number, position, or configuration of the hydroxyl groups in the sugar molecule. Therefore, glycoside hydrolases have found multiple biotechnology applications, such as in biofuel production⁸, paper pulp bleaching and the food industry⁹. In humankind, deficiency of GHs leads to multiple metabolic disorders such lysosomal storage disorders¹⁰ and lactose intolerance¹¹. Hence, glycosidases inhibition has been an attractive subject of research, and the identified inhibitors have found extensive use as agrochemicals and therapeutic agents¹², such as antifungal agents, insecticides, antidiabetics, anti-obesity compounds, antivirals and compounds to correct lysosomal storage disorders^{13, 14}. To discover novel glycosidases from genomic sequences, an enormous effort was dedicated to classify this historically important family of enzymes using several classification systems, including those based on the substrate or product specificity, mode of attack (exo-glycosidic versus endo-glycosidic enzymes) and the stereochemical mechanism. In 1991, a classification of glycoside hydrolases based upon amino acid sequence similarities was introduced, which is now provides more than 140 sequence-based families of glycoside hydrolases, and structures of members of at least 120 families have been solved (www.cazy.org)¹⁵. Among the largest GH families are the retaining β -glycosidases GH5, GH30 and GH11. Although these three families differ in terms of structures and sequences, all of them include members with the same substrate specificity, such as β -glucosidases, endo- β -1-4 xylanases and β -glycosylceramidases from different organisms^{16, 17}.

β -glycosidases have variable structures and substrate specificities, therefore, each GH family has been classified into different Clans¹⁸. The GH5 and GH30 β -glycosidases classify as the GH Clan A, which consists of proteins with an $(\beta/\alpha)_8$ -barrel catalytic domain fold, while GH11 is in the GH Clan C, with a β -jelly roll catalytic domain fold. Due to their industrial and therapeutic importance, the focus here is to discuss the general features of their fold topology, dynamics, conformational stability and inhibition, with the aim to provide the reader with a general overview of the structural and biophysical characteristics of these three families of enzymes.

β -glycosidases catalytic mechanism

Retaining β -glycosidases perform their catalytic reaction in two steps first described by Koshland, using a catalytic dyad functioning as a nucleophile and acid/base¹⁹. The first step is a glycosylation of the enzyme by nucleophilic attack of the anomeric carbon of the substrate, which induces an electronic rearrangement and a hydrolysis of the glycosidic linkage. The nucleophilic attack is concomitant with a proton transfer from the acid/base residue and the departure of the leaving group from the aglycon site. In the second step, an activated water molecule acts as a nucleophile with the assistance of the general acid/base to deglycosylate the nucleophile residue. The product is released from the glycon pocket and a new catalytic cycle could take place (**Figure 1.1.a**). It is proposed that the two steps of the reaction pass through a transient oxocarbenium like state and depending on the sugar ring configuration the substrate could adopt different itineraries pathway during catalysis¹⁹. In the case of GH5 and GH30, the substrate itinerary is supposed to pass by the ${}^3S_1 \rightarrow {}^3H_4^* \rightarrow {}^1C_4$ pathway for the Michaelis complex \rightarrow TS \rightarrow intermediate enzymatic half reaction²⁰ (**Figure 1.1.b**). On the other hand, the substrate itinerary for GH11 xylanases has been proposed to follow a path of ${}^4C_1 \rightarrow {}^0E \rightarrow {}^0S_2^* \rightarrow B_{2,5}$ for the xylose residue at -1 subsite²¹. However, this issue remains as yet unresolved. Early structures of intermediate complexes trapped with 2-fluoro sugars were interpreted as ${}^{2,5}B$ conformations²², suggesting a ${}^2S_0 \rightarrow {}^{2,5}B \rightarrow {}^5S_1$ itinerary. The Michaelis complex of xylohexaose bound to the xylanase XynII from *T. reesi* revealed a slightly distorted 4C_1 conformation²¹. Thus, the sugar ring itinerary of GH11 families number is still under debate.

Retaining β -glycosidases can also perform a transglycosylation reaction by simply changing the temperature²³ or the pH²⁴ of the enzymatic assay or by providing the enzyme with a suitable aglycon acceptor²⁵ (**Figure 1.1a**). This reaction has been successfully applied to synthesize oligosaccharides and glycoconjugates. The transglycosylation capacity of (mutant) β -glycosidases, in combination with their high regio- and stereospecificity, makes them an attractive instrument to synthesize complex carbohydrates.

enzymes, being composed of only 8 β -strands in a barrel geometry (**Figure 1.2e**). Exceptionally, the TIM barrel of EGCII is not capped by the small β -strand sheet observed in most other GH5 family members²⁹. Unlike EGCII, EGC I (another endoglycoceramidase from *Rhodococcus equi* with broader substrate specificity than EGCII) displays a typical GH5 TIM barrel fold sealed with two β -strands at the non-catalytic face of the domain. However, in addition, the TIM barrel of this enzyme is also fused to a β -sandwich structure³⁰ (**Figure 1.2a**). Thus, EGC I is a typical GH5 enzyme while EGCII shows structural features of members of both GH5 and GH30 families. The evolutionary relationship between these enzymes remains unclear.

In humans, no endoglycoceramidase is characterized yet, although an endo hydrolysis activity towards gangliosides has been noted for human cancer cells and tissues of other mammals^{31,32}.

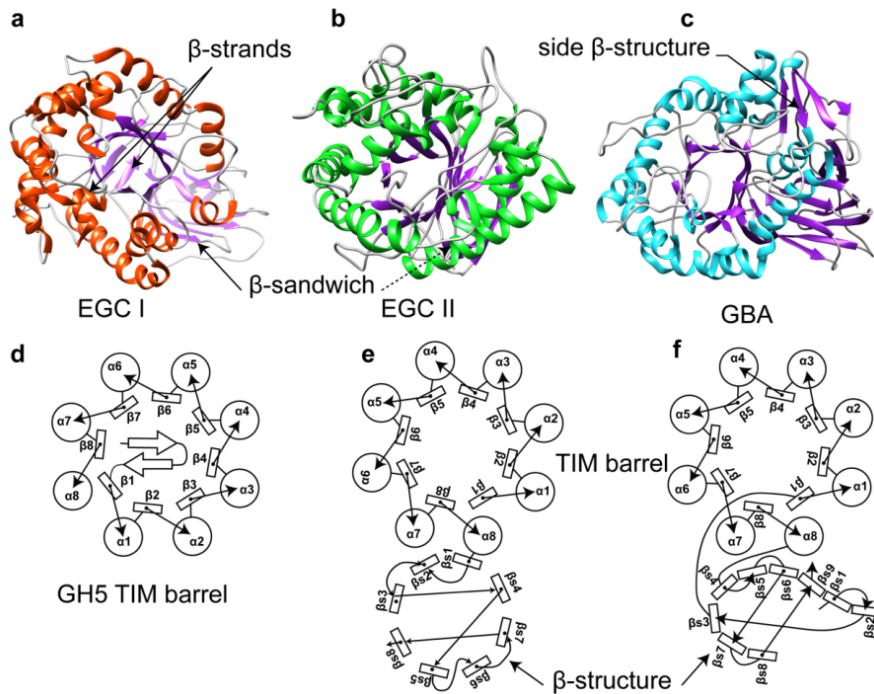


Figure 1.2. GH5 and GH30 general fold and secondary structure arrangement. **(a)** EGC I 3D structure (PDB ID: 5j7z)³⁰. **(b)** EGCII 3D structure (PDB ID: 2osx)²⁹. **(c)** GBA 3D structure (PDB ID:2v3e)³³. **(d)** Diagram of the GH5 family members secondary structure organization adopted from (16). **(e)** EGCII secondary structure arrangement (PDB: 2osx). **(f)** GBA (PDB: 1ogs) secondary structure elements of GH30 members¹⁶. β # refers to TIM barrel domain β -strand number and β s# refers to a β -strand number of the β -side domain.

GH11 fold topology

GH11 is one of the best characterized GH families, which is reflected by the 31 structures deposited in the PDB and CAZyme databases. This family includes bacterial and fungal enzymes considered to be true xylanases, due to their high substrate specificity toward non-decorated xylan polymers and their high catalytic efficiency³⁴. GH11 enzymes display unique biophysical properties such as a low molecular weight (20 kDa) and variable pH and temperature optima, making them attractive candidates for several industrial and biotechnological applications³⁵. For instance, xylanases are widely used in paper pulp bleaching³⁶ biofuel production⁸, and food industries⁹. This class of enzymes has a globular catalytic domain with an approximate gyration radius of 17 Å and a β -jelly-roll fold composed of antiparallel β -sheets A and B that shape a long (~25 Å), deep (~9 Å) and wide (4 Å) catalytic cleft³⁷ (**Figure 1.3a**). The overall shape of this fold is often compared to a right-hand fist³⁷. The β -strands A are nearly planar and distorted at the end to form a hand palm and fingers, and the B strands are in a perpendicular position to the A strands sculpting the binding cleft including, the thumb region. The two sides of the cleft are connected by a long loop called the cord³⁸. The fold includes a single α -helix, sitting under the β -strands B structure. Around 20 % of the amino acids comprises serines and threonines, providing an extensive hydrogen bond network that rigidifies the fold. A sequence alignment of the GH11 family members, using 236 unique sequences out of 456 PSI-BLAST hits (the 220 excluded sequences were found to be more than 95% conserved) revealed a high conservation, (**Figure 1.3b**) most variability is observed for the surrounding residues located on the protein surface. The residues lining the catalytic cleft are highly conserved, both in space and in sequence, and a “backbone” like pattern is formed by multiple aromatic side chains at the bottom of the cleft (**Figure 1.3a**). Among the aromatic residues (residue numbering refers to 1BCX), many are highly (more than 80%) conserved regarding the type of the aromatic side chain (Trp9, Tyr69, Trp71 and Tyr80) while other positions seem to be more flexible (Trp129 and Tyr174 can be substituted by Phe and Trp, respectively). Tyr165 is more variable (less than 50% conserved) and can sometimes be substituted by Glu, which could mean that a polar group is more important than an aromatic residue at this position.

The PSIXG sequence motif of the thumb region is highly conserved, suggesting the importance of this hairpin loop for the protein function (**Figure 1.3a**). The amino acid sequence that harbours the nucleophilic glutamic residue is also conserved (ATEG) with one exception, where a glutamine is present instead of a glutamic acid. The sequence in which the acid/base residue (Glu) is located is more variable, and in some cases, the acid/base residue is substituted by either a glutamine or an arginine. These type changes of the catalytic dyad could reflect a different mode of action of these enzymes or a change of their pH optima. Overall, the strong sequence conservation of the GH11 family is remarkable because generally, proteins structures are better conserved than sequences³⁹.

GH11 family members exhibit a wide variability of their biochemical properties with different pH and temperature optima. These variabilities seem to be caused by only minor sequence differences.

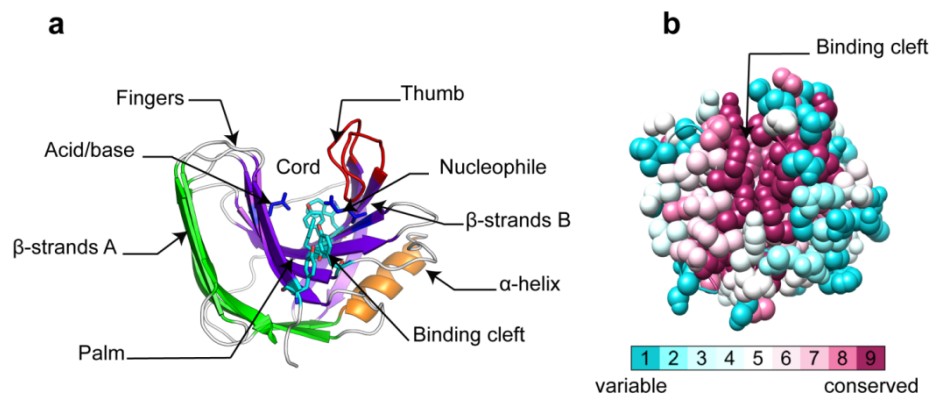


Figure 1.3. (a) GH11 β -jelly-roll fold. (b) GH11 amino acid conservation based on sequence alignment using the ConSurf Server.

β -glycosidases dynamics and stability

GH5 and GH30 TIM barrel dynamics and stability

Enzymes are very dynamic entities, exerting their function by sampling multiple conformational substates during catalysis⁴⁰. Thus, it is insufficient to describe only the ground state structure of the resting state if a complete understanding of the catalytic function is to be achieved. Although there are numerous β -glycosidases structures available, few efforts were dedicated to investigating their molecular dynamics. The scarcity in dynamics studies could stem from the robust understanding of the chemistry that governs β -glycosidases catalytic reactions and also from the challenges of studying protein dynamics experimentally. The biophysical and theoretical techniques that have been employed to study the global dynamics of retaining β -glycosidases include molecular dynamic simulations (MD), frequency decay fluorometry that exploit tryptophan emission, hydrogen/deuterium exchange (HDX) mass spectrometry and the versatile technique NMR spectroscopy, which can cover a broad spectrum of protein time scale motions from ps to hours with an atomic resolution.

Clan A β -glycosidases have a TIM barrel catalytic domain fold, so studying the dynamics of a particular member could provide a general trend for the dynamics of this recurrent topology. For instance, David *et al.* have studied the dynamics of the catalytic domain of the β -(1,4)-glycosidase Cex (or CfxYn10A) from the soil bacterium *Cellulomonas fimi* from ns to ms time scale using NMR spectroscopy⁴¹. The conclusion from this study was that the TIM barrel domain is uniformly rigid on the different probed time scales. Few dynamic changes were observed for the glycosyl-enzyme intermediate state complex,

CHAPTER 1

although an enhancement of the thermal stability and proteolysis resistance of the domain was observed. A lower resolution technique was also employed to follow the conformational dynamics of a thermophilic and a mesophilic Clan A β -glycosidase from extremophilic archaeon *Sulfolobus solfataricus* (S β gly) and from *Escherichia coli* (C β gal), using multityryptophan emission decay⁴². The thermophilic variant harbours twelve tryptophans distributed over the core of the protein TIM barrel domain and some of them are located on flexible loops. The study showed that there are two groups of tryptophan fluorescence decay: A short-lived and a long-lived tryptophan life time decay, reflecting the well packed and rigid TIM barrel core and the flexibility of the protein surface loops, respectively. However, when incubated with the irreversible inhibitor cyclophellitol (*see below*), a quenching of tryptophan short lived residues fluorescence was observed, pointing toward a structural rigidification of the TIM barrel flexible loops. In contrast, the mesophilic β -galactosidase variant exhibits a uniform distribution of tryptophan fluorescence decay, an indication of a looser structure of the TIM barrel domain. The same trend was also observed in case of β -glucosylceramidase (GBA) where HDX mass spectrometry was employed. The study showed that the residues that reside within the core of TIM barrel domain are highly protected against the H/D exchange process, and loops that connect the α -helices and β -sheet of the catalytic domain are the ones with the lowest protection factor⁴³. All of these observations lead to the conclusion that the TIM barrel domain is globally rigid, yet includes flexible loops that might have a determinant role in protein function. It is proposed that the rigid TIM barrel fold provides the correct frame for favourable interactions with carbohydrate substrates and this rigidity could be necessary to bind, distort, and subsequently hydrolyze the glycosidic linkage within the enzyme active site⁴¹.

GH11 β -jelly roll dynamics and stability

The β -jelly roll fold is common among a variety of proteins with no functional correlation³¹. To interrogate GH11 β -jelly roll fold dynamics and the contribution of the protein motion in its catalytic reaction β -1-4-xylanase from *Bacillus circulans* (BCX) was selected to be studied by NMR due to its well-characterized structure and suitable biophysical properties⁴⁴. BCX comprises 185 residues with a molecular weight of 20 kDa and a stokes radius of $\sim 17 \text{ \AA}$ ³⁷. Its small size and well-dispersed NMR spectra facilitated a thorough study of its dynamics. A survey carried out by Connelly *et al.* has revealed that the protein in its substrate-free form displays a high average order relaxation parameter ($S^2 = 0.86 \pm 0.04$), indicative of restricted motion on the pico-nanosecond time scale, which is in agreement with the very compact and globular fold observed with crystallographic and hydrodynamic experiments⁴⁵. The dynamics uniformity of BCX is in line with the extensive intramolecular hydrogen bond network. By examining the BCX crystal structure, 146 backbone amides out of 185 participate in this network. The same

CHAPTER 1

dynamic behaviour on the fast timescale was observed when studying the complex of the protein with 2-deoxy-2-fluoro- β -xylobioside. However, these findings do not exclude the possibility of slower dynamics on the millisecond time scale, which is more relevant for catalysis as it covers the rate of the substrate turnover (20 s⁻¹ against 2,5-DNPX2 substrate)⁴⁶.

A unique feature of GH11 is the presence of a thumb loop region that is believed to play a determinant role in selective substrate binding and product release⁴⁷. Multiple molecular dynamics simulations have suggested the opening of the thumb loop to induce the product dissociation⁴⁸⁻⁵⁰. The thumb region displays a well-structured classical hairpin, containing a type I β -turn (residues 117-120 in BCX) with six internal hydrogen bonds. The only evidence of a full opening of the thumb was observed in the case of a specific xylanase mutant from *B. subtilis* in the crystalline state⁵¹. A recently published study of xylanase millisecond time scale dynamics, using the relaxation dispersion CPMG technique⁵², showed that the protein in its free form experiences a millisecond motion for multiple residues localized within the binding site⁵³. Residues of the thumb regions were not detected due to peak broadening. In the presence of its substrate, an enhancement of the millisecond (ms) time scale motion was observed. This study has provided the first evidence of such motion in GH11 family enzyme. It is difficult to interpret relaxation dispersion effects in structural terms. These ms dynamics might reflect a chemical exchange of the backbone amides that could be due to side chain reorientations and not due to conformational changes in the protein backbone.

A thorough MD investigation on GH11 family enzymes was undertaken for XYNII from *Trichoderma reesei*⁵⁴. By combining the different crystal structures, it was proposed that the protein samples three sequential substates during its catalytic reaction. First, the protein adopts an open state to allow substrate accommodation within the cleft. Substrate binding induces a closed conformation necessary for positioning the substrate into the correct configuration for glycosidic bond hydrolysis. The last state is a loose structure from which the product is released. The study provided a model for the enzyme catalytic cycle based on the available crystal structures that still needs to be validated with studies in solution.

Overall, the conclusion that could be deduced from these studies is that the β -jelly roll catalytic domain of GH11 has an inherent structural rigidity emerging from the strong hydrogen network between its secondary structure elements. Most of the GH11 family members are secreted enzymes⁵⁵. Thus, the lack of their conformational flexibility might be an adaption mechanism to function in harsh extracellular conditions. Besides, no allosteric regulation was identified for GH11 xylanases so far. Therefore, it is speculated that they do not need to contain flexible regions to facilitate effector binding. Additionally, this structural rigidity could also be required for sugar ring distortion necessary for the hydrolysis of the glycosylic link. To this point, all of the experimental observations point toward a globular and rigid fold of GH11 during its reaction pathway with minor

conformational changes of the protein structure and a plausible local opening of the thumb region.

β -glycosidases inhibitors and their applications

The high abundance of β -glycosidases encoding genes in all organisms is reflecting their pivotal roles in multiple biological processes. In humankind, β -glycosidases function or dysfunction is related to different pathological states, leading to an increased interest in the therapeutic application of inhibitors. Cognate β -glycosidases inhibitors can be divided in different classes based on their mode of action and covalency. In the following section, the focus is on the most frequently used β -glycosidases inhibitors.

Covalent mechanism-based inhibitors: Mechanism-based inhibitors are covalent inhibitors (or inactivators) that obliterate the enzyme activity by forming a covalent bond between the enzyme and a functional group of the inactivator⁵⁶. The bond is typically formed by a nucleophilic attack of an activated center on the inactivator leading to the formation of a covalent complex. Inactivation can be caused by blocking the substrate accessibility to the enzyme active site or by modifying one of the enzyme catalytic residues. This class of inhibitors has attracted interest to probe β -glycosidases structure and function and to identify catalytic residues⁵⁷.

Epoxide- and aziridine-based inactivators: This type of inactivators has found successful applications due to their high inactivation efficiency and stability. Aziridine and epoxide are widely utilized to identify glycosidases nucleophile catalytic residues as they exploit the first step of the catalytic enzyme mechanism. The inactivation mechanism involves the attack of the epoxide or aziridine by the enzyme nucleophile, resulting in ring opening and the formation of an adduct bond between the enzyme and the inhibitor, which emulates the intermediate state of the natural substrate hydrolysis reaction. The process is facilitated by protonation of the inactivator by the general acid/base residue (**Figure 1.4a**)⁵⁷. In 1974 Quaroni et al. have used conduritol B-epoxide (CBE) **1** (**Figure 1.4a**) to identify the catalytic carboxylate in both sucrase and isomaltase⁵⁸. Radioactive CBE derivatives were also used to identify catalytic active site residues in different glycosidases⁵⁹ before bioinformatics emerged as a predictive method. The structural symmetry of CBE allows it to label both α and β -glycosidases^{60,61}. Moreover, CBE has been shown to interact not only with nucleophile residues involved in catalysis but in some cases also with other active site residues. For instance, identification of the β -lac Z, β -glucosylceramidase and almond β -glucosidase nucleophile residues by CBE was initially mistaken due to the inhibitor promiscuity, and it was later corrected^{62,63}. Epoxide derivatives, such as exo-alkyl epoxide glycosides **2** (**Figure 1.4a**), a type of molecule that contains an epoxide moiety linked to a glucoside by an alkyl chain, were also effectively

CHAPTER 1

used to label the nucleophile catalytic residue for a variety of enzymes and X-ray crystallography was used to solve the 3D structure of their complexes⁶⁴. It was observed that the linked residue depends on the alkyl chain length, such as in retaining β -1-4-xylanase from *T. reesi*, in which 2,3-epoxypropyl β -D-xyloside and 3,4-epoxybutyl β -D-xyloside labelled the nucleophile and the acid/base residues, respectively⁶⁵. It was speculated that these results are mainly due to the alkyl chain flexibility and the different inactivator orientations adopted within the enzyme active site. The aza-analogue of CBE (aziridine) **3** (**Figure 1.4a**) was found to be a moderate inactivator for both Abg β -glycosidase and yeast α -glucosidase, with slightly higher activity against the latter⁶⁶. Aziridine based inactivators exhibit a positive charge, thus, they are specifically directed toward the negative active site of the enzyme, precluding non-specific interactions with other parts of the protein. These compounds have been shown to be more reactive than their epoxide counterpart due to the lower stability of the aziridine cycle⁶⁶.

CBE was extensively used to study and characterize human β -glucosylceramidase (GBA) structure/function relationships^{68,69}. Aerts and co-workers have used CBE in the discovery of a novel cytosolic human GBA⁷⁰. Irreversible binding of CBE to GBA was exploited to knock out GBA activity in both cell cultures and animals, allowing the study of GBA roles in maintaining cellular homeostasis and to establish the role of glucosylceramides accumulation in cancer cell^{71,72}. CBE was also used to produce cellular and animal models for Gaucher disease and to study the morphology of Gaucher disease macrophages and its neurological manifestations^{73,74}. Injection of CBE into healthy mice has helped to evaluate the minimum GCCase activity (12-16%) required for maintaining a correct cellular functioning⁷⁵.

Although CBE has proven to be an effective β -glycosidases inactivator, its inherent symmetry limits its specificity toward different β -glycosidases. Thus, it has been proposed that the addition of a hydroxymethylene group on the C5 of CBE pyranose ring would enhance its potency and selectivity toward β -glycosidases⁶⁵. Indeed, a natural compound identical to the proposed CBE derivative has been extracted from the mushroom *Phellinus* sp. by Atsumi *et al.*⁷⁶, and it showed to be selective exclusively toward β -glycosidases. The compound was called cyclophellitol **4** (**Figure 1.4a**) and it has been used in the same manner as CBE against human GCCase to induce a Gaucher disease-like state in cell cultures and in animal model^{77,78}. The crystal structure of cyclophellitol covalently bound to a β -glycosidase has given clear insight into the intermediate state sugar ring distortion of this family of enzymes. The compound has been shown to adopt a ⁴C₁ chair conformation⁷⁹. These new structural insights have guided Witte *et al.* to rationally design selective activity-based probes (ABPs) toward GBA by incorporating a reporter group (biotin or BODIPY) attached via an alkyl or acyl linker to the cyclophellitol scaffold or its aziridine analogue⁸⁰. The ABPs have found various biological applications and further β and α -glucosidases ABPs have been synthesized based on this principle^{81,82}.

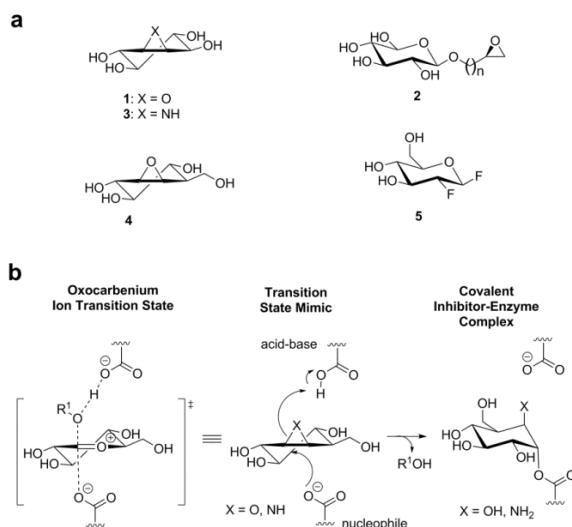


Figure 1.4. Retaining β -glycosidases mechanism-based inhibitors. (a) Epoxide- and aziridine-based inactivators. (b) CBE inactivation mechanism.

Activated fluorinated glycosides inhibitors: The activated 2-deoxy-2-fluoro glycosides **5** (Figure 1.4a) are one of the most selective retaining β -glycosidases inactivators. These inactivators mimic the natural substrate of the enzyme by incorporating an activated aglycon leaving group linked to a glycoside with a fluoride at the position C2. Thus, they are usually considered as slow substrates. The occupancy of C2 position by a fluoride helps to stabilize the intermediate state by destabilizing the oxocarbenium ion like transition states (Figure 1.5)⁸³. The spontaneous hydrolysis of the enzyme-glycosyl intermediate has variable rates and its lifetime can vary from seconds to months. The enzyme catalytic activity could be rescued by using a suitable acceptor to transfer the fluorinated glycoside and liberate the nucleophile residue⁸³. Like CBE and cyclophellitol, activated fluorinated glycosides have been extensively used to investigate the structure/activity relationship of a variety of retaining β -glycosidase enzymes using various biophysical techniques⁸⁴. Additionally, NMR spectroscopy has been employed to generate a model of the oxocarbenium ion-like transition state itinerary and to investigate the dynamic aspects of β -glycosidases during the catalytic pathway, using this class of inactivators as a tool^{41,85}.

Fluorinated glycosides have also found multiple biological applications. They were used to identify novel mammalian retaining β -glucosidases⁸⁶ and to characterize the mammalian lactase phlorizin hydrolase binding pocket⁸⁷. The ability to trap β -glycosidases in their intermediate state has also been used to explore the role of their aglycon binding site and its specificity. The kinetics of recovery of the enzyme activity,

after complex formation with fluorinated glycosides, was shown to be related to the binding affinity of the acceptor to the aglycon site⁸⁸. This class of “slow substrates” was also used as a warhead to generate ABPs by linking the compounds to a fluorogenic reporter⁸⁹. These ABPs were successfully used to selectively label β -glycosidases in complex biological samples and to discover novel β -glycosidases enzymes in *Cellulomonas fimi*⁹⁰.

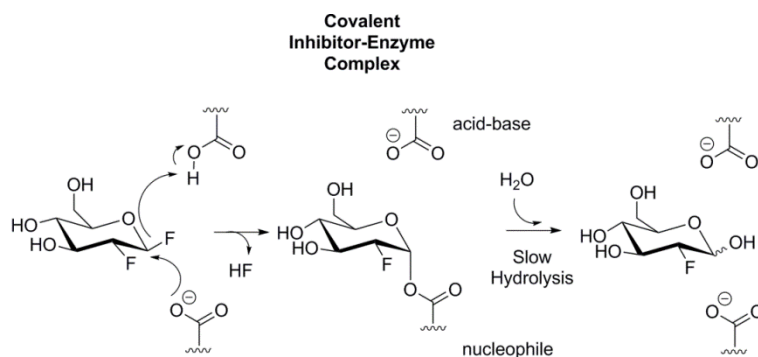


Figure 1.5. The inactivation mechanism of activated fluorinated glycoside inhibitors for retaining β -glycosidases.

Non-covalent inhibitors: Non-covalent β -glycosidases inhibitors are more therapeutically attractive as they can reversibly inhibit the enzyme activity in a dose-dependent manner. Therefore, several β -glycosidases inhibitors comprising disaccharides, iminosugars, cabasugars, thiosugars and non-glycosidic inhibitors were either synthesized or extracted from natural sources⁹¹. In the following section, the focus is mainly on the iminosugars inhibitors because of their successful therapeutic application in a variety of human lysosomal storage disorders.

Iminosugars are low molecular weight compounds also called polyhydroxylated alkaloids that exhibit at least two hydroxyl groups and one heterocyclic nitrogen atom. These compounds are abundant in plants and microorganisms⁹². The substitution of the oxygen or anomeric carbon of the pyranose ring by a protonated nitrogen has been proposed to mimic the positive charge generated in these positions upon partial cleavage of the glycosidic bond, thus emulating the transition state, which triggers a high inhibition potency⁹³ (**Figure 1.6b**).

One of the first iminosugars described was nojirimycin (NJ) **6** (**Figure 1.6a**), isolated from several strains of *Bacillus* and *Streptomyces* as well as mulberry tree leaf. It contains an endocycle nitrogen in the place of the oxygen pyranosidic atom, and it was shown to be a potent inhibitor of both α and β -glycosidases inhibitors⁹¹. However, the presence of C1 hydroxylic group renders this compound unstable, hindering utilisation. 1-Deoxynojirimycin (DNJ) **7** (**Figure 1.6a**) is a reduced version of nojirimycin that lacks the hydroxyl group from the anomeric carbon enhancing the stability and inhibition

CHAPTER 1

potency of the compound⁹¹. This compound also acts on both β and α -glycosidases. Changing the position of the heterocycle nitrogen atom to the anomeric carbon position of the DNJ pyranosidic ring led to a 440-fold inhibition enhancement toward β -glycosidases with a moderate inhibition toward α -glycosidases⁹⁴. It has been proposed that this enhancement of the inhibition potency is due to the better ability of the new compound in mimicking the β -glycosidases transition state. The new analogues are named 1-azasugars, represented by isofagomine (IFG) **8** (**Figure 1.6a**). IFG has the anomeric carbon and the ring oxygen of glucose replaced by nitrogen and carbon, respectively, and the C2 hydroxylic group is absent. The remaining hydroxyl groups are maintained, preserving a D-glucose like configuration. However, it was suggested that by keeping the hydroxyl group at C2 a stronger β -glycosidases inhibition would be observed, presumably due the addition of a hydrogen bond interaction with the enzyme active site. The compound having these characteristics is named noeuromycin **9**, and it showed high inhibition specificity toward β -glycosidases⁹⁵.

The superior specificity of azasugars toward β -glycosidases has prompted their use as potential therapeutic substances, especially in the case of the lysosomal storage disorder such as Gaucher disease⁹⁶. GBA is the enzyme responsible for cleaving the glucosidic bonds between the glucose and ceramide moieties of glucosylceramides in the lysosomal compartment of the cell. Reported single point mutations in GBA have been shown to decrease the half-life of the protein by destabilizing its native fold or by leading to the production of a misfolded protein. The deleterious GBA mutants are degraded by the cell control machinery, thus hampering the enzyme from reaching its lysosomal destination and leading to the accumulation of its glucosylceramide substrate⁹⁶. IFG is one of the best structurally characterized azasugars, and due its high specificity and potency toward GBA, it was proposed to be used as a pharmacological chaperone to rescue GBA proteostasis in GD patients. *In vitro* and *in vivo* studies provided evidence for its stabilization effects on multiple GBA variants⁹⁷. For instance, IFG was found to have a higher binding affinity to GBA at neutral pH (as found in the ER compartment) compared to acid pH (as found in the lysosomal compartment)⁴³. This pH binding dependency is a pivotal property in assisting the folding of GBA mutants in the ER compartment to escape the cellular quality control machinery and to be released in the lysosome. IFG increases the thermal stability of the enzyme at neutral pH and raises the cellular level of GBA N370S and L444P mutants in GD patients tissues⁹⁸. IFG is supposed to cross the blood-brain barrier and correct GD manifestation in the nervous system due its small size. Despite these promising results, IFG has failed in clinical trials, presumably due to its hydrophilicity, resulting in poor biodistribution. Thus, N-alkylated derivatives were produced and demonstrated to have a superior chaperone performance⁹⁸. One of the successful compounds is N-butyl-deoxynojirimycin (NB-DNJ, Miglustat) **10** (**Figure 1.6b**), which has dual beneficial effects on glucosylceramide depletion and on the

stabilization of GBA mutants⁹⁹. Another derivative is N-nonyl-deoxyojirimycin (NN-DNJ) **11** (Figure 1.6b), which showed an enhanced binding affinity toward GCCase when tested *in vivo*, presumably due to its longer alkyl chain length¹⁰⁰. Tuning of the alkyl chain length of these compounds and elucidating the stabilization mechanism toward GBA might provide valuable information that could pave the way for the development of a new generation of pharmacological chaperones.

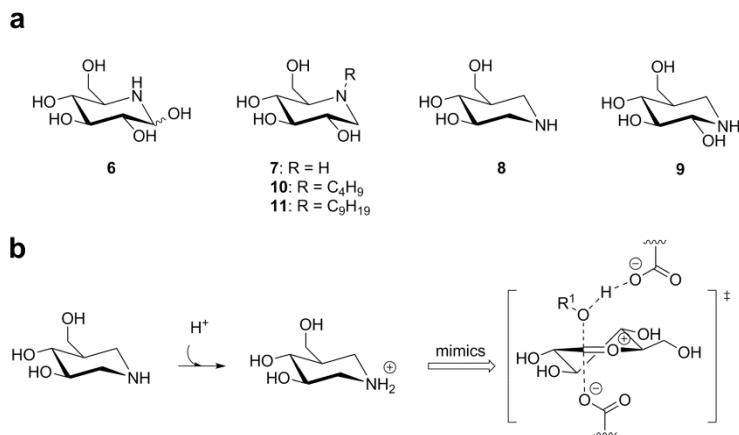


Figure 1.6. Retaining β -glycosidases iminosugar inhibitors. (a) Different type of iminosugars used against retaining β -glycosidases as reversible inhibitors. (a) Isofagomine inhibition mechanism.

Conclusion and perspective

The structure/function relationship studies of β -glycosidases have provided an enormous amount of information about their physical characteristics. Uncovering the substrate itinerary during catalysis has helped to produce more potent and efficient inhibitors, although the full potential of this information has yet to be explored for a large number of retaining β -glycosidases, and, besides, the inhibitory stabilization mechanism is still poorly understood.

Despite these tremendous insights, understanding of retaining β -glycosidases dynamics in relation to substrate binding and distortion as well as product release is still limited. Studies of the dynamics could address the paradox between the high structural conservation and wide variety of functions. The unique characteristic of β -glycosidases to shift the equilibrium of their hydrolysis reaction toward polymer synthesis under specific conditions has encouraged their use to produce relevant carbohydrates with a wide spectrum of therapeutic, industrial and research applications. Enzymatic synthesis of carbohydrates offers a one-step reaction under mild conditions with stereospecificity and without by-product generation and less environmental pollution, compared to classical chemical methods, which still require several protection, activation, coupling and deprotection steps.

Depletion of fossil fuels at an enhanced rate and the effect of its utilization on the global economy and environment have pressed the quest for a renewable and clean source of energy. Bioethanol has been considered as a potential alternative fuel as its raw material (cellulose) is highly abundant¹⁰¹. β -glycosidases hold a promising future regarding their use in cellulose bioconversion process and biofuel production¹⁰². Fundamental studies of this family of enzymes will help to compose the right cocktail of enzymes for maximum cellulose bioconversion and to guide their re-engineering for optimal function under large scale industrial conditions.

References

1. Kato, K., and Ishiwa, A. (2015) The Role of Carbohydrates in Infection Strategies of Enteric Pathogens, *Trop. Med. Health* 43, 41-52.
2. Kim, Y. O., Park, K. S., Hessel, C., Weng, S. Y., Popov, Y., Gasteiger, G., and Schuppan, D. (2017) High carbohydrate diet induces acute liver injury, enhanced de novo lipogenesis, inflammation and fibrosis but reversible by M2 macrophage polarization, *J. Hepatol.* 66, S611-S611.
3. Mann, J. (2007) Dietary carbohydrate: relationship to cardiovascular disease and disorders of carbohydrate metabolism, *Eur. J. Clin. Nutr.* 61, S100-S111.
4. Lichtenthaler, F. W. (2007) Carbohydrates as Renewable Raw Materials: A Major Challenge of Green Chemistry, In *Methods and Reagents for Green Chemistry*, pp 23-63, John Wiley & Sons, Inc.
5. Laine, R. A. (1994) A calculation of all possible oligosaccharide isomers both branched and linear yields 1.05×10^{12} structures for a reducing hexasaccharide - the isomer-barrier to development of single-method saccharide sequencing or synthesis systems, *Glycobiology* 4, 759-767.
6. Davies, G. J., Gloster, T. M., and Henrissat, B. (2005) Recent structural insights into the expanding world of carbohydrate-active enzymes, *Curr. Opin. Struct. Biol.* 15, 637-645.
7. Wolfenden, R., Lu, X. D., and Young, G. (1998) Spontaneous hydrolysis of glycosides, *J. Am. Chem. Soc.* 120, 6814-6815.
8. Garg, S. (2016) Xylanase: Applications in Biofuel Production, *Current Metabolomics* 4, 23-37.
9. Collins, T., Hoyoux, A., Dutron, A., Georis, J., Genot, B., Dauvrin, T., Arnaut, F., Gerday, C., and Feller, G. (2006) Use of glycoside hydrolase family 8 xylanases in baking, *J. Cereal. Sci.* 43, 79-84.
10. Filocamo, M., and Morone, A. (2011) Lysosomal storage disorders: Molecular basis and laboratory testing, *Hum. Genomics* 5, 156-169.
11. Neale, G. (1971) Disaccharidase deficiencies, *J. Clin. Pathol. Suppl. (R. Coll. Pathol.)* 5, 22-28.
12. Asano, N., Nash, R. J., Molyneux, R. J., and Fleet, G. W. J. (2000) Sugar-mimic glycosidase inhibitors: natural occurrence, biological activity and prospects for therapeutic application, *Tetrahedron-Asymmetry* 11, 1645-1680.
13. vonItzstein, M., and Colman, P. (1996) Design and synthesis of carbohydrate-based inhibitors of protein-carbohydrate interactions, *Curr. Opin. Struct. Biol.* 6, 703-709.
14. Asano, N. (2003) Glycosidase inhibitors: update and perspectives on practical use, *Glycobiology* 13, 93R-104R.
15. Henrissat, B. (1991) A classification of glycosyl hydrolases based on amino-acid-sequence similarities, *Biochem. J.* 280, 309-316.
16. St John, F. J., Gonzalez, J. M., and Pozharski, E. (2010) Consolidation of glycosyl hydrolase family 30: A dual domain 4/7 hydrolase family consisting of two structurally distinct groups, *FEBS Lett.* 584, 4435-4441.
17. Aspeborg, H., Coutinho, P. M., Wang, Y., Brumer, H., and Henrissat, B. (2012) Evolution, substrate specificity and subfamily classification of glycoside hydrolase family 5 (GH5), *BMC Evol. Biol.* 12.
18. Naumoff, D. G. (2014) Hierarchical classification of glycoside hydrolases, *FEBS J.* 281, 569-569.
19. Rye, C. S., and Withers, S. G. (2000) Glycosidase mechanisms, *Curr. Opin. Chem. Biol.* 4, 573-580.
20. Speciale, G., Thompson, A. J., Davies, G. J., and Williams, S. J. (2014) Dissecting conformational contributions to glycosidase catalysis and inhibition, *Curr. Opin. Struct. Biol.* 28, 1-13.
21. Wan, Q., Zhang, Q., Hamilton-Brehm, S., Weiss, K., Mustyakimov, M., Coates, L., Langan, P., Graham, D., and Kovalevsky, A. (2014) X-ray crystallographic studies of family 11 xylanase Michaelis and product complexes: implications for the catalytic mechanism, *Acta Crystallogr. Sect. D. Biol. Crystallogr.* 70, 11-23.
22. Sabini, E., Sulzenbacher, G., Dauter, M., Dauter, Z., Jørgensen, P. L., Schülein, M., Dupont, C., Davies, G. J., and Wilson, K. S. (1999) Catalysis and specificity in enzymatic glycoside hydrolysis: a 2,5B conformation for the glycosyl-enzyme intermediate revealed by the structure of the *Bacillus agaradhaerens* family 11 xylanase, *Chem. Biol.* 6, 483-492.
23. Ribeiro, M., Pereira-Chioccola, V. L., Eichinger, D., Rodrigues, M. M., and Schenkman, S. (1997) Temperature differences for trans-glycosylation and hydrolysis reaction reveal an acceptor binding site in the catalytic mechanism of *Trypanosoma cruzi* trans-sialidase, *Glycobiology* 7, 1237-1246.
24. Eneyskaya, E. V., Brumer, H., Backinowsky, L. V., Ivanen, D. R., Kulminskaya, A. A., Shabalin, K. A., and Neustroev, K. N. (2003) Enzymatic synthesis of β -xylanase substrates: transglycosylation reactions of the β -xylosidase from *Aspergillus* sp, *Carbohydr. Res.* 338, 313-325.

CHAPTER 1

25. Danby, P. M., and Withers, S. G. (2016) Advances in enzymatic glycoside synthesis, *ACS Chem. Biol.* 11, 1784-1794.
26. Davies, G., and Henrissat, B. (1995) Structures and mechanisms of glycosyl hydrolases, *Structure* 3, 853-859.
27. Durand, P., Lehn, P., Callebaut, I., Fabrega, S., Henrissat, B., and Mornon, J.-P. (1997) Active-site motifs of lysosomal acid hydrolases: invariant features of clan GH-A glycosyl hydrolases deduced from hydrophobic cluster analysis, *Glycobiology* 7, 277-284.
28. Ito, M., and Yamagata, T. (1986) A novel glycosphingolipid-degrading enzyme cleaves the linkage between the oligosaccharide and ceramide of neutral and acidic glycosphingolipids, *J. Biol. Chem.* 261, 14278-14282.
29. Caines, M. E., Vaughan, M. D., Tarling, C. A., Hancock, S. M., Warren, R. A. J., Withers, S. G., and Strynadka, N. C. (2007) Structural and mechanistic analyses of endo-glycoceramidase II, a membrane-associated family 5 glycosidase in the Apo and GM3 ganglioside-bound forms, *J. Biol. Chem.* 282, 14300-14308.
30. Han, Y.-B., Chen, L.-Q., Li, Z., Tan, Y.-M., Feng, Y., and Yang, G.-Y. (2017) Structural Insights into the Broad Substrate Specificity of a Novel Endoglycoceramidase I Belonging to a New Subfamily of GH5 Glycosidases, *J. Biol. Chem.* 292, 4789-4800.
31. Basu, M., Kelly, P., O'donnell, P., Miguel, M., Bradley, M., Sonnino, S., Banerjee, S., and Basu, S. (1999) Ceramide glycanase activities in human cancer cells, *Biosci. Rep.* 19, 449-460.
32. Basu, M., Kelly, P., Girzadas, M., Li, Z., and Basu, S. (2000) [31] Properties of animal ceramide glycanases, *Methods Enzymol.* 311, 287-297.
33. Brumshtein, B., Greenblatt, H.M., Butters, T.D., Shaaltiel, Y., Aviezer, D., Silman, I., Futerman, A.H., Sussman, J.L. (2007), Crystal Structures of Complexes of N-Butyl- and N-Nonyl-Deoxyojirimycin Bound to Acid β -Glucosidase Insights into the mechanism of chemical chaperone action in gaucher disease. *J. Biol. Chem.*, **282**(39): p. 29052-29058.
34. Sizova, M. V., Izquierdo, J. A., Panikov, N. S., and Lynd, L. R. (2011) Cellulose- and Xylan-Degrading Thermophilic Anaerobic Bacteria from Biocompost, *Appl. Environ. Microbiol.* 77, 2282-2291.
35. Collins, T., Gerday, C., and Feller, G. (2005) Xylanases, xylanase families and extremophilic xylanases, *FEMS Microbiol. Rev.* 29, 3-23.
36. Walia, A., Guleria, S., Mehta, P., Chauhan, A., and Parkash, J. (2017) Microbial xylanases and their industrial application in pulp and paper biobleaching: a review, *3 Biotech* 7, 12.
37. Kozak, M. (2006) Solution scattering studies of conformation stability of xylanase XYNII from *Trichoderma longibrachiatum*, *Biopolymers* 83, 95-102.
38. Paes, G., Berrin, J. G., and Beaugrand, J. (2012) GH11 xylanases: Structure/function/properties relationships and applications, *Biotechnol. Adv.* 30, 564-592.
39. Orengo, C. A., Jones, D. T., and Thornton, J. M. (1994) Protein superfamilies and domain superfolds, *Nature* 372, 631-634.
40. Henzler-Wildman, K., and Kern, D. (2007) Dynamic personalities of proteins, *Nature* 450, 964-972.
41. Poon, D. K. Y., Ludwiczek, M. L., Schubert, M., Kwan, E. M., Withers, S. G., and McIntosh, L. P. (2007) NMR spectroscopic characterization of a beta-(1,4)-glycosidase along its reaction pathway: Stabilization upon formation of the glycosyl-enzyme intermediate, *Biochemistry* 46, 1759-1770.
42. Bismuto, E., Nucci, R., Rossi, M., and Irace, G. (1999) Structural and dynamic aspects of beta-glycosidase from mesophilic and thermophilic bacteria by multityrophanyl emission decay studies, *Proteins: Struct., Funct., Genet.* 35, 163-172.
43. Kornhaber, G. J., Tropak, M. B., Maegawa, G. H., Tuske, S. J., Coales, S. J., Mahuran, D. J., and Hamuro, Y. (2008) Isofagomine Induced Stabilization of Glucocerebrosidase, *ChemBioChem* 9, 2643-2649.
44. Plesniak, L. A., Wakarchuk, W. W., and McIntosh, L. P. (1996) Secondary structure and NMR assignments of *Bacillus circulans* xylanase, *Protein Sci.* 5, 1118-1135.
45. Connelly, G. P., Withers, S. G., and McIntosh, L. P. (2000) Analysis of the dynamic properties of *Bacillus circulans* xylanase upon formation of a covalent glycosyl-enzyme intermediate, *Protein Sci.* 9, 512-524.
46. Zechel, D. L., Konermann, L., Withers, S. G., and Douglas, D. (1998) Pre-steady state kinetic analysis of an enzymatic reaction monitored by time-resolved electrospray ionization mass spectrometry, *Biochemistry* 37, 7664-7669.
47. Paës, G., Tran, V., Takahashi, M., Boukari, I., and O'donohue, M. J. (2007) New insights into the role of the thumb-like loop in GH-11 xylanases, *Protein Eng. Des. Sel.* 20, 15-23.
48. Mhlongo, N. N., Ebrahim, M., Skelton, A. A., Kruger, H. G., Williams, I. H., and Soliman, M. E. S. (2015) Dynamics of the thumb-finger regions in a GH11 xylanase *Bacillus circulans*: comparison between the Michaelis and covalent intermediate, *RSC Advances* 5, 82381-82394.

CHAPTER 1

49. Paës, G., Cortés, J., Siméon, T., O'Donohue, M. J., and Tran, V. (2012) Thumb-loops up for catalysis: a structure/function investigation of a functional loop movement in a GH11 xylanase, *Comput. Struct. Biotechnol. J.* e201207001.
50. Murakami, M. T., Arni, R. K., Vieira, D. S., Degrève, L., Ruller, R., and Ward, R. J. (2005) Correlation of temperature induced conformation change with optimum catalytic activity in the recombinant G/11 xylanase A from *Bacillus subtilis* strain 168 (1A1), *FEBS Lett.* 579, 6505-6510.
51. Pollet, A., Vandermarliere, E., Lammertyn, J., Strelkov, S. V., Delcour, J. A., and Courtin, C. M. (2009) Crystallographic and activity-based evidence for thumb flexibility and its relevance in glycoside hydrolase family 11 xylanases, *Proteins.* 77, 395-403.
52. Hansen, D. F., Vallurupalli, P., and Kay, L. E. (2008) An improved 15N relaxation dispersion experiment for the measurement of millisecond time-scale dynamics in proteins, *J. Phys. Chem. B.* 112, 5898-5904.
53. Gagné, D., Narayanan, C., Nguyen-Thi, N., Roux, L. D., Bernard, D. N., Brunzelle, J. S., Couture, J.-F., Agarwal, P. K., and Doucet, N. (2016) Ligand binding enhances millisecond conformational exchange in xylanase B2 from *Streptomyces lividans*, *Biochemistry* 55, 4184-4196.
54. Muilu, J., Törrönen, A., Peräkylä, M., and Rouvinen, J. (1998) Functional conformational changes of endo-1, 4-xylanase II from *Trichoderma reesei*: A molecular dynamics study, *Proteins.* 31, 434-444.
55. Rapp, P., and Wagner, F. (1986) Production and properties of xylan-degrading enzymes from *Cellulomonas uda*, *Appl. Environ. Microbiol.* 51, 746-752.
56. Legler, G. (1990) Glycoside hydrolases: mechanistic information from studies with reversible and irreversible inhibitors, *Adv. Carbohydr. Chem. Biochem.* 48, 319-384.
57. Withers, S. G., and Aebersold, R. (1995) Approaches to labeling and identification of active site residues in glycosidases, *Protein Sci.* 4, 361-372.
58. Quaroni, A., Gershon, E., and Semenza, G. (1974) Affinity labeling of the active sites in the sucrase-isomaltase complex from small intestine, *J. Biol. Chem.* 249, 6424-6433.
59. Rempel, B. P., and Withers, S. G. (2008) Covalent inhibitors of glycosidases and their applications in biochemistry and biology, *Glycobiology* 18, 570-586.
60. Hermans, M., Kroos, M., Van Beeumen, J., Oostra, B., and Reuser, A. (1991) Human lysosomal alpha-glucosidase. Characterization of the catalytic site, *J. Biol. Chem.* 266, 13507-13512.
61. Herrchen, M., and Legler, G. (1984) Identification of an essential carboxylate group at the active site of lacZ β -galactosidase from *Escherichia coli*, *The FEBS Journal* 138, 527-531.
62. Gebler, J., Aebersold, R., and Withers, S. (1992) Glu-537, not Glu-461, is the nucleophile in the active site of (lac Z) beta-galactosidase from *Escherichia coli*, *J. Biol. Chem.* 267, 11126-11130.
63. Miao, S., McCarter, J. D., Grace, M. E., Grabowski, G. A., Aebersold, R., and Withers, S. G. (1994) Identification of Glu340 as the active-site nucleophile in human glucocerebrosidase by use of electrospray tandem mass spectrometry, *J. Biol. Chem.* 269, 10975-10978.
64. Sulzenbacher, G., Schülein, M., and Davies, G. J. (1997) Structure of the endoglucanase I from *Fusarium oxysporum*: Native, cellobiose, and 3, 4-epoxybutyl β -D-cellobioside-inhibited forms, at 2.3 Å resolution, *Biochemistry* 36, 5902-5911.
65. Havukainen, R., Törrönen, A., Laitinen, T., and Rouvinen, J. (1996) Covalent binding of three epoxyalkyl xylosides to the active site of endo-1, 4-xylanase II from *Trichoderma reesei*, *Biochemistry* 35, 9617-9624.
66. Caron, G., and Withers, S. (1989) Conduritol aziridine: a new mechanism-based glucosidase inactivator, *Biochem. Biophys. Res. Commun.* 163, 495-499.
67. Willems, L. I., Jiang, J., Li, K. Y., Witte, M. D., Kalleméijn, W. W., Beenakker, T. J., Schröder, S. P., Aerts, J. M., van der Marel, G. A., and Codée, J. D. (2014) From Covalent Glycosidase Inhibitors to Activity-Based Glycosidase Probes, *Chem. Eur. J.* 20, 10864-10872.
68. Premkumar, L., Sawkar, A. R., Boldin-Adamsky, S., Toker, L., Silman, I., Kelly, J. W., Futerman, A. H., and Sussman, J. L. (2005) X-ray Structure of Human Acid- β -Glucosidase Covalently Bound to Conduritol-B-Epoxyde Implications for gaucher disease, *J. Biol. Chem.* 280, 23815-23819.
69. Daniels, L. B., Glew, R. H., Radin, N. S., and Vunnam, R. R. (1980) A revised fluorometric assay for Gaucher's disease using conduritol- β -epoxyde with liver as the source of β -glucosidase, *Clin. Chim. Acta* 106, 155-163.
70. Boot, R. G., Verhoek, M., Donker-Koopman, W., Strijland, A., van Marle, J., Overkleeft, H. S., Wennekes, T., and Aerts, J. M. (2007) Identification of the non-lysosomal glucosylceramidase as β -glucosidase 2, *J. Biol. Chem.* 282, 1305-1312.
71. Hays, W. S., Wheeler, D. E., Eghtesad, B., Glew, R. H., and Johnston, D. E. (1998) Expression of cytosolic β -glucosidase in guinea pig liver cells, *Hepatology* 28, 156-163.

CHAPTER 1

72. Morjani, H., Aouali, N., Belhoussine, R., Veldman, R. J., Levade, T., and Manfait, M. (2001) Elevation of glucosylceramide in multidrug-resistant cancer cells and accumulation in cytoplasmic droplets, *Int. J. Cancer* 94, 157-165.
73. Yatziv, S., Newburg, D., Livni, N., Barfi, G., and Kolodny, E. (1988) Gaucher-like changes in human blood-derived macrophages induced by beta-glucocerebrosidase inhibition, *J. Lab. Clin. Med.* 111, 416-420.
74. Prencz, E., Chaturvedi, P., and Newburg, D. (1996) In vitro accumulation of glucocerebroside in neuroblastoma cells: a model for study of Gaucher disease pathobiology, *J. Neurosci. Res.* 43, 365-371.
75. Stephens, M., Bernatsky, A., Burachinsky, V., Legler, G., and Kanfer, J. (1978) The Gaucher mouse: differential action of conduritol B epoxide and reversibility of its effects, *J. Neurochem.* 30, 1023-1027.
76. Atsumi, S., Umezawa, K., Iinuma, H., Naganawa, H., Nakamura, H., Itaka, Y., and Takeuchi, T. (1990) Production, isolation and structure determination of a novel β -glucosidase inhibitor, cyclophellitol, from *Phellinus* sp., *J. Antibiot.* 43, 49-53.
77. Atsumi, S., Nosaka, C., Iinuma, H., and Umezawa, K. (1992) Inhibition of glucocerebrosidase and induction of neural abnormality by cyclophellitol in mice, *Arch. Biochem. Biophys.* 297, 362-367.
78. Atsumi, S., Nosaka, C., Iinuma, H., and Umezawa, K. (1993) Accumulation of tissue glucosylsphingosine in Gaucher-like mouse induced by the glucosylceramidase inhibitor cyclophellitol, *Arch. Biochem. Biophys.* 304, 302-304.
79. Gloster, T. M., Madsen, R., and Davies, G. J. (2007) Structural basis for cyclophellitol inhibition of a β -glucosidase, *Org. Biomol. Chem.* 5, 444-446.
80. Witte, M. D., Kallemeijn, W. W., Aten, J., Li, K.-Y., Strijland, A., Donker-Koopman, W. E., Van Den Nieuwendijk, A. M., Bleijlevens, B., Kramer, G., and Florea, B. I. (2010) Ultrasensitive in situ visualization of active glucocerebrosidase molecules, *Nat. Chem. Biol.* 6, 907-913.
81. Kallemeijn, W. W., Li, K. Y., Witte, M. D., Marques, A. R., Aten, J., Scheij, S., Jiang, J., Willems, L. I., Voorn-Brouwer, T. M., and van Roomen, C. P. (2012) Novel Activity-Based Probes for Broad-Spectrum Profiling of Retaining β -Exoglucosidases In Situ and In Vivo, *Angew. Chem. Int. Ed.* 51, 12529-12533.
82. Caner, S., Zhang, X., Jiang, J., Chen, H. M., Nguyen, N. T., Overkleeft, H., Brayer, G. D., and Withers, S. G. (2016) Glucosyl epi-cyclophellitol allows mechanism-based inactivation and structural analysis of human pancreatic α -amylase, *FEBS Lett.* 590, 1143-1151.
83. Wicki, J., Rose, D. R., and Withers, S. G. (2002) Trapping covalent intermediates on beta-glycosidases, *Methods Enzymol.* 354, 84-105.
84. Vocadlo, D. J., Davies, G. J., Laine, R., and Withers, S. G. (2001) Catalysis by hen egg-white lysozyme proceeds via a covalent intermediate, *Nature* 412, 835.
85. Withers, S. G., and Street, I. P. (1988) Identification of a covalent. alpha.-D-glucopyranosyl enzyme intermediate formed on a beta.-glucosidase, *J. Am. Chem. Soc.* 110, 8551-8553.
86. McMahon, L. G., Nakano, H., Levy, M.-D., and Gregory, J. F. (1997) Cytosolic Pyridoxine- β -d-Glucoside Hydrolase from Porcine Jejunal Mucosa Purification, properties, and comparison with broad specificity β -glucosidase, *J. Biol. Chem.* 272, 32025-32033.
87. Arribas, J. C. D., Herrero, A. G., Martín-Lomas, M., Cañada, F. J., He, S., and Withers, S. G. (2000) Differential mechanism-based labeling and unequivocal activity assignment of the two active sites of intestinal lactase/phlorizin hydrolase, *The FEBS Journal* 267, 6996-7005.
88. Blanchard, J. E., and Withers, S. G. (2001) Rapid screening of the aglycone specificity of glycosidases: applications to enzymatic synthesis of oligosaccharides, *Chem. Biol.* 8, 627-633.
89. Vocadlo, D. J., and Bertozzi, C. R. (2004) A strategy for functional proteomic analysis of glycosidase activity from cell lysates, *Angew. Chem. Int. Ed.* 43, 5338-5342.
90. Hekmat, O., Kim, Y.-W., Williams, S. J., He, S., and Withers, S. G. (2005) Active-site Peptide "Fingerprinting" of Glycosidases in Complex Mixtures by Mass Spectrometry Discovery of a novel retaining β -1, 4-glycanase in *Cellulomonas fimi*, *J. Biol. Chem.* 280, 35126-35135.
91. de Melo, E. B., da Silveira Gomes, A., and Carvalho, I. (2006) α - and β -Glucosidase inhibitors: chemical structure and biological activity, *Tetrahedron* 62, 10277-10302.
92. Watson, A. A., Fleet, G. W., Asano, N., Molyneux, R. J., and Nash, R. J. (2001) Polyhydroxylated alkaloids—natural occurrence and therapeutic applications, *Phytochemistry* 56, 265-295.
93. Sinnott, M. L. (1990) Catalytic mechanism of enzymic glycosyl transfer, *Chem. Rev.* 90, 1171-1202.
94. Pandey, G., Kapur, M., Khan, M. I., and Gaikwad, S. M. (2003) A new access to polyhydroxy piperidines of the azasugar class: synthesis and glycosidase inhibition studies, *Org. Biomol. Chem.* 1, 3321-3326.
95. Liu, H., Liang, X., Søhoel, H., Bülow, A., and Bols, M. (2001) Noeumycin, 1 A Glucosyl Cation Mimic that Strongly Inhibits Glycosidases, *J. Am. Chem. Soc.* 123, 5116-5117.

CHAPTER 1

96. Benito, J. M., García Fernández, J. M., and Mellet, C. O. (2011) Pharmacological chaperone therapy for Gaucher disease: a patent review, *Expert Opin. Ther. Pat.* 21, 885-903.
97. Khanna, R., Benjamin, E. R., Pellegrino, L., Schilling, A., Rigat, B. A., Soska, R., Nafar, H., Ranes, B. E., Feng, J., and Lun, Y. (2010) The pharmacological chaperone isofagomine increases the activity of the Gaucher disease L444P mutant form of β -glucosidase, *The FEBS journal* 277, 1618-1638.
98. Sawkar, A. R., Adamski-Werner, S. L., Cheng, W.-C., Wong, C.-H., Beutler, E., Zimmer, K.-P., and Kelly, J. W. (2005) Gaucher disease-associated glucocerebrosidases show mutation-dependent chemical chaperoning profiles, *Chem. Biol.* 12, 1235-1244.
99. Abian, O., Alfonso, P., Velazquez-Campoy, A., Giraldo, P., Pocovi, M., and Sancho, J. (2011) Therapeutic strategies for Gaucher disease: miglustat (NB-DNJ) as a pharmacological chaperone for glucocerebrosidase and the different thermostability of velaglucerase alfa and imiglucerase, *Mol. Pharm.* 8, 2390-2397.
100. Sawkar, A. R., Cheng, W.-C., Beutler, E., Wong, C.-H., Balch, W. E., and Kelly, J. W. (2002) Chemical chaperones increase the cellular activity of N370S β -glucosidase: a therapeutic strategy for Gaucher disease, *Proc. Natl. Acad. Sci. U.S.A.* 99, 15428-15433.
101. Somerville, C. (2007) Biofuels, *Curr. Biol.* 17, R115-R119.
102. Dodd, D., and Cann, I. K. (2009) Enzymatic deconstruction of xylan for biofuel production, *GCB Bioenergy* 1, 2-17.

THESIS OUTLINE

The work presented in this thesis is devoted to deepening our understanding of the functional dynamics and conformational stability of retaining β -glycosidases. Over the years, tremendous efforts were dedicated to elucidate the structure/function relationship of this ubiquitous family of enzymes and to discern their substrate itineraries during catalysis. Nevertheless, the mechanism of stabilization of β -glycosidases by active site binders and the contribution of dynamics in catalysis remains poorly explored. Therefore, in this thesis it is aimed to address these aspects, relying on activity-based probes technology in conjunction with standard biochemistry and advanced NMR techniques. **CHAPTER 1** gives a general introduction of the biophysical properties of GH5, GH11 and GH30 β -glycosidase families and the inhibitors used to modulate their functions, both in fundamental research and in therapy. **CHAPTER 2** describes the application of ABPs to characterize the conformational stability of endo-glycoceramidase EGCII, a bacterial homologue of GBA that holds promise as a therapeutic application against a number of inherited glycosphingolipidoses caused by deficiency in lysosomal exoglycosidases. **CHAPTER 3** describes the application of ABPs and reversible β -glycosidase inhibitors to dissect the stabilization mechanism of GBA by active site occupancy *in vitro* and *in vivo*, as a proof of the principal for the pharmacological chaperone treatment against Gaucher disease. **CHAPTER 4** describes the conformational landscape and dynamics of β -glycosidases and their possible roles in the catalytic mechanism, using GH11 xylanase as a model. **CHAPTER 5** gives general conclusions of this work and future perspectives.

CHAPTER 2

Hydrophobic Interactions Contribute to Conformational Stabilization Endoglycoceramidase II by Mechanism-Based Probes

Abstract

Small compound active site interactors receive considerable attention for their ability to positively influence the fold of glycosidases. Endoglycoceramidase II (EGCII) from *Rhodococcus* sp. is an endo- β -glucosidase releasing the complete glycan from ceramide in glycosphingolipids. Cleavage of the β -glycosidic linkage between glucose and ceramide is also catalysed by glucocerebrosidase (GBA), the exo- β -glucosidase deficient in Gaucher disease. In this work, it is demonstrated that established β -glucoside-configured cyclophellitol-type activity-based probes (ABPs) for GBA also are effective, mechanism-based, and irreversible inhibitors of EGCII. The stability of EGCII is markedly enhanced by formation of covalent complexes with cyclophellitol ABPs substituted with hydrophobic moieties, as evidenced by an increased melting temperature, resistance against tryptic digestion, changes in ^{15}N - ^1H transverse relaxation optimized spectroscopy spectra of the [^{15}N]-Leu-labeled enzyme, and relative hydrophobicity as determined by 8-anilino-1-naphthalenesulfonic acid fluorescence. The stabilization of the EGCII conformation correlates with the shape and hydrophobicity of the substituents of the ABPs. It is concluded that the amphipathic active site binders with aliphatic moieties act as a “hydrophobic zipper” on the flexible EGCII protein structure.

This work was published as: Ben Bdira, F., et al., Hydrophobic Interactions Contribute to Conformational Stabilization of Endoglycoceramidase II by Mechanism-Based Probes. *Biochemistry*, 2016. 55(34): p. 4823-4835.

Introduction

Glycosphingolipids, an important class of cellular membrane lipids, contain a ceramide, and its primary hydroxyl is glycosylated with either a glucose or galactose residue to which further sugars may be attached. Two pathways for degradation of glycosphingolipids are known to exist in nature. Non-mammalian endoglycoceramidasases are able to remove in one step the entire oligosaccharide chain from the ceramide moiety. Endoglycoceramidase II (EGCII) from *Rhodococcus* sp.¹ was the first endoglycoceramidase identified (grouped in glucosyl-hydrolase family 5). Later, other non-homologous endoglycosidases degrading glycosphingolipids from leeches² and earthworms³ were discovered. No mammalian endoglycoceramidase has been identified so far, although a similar enzymatic activity has been reported for rat and rabbit mammary glands⁴ and human cancer cells⁵. In mammalian cells, the degradation of glycosphingolipids takes place via a very different pathway. Inside lysosomes, the subcellular compartments that specialize in the breakdown of macromolecules, terminal sugars of glycosphingolipids are removed stepwise by specific exoglycosidases, ultimately generating the free lipid, ceramide. The physiological relevance of lysosomal degradation of glycosphingolipids is illustrated by associated pathologies. Inherited defects in glycosphingolipid degrading exoglycosidases cause a number of storage diseases in humans, collectively named glycosphingolipidoses. Most prevalent among these disorders is Gaucher disease, in which deficiency of the lysosomal β -glucosidase, named glucocerebrosidase (EC 3.2.1.45, GBA), a member of glycosidase family 30 (www.cazy.org), causes accumulation of the substrate glucosylceramide. A number of GBA active site binders, called pharmacological chaperones, are being investigated as enzyme stabilizers with envisioned therapeutic application in Gaucher disease patients. One of the best studied compounds in this respect is the iminosugar isofagomine (IFG), a competitive GBA inhibitor^{6,7}. The retaining β -glucosidase GBA employs a Koshland double-displacement mechanism following a ${}^1S_3 \rightarrow {}^4H_3 \rightarrow {}^4C_1$ reaction itinerary⁸. In the first displacement event, a covalent α -enzyme glucosyl intermediate is formed, with the glucopyranose moiety adopting a 4C_1 conformation. After binding of the substrate β -glucoside, a transition state emerges with high oxocarbenium ion character with a concomitant conformational change of the substrate in the Michaelis complex (1S_3) to a 4H_3 half-chair⁹. It is the enzyme glucosyl intermediate state of the hydrolysis reaction that is emulated by cyclophellitol **1** (see **Figure 2.1a** for the compounds used in this study). Thus, cyclophellitol binds with high specificity to the β -glucosidase active site. Cyclophellitol **1**, first isolated from a *Phellinus* sp. culture by Atsumi and co-workers¹⁰, irreversibly inhibits GBA by forming a stable, covalent adduct to residue Glu340¹¹. The cyclophellitol epoxide is ideally positioned for acid-catalyzed nucleophilic opening involving the active site residues. As a result, a covalent enzyme-inhibitor complex is

CHAPTER 2

formed (with the inhibitor now also adopting a 4C_1 conformation), with the ester bond much more stable and thereby irreversible compared to the acylal linkage that characterizes the enzyme-substrate covalent intermediate (**Figure 2.1b**)⁹. Substitution of the epoxide oxygen with nitrogen yields cyclophellitol aziridine **2**, an equally strong inhibitor¹². Cyclophellitol **1** and cyclophellitol aziridine **2** functionalized to contain a fluorophore have been applied as activity-based glycosidase probes for sensitive *in vitro* and *in situ* detection of GBA molecules^{11,13}. Conduritol B epoxide (CBE) **10**, an analogue of cyclophellitol lacking the C8 methylene, likewise irreversibly inhibits GBA but with lower affinity and specificity¹⁴. Freezing of the enzyme midway through its catalytic reaction through covalent inhibition offers an important tool for investigating the characteristics of the formed complex and elucidating which parts of the inhibitors are important for efficient stabilization activity. Despite the significant differences in their amino acid sequences, as they belong to different families of glycoside hydrolases (**Figure A1.1**), GBA and EGCII share a similar folding topology of their polypeptide chains. Both of them display a TIM barrel (triose-phosphate isomerase barrel) catalytic domain formed by $(\alpha/\beta)_8$, which makes them both members of GH-A clan (www.cazy.org). The superposition of the three-dimensional (3D) structure of the TIM barrels has a root-mean-square deviation (rmsd) of 3.1 Å for the C α atoms [Protein Data Bank (PDB) entry 2v3e for GBA and PDB entry 2osx for EGCII] yet shows a remarkable superposition of the acid/base and the nucleophile catalytic residues, which are separated by an average distance of ~ 5.2 Å, consistent with their role in a double displacement mechanism with net retention of stereochemistry (see **Figure 2.2a,c**). The two proteins also have the aglycan sites in the same position relative to the active site. The analysis of the GBA crystal structure in the presence of nonyl-deoxynojirimycin (NN-DNJ), a potent inhibitor of GBA, shows that the aliphatic tail of the substrate is accommodated within a narrow hydrophobic channel where it interacts with residues Leu241, Phe246, Tyr313, Leu314, and Tyr244. Similarly, the ceramide moiety of GM3 ganglioside, the natural substrate for EGCII, makes several hydrophobic interactions with residues Leu180, Tyr182, Ile183, Phe235, Ala275, Ile276, Tyr306, and Leu308 (**Figure 2.2b,c**). In view of the similarities between the two protein binding sites, it is not surprising that NN-DNJ can also inhibit EGCII and fits well in the active site of the EGCII crystal structure (PDB entry 2OSX)¹⁵ (**Figure 2.2c**). The GBA glycan binding site is much narrower than that of EGCII, which allows GBA to accommodate only a single glucose ring, precluding the binding of longer saccharide moieties and suggesting an explanation for the different exo and endo hydrolysis specificities for GBA and EGCII, respectively. The location of the reactive residues and primary sugar is, however, essentially the same in both active sites, suggesting that the mechanism of cleavage of the β -glycosidic linkage connecting glucose and ceramide is the same. The analogies between the two retaining β -glucosidases stimulated us to test the impact of a series of mechanism-based irreversible inhibitors known to bind covalently in the active site of GBA on EGCII conformational stability.

CHAPTER 2

Here, it is demonstrated that in its free state in solution EGCII is thermolabile and highly flexible. An equilibrium between monomeric and dimeric states is observed for the resting state enzyme, because of the large solvent-exposed hydrophobic surface area of EGCII. Upon formation of the complex with the amphiphilic cyclophellitol analogues (**4-8**), marked stabilization and rigidification are observed, correlating with the lipophilic potential of the compounds. No changes are observed in the protein stability or rigidity after incubation with non-hydrophobic compounds (**1** and **2**). These findings demonstrate the importance of the length and shape of the non-glycan moiety of substituted cyclophellitols for the enzyme stabilization.

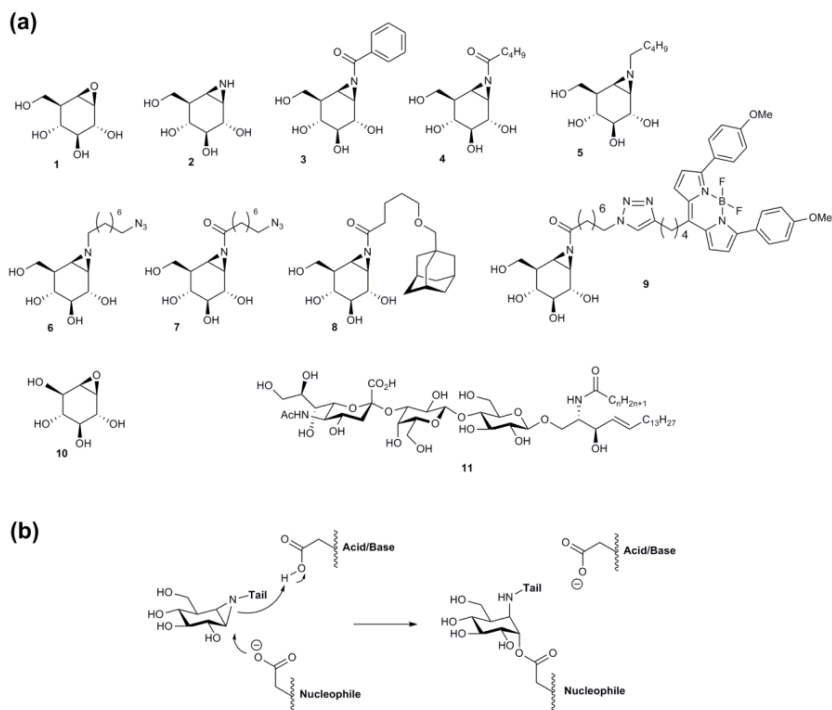


Figure 2.1. (a) Structures of β -glucoside-configured cyclophellitols used and (b) Mechanism-based inactivation of β -glucosidases by covalent binding to a catalytic nucleophile.

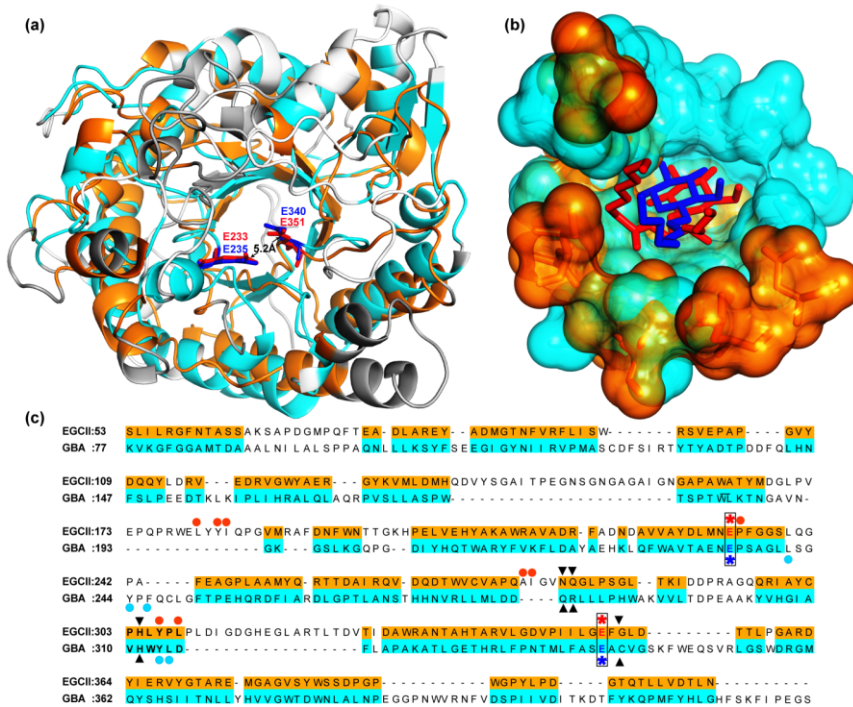


Figure 2.2. Comparison of the folding topology and aglycan binding sites of GBA and EGCII. (a) Structural alignment of the TIM barrel catalytic domain of EGCII (orange cartoon) and GBA (cyan cartoon) using the jFATCAT algorithm³⁹ (RCSB comparison tool). The acid/base and nucleophile catalytic residues are shown as sticks and colored red for EGCII and blue for GBA. For the sake of clarity, non-overlapping loops were hidden. (b) Aglycan binding site cavities of EGCII (orange) and GBA (cyan) as observed in the superposition of the residues interacting with the aliphatic tail of the ligands is shown; β -D-glucose-ceramide (in EGCII) is colored red and NN-DNJ (in GBA) blue. (c) Primary sequences of EGCII and GBA with the structurally homologous parts highlighted in orange and cyan, respectively. Acid/base catalytic residues are marked with stars and a black box. Hydrophobic residues interacting with the NN-DNJ alkyl chain and the ceramide moiety of GM3 are marked with cyan and orange circles, respectively. Non-hydrophobic interacting residues within the aglycan binding sites are marked by black triangles.

Results

Readouts for Active EGCII Molecules. It is first identified convenient readouts for active EGCII molecules. It is determined whether 4-methylumbelliferyl lactoside (4MU-Lac) is a suitable fluorogenic substrate for recombinant EGCII. This proves to be the case. The enzyme exhibits an optimal activity at pH 5.5 (**Figure 2.3a**), with hydrolysis occurring in a time-dependent manner (**Figure 2.3b**). Next, it is demonstrated that EGCII can be labeled in a mechanism-based manner by a β -glucoside-configured cyclophellitol **10** and cyclophellitol-aziridine substituted with a BODIPY fluorophore **9** (**Figure 2.3c**).

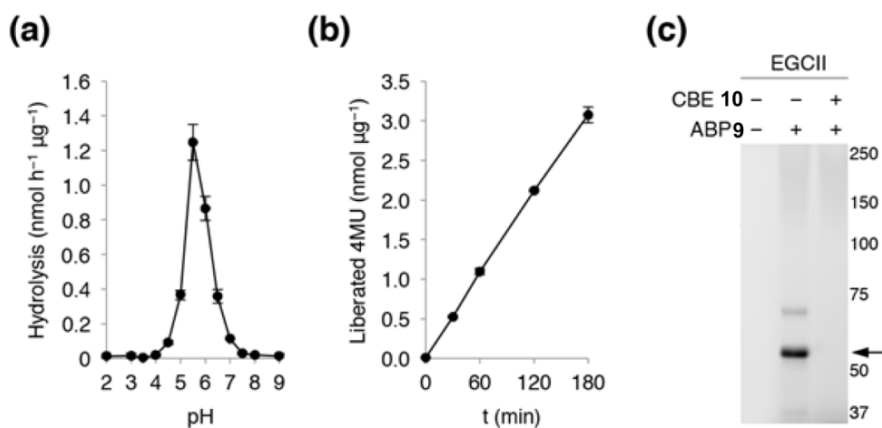


Figure 2.3. Read-outs of active EGCII molecules. (a) Hydrolysis of 4MU-Lac by EGCII across a pH range, at 17 °C in 150 mM McIlvaine's buffer. (b) Time-dependent liberation of 4MU from 4MU-Lac by EGCII at 17 °C and in 150 mM McIlvaine's buffer pH 5.5 (c) Labeling of EGCII with cyclophellitol-aziridine ABP **9** at pH 5.5 and 17 °C and its competition by pre-incubation with CBE **10** in 150 mM McIlvaine's buffer pH 5.5. The main EGCII protein band is marked with an arrow.

Thermal stability of EGCII

Under optimal conditions for enzymatic activity [150 mM McIlvaine's buffer (pH 5.5)]¹⁶ was monitored by recording the temperature dependence of the dichroic signal at 222 nm and applying a range of heating rates from 1 to 5 °C/min (**Figure 2.4a**). The obtained unfolding curve at a heating rate of 1 °C/min shows an apparent T_m of 42 °C, close to the enzyme optimal catalytic temperature (37 °C) (**Figure 2.4b**)¹. The apparent T_m value depends on the scanning rate, suggesting an irreversible denaturation process toward aggregation, which is visible by eye due to the turbidity of the protein solution. The unfolding kinetics of EGCII at 37 °C (pH 5.5) were determined by recording a CD spectrum every 10 min for 50 min. EGCII shows an exponential decay of its ellipticity signal at 222 nm with a half-life of ~10 min and forms a visible aggregate. The enzymatic

activity was also tested with 4MU-Lac as a substrate. A parallel decay was observed (**Figure 2.4c**), correlating unfolding kinetics with loss of activity. During the kinetic unfolding, the amount of residual active protein was also followed by labeling with the activity-based probe compound **9** (**Figure 2.4c**, bottom panel). A similar decay of the fluorescently labeled EGCII over the incubation time was observed. EGCII denaturation was also followed at 25 °C by CD (**Figure 2.4d**). At this temperature, the enzyme's activity is close to optimal (**Figure 2.4b**). At 25 °C [150 mM McIlvaine's buffer (pH 5.5)], EGCII is stable with no changes in its secondary structure and its active state as monitored by ABP (**Figure 2.4d**, bottom panel). These results show that EGCII is a thermolabile protein with an apparent T_m of 42 °C at a heating rate of 1 °C/min and tends to form an aggregate as a final step in the irreversible unfolding process. Therefore, for experiments requiring prolonged incubations, it is practical to work at 25 °C.

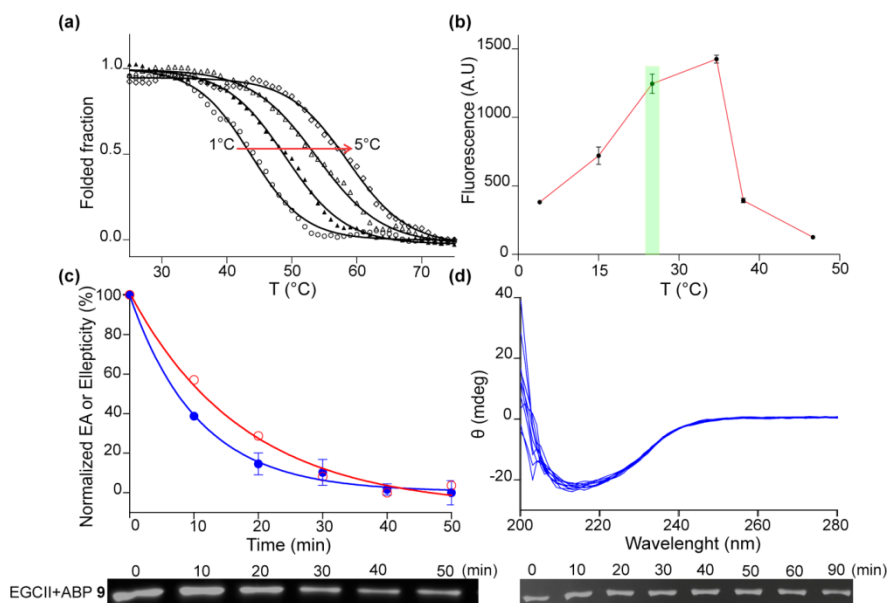


Figure 2.4. Thermodynamic stability of EGCII. **(a)** Thermal denaturation curves of EGCII at varying scanning rates (1-5 °C/min), at a protein concentration of 5 μ M. **(b)** Temperature dependence of EGCII activity toward 4MU-Lac in 150 mM McIlvaine's buffer (pH 5.5), with an incubation time of 1 h. The activity at 25 °C is highlighted by the green rectangle; the error bars represent the standard deviations of a duplicate experiment. **(c)** Decays over time of the ellipticity at 222 nm (red empty circle and curve), the specific activity (blue filled circle and curve), and SDS-PAGE of ABP labeling of EGCII samples at 37 °C in 150 mM McIlvaine's buffer (pH 5.5) (bottom panel). The red and blue curves are exponential decay fits of the ellipticity and enzymatic activity (EA), respectively. The half-life decays are 12 min (ellipticity) and 7 min (enzymatic activity). The error bars represent standard deviations of a duplicate experiment. **(d)** EGCII kinetic stability at 25 °C monitored by circular dichroism spectra (blue lines), recorded every 10 min for 90 min, and SDS-PAGE of ABP selective labeling of EGCII (bottom panel).

EGCII flexibility and conformations in solution

Limited proteolysis with trypsin at a trypsin: EGCII ratio of 1:100 was employed to investigate the flexibility of EGCII in solution. Proteolysis under different conditions and as a function of incubation time was analyzed via SDS-PAGE. At 25 °C, directly after trypsin addition, an additional band rapidly appears on the gel close to the intact protein. This could result from cleavage of one of the flexible ends of the protein. After incubation for 10 min, approximately 50% of the protein has been digested with the appearance of two major protein fragments with apparent molecular weight of 34 and 25 kDa (**Figure 2.6a**). These fragment species remain relatively resistant to °C, the protein was fully digested into these two bands within 10 min, the digestion already being observed immediately upon addition of the protease (time zero) (**Figure 2.6c**). The peptic fragment pattern is similar at 37 and 25 °C, suggesting that digestion occurs at the same position in the polypeptide. To correct for the difference in trypsin activity at 25 and 37 °C, the digestion at 25 °C was conducted by adding 3 and 10 times more trypsin. The tryptic pattern of EGCII was not affected by the additional trypsin activity (**Figure 2.5**). The subsequent rapid disappearance of the tryptic fragments at 37 °C, as compared to that at 25 °C, suggests that at the lower temperature the nicked polypeptide remains folded, whereas at higher temperature it unfolds, allowing further proteolysis of the two fragments. We tried to identify the site of digestion by mass spectrometry.

The in-gel digestion and analysis by LC/MS of the produced tryptic fragments suggested that the major digestion occurs after Arg332. However, LC/MS of the intact fragments (that is, without further digestion into smaller peptides) suggested that the major digestion site is located after the preceding arginine residue at position 321 (observed mass for C-terminal fragment 18622 Da, expected 18624 Da). It is concluded that either or both of these arginines represent the primary cutting site. Interestingly, in the EGCII crystal structure, both arginines are located in a long, well-structured α -helix (**Figure 2.6e**). In a modeling study, Hubbard et al. concluded that a local disorder or unfolding of the protein polypeptide chain of at least 12 residues is required to allow access into a protease active site¹⁷. Therefore, those results suggest that this part of the protein is less structured in solution than in the crystalline state. In the presence of the detergent lauryl glucoside (**Figure 2.6b**) or Triton X-100 (**Figure 2.6d**), the protein is strikingly resistant to tryptic digestion. It has been reported that the used surfactants have no inhibitory effects on trypsin¹⁸. This tryptic resistance of the protein in the presence of detergents could be due to interaction with the micelles, shielding the protein surface, leading to a more rigid and compact structure. Moreover, lauryl glucoside has an amphiphilic structure quite similar to that of EGCII natural substrates **11** (**Figure 2.1a**), and thus, it might interact with the binding pocket of the protein, stabilizing it in a rigid conformation (see below). Crystals of EGCII were obtained in the presence of 1% (v/v) Triton X-100, 10% (v/v) glycerol, and 25% (w/v) PEG¹⁹. The possibility that under these conditions, and because of crystal

CHAPTER 2

packing effects, the protein could adopt a rigid conformation that is not representative of the lowest-energy state present in solution cannot be excluded.

Next, EGCII in solution was studied by size exclusion chromatography (SEC) to monitor changes in the hydro- dynamic dimensions accompanying unfolding, dimerization, or conformational changes of globular proteins in solution^{20,21}. It is observed that EGCII elutes as two fractions from the SEC column (P1 and P2) with elution volumes of 8.5 and 9.5 mL, respectively. The integration of the chromatogram peaks area yields percentages of 30 and 70% for peaks 1 and 2, respectively (**Figure 2.7a**). The re-injection of the extremity of the collected fractions of the two peaks shows an exchange between the two states of the protein even at low concentrations (**Figure 2.7c**). The enzymatic activity of both peak fractions was the same within error (**Figure 2.7b**). They also exhibit the same molecular weight on SDS-PAGE. Therefore, both fractions represent a native and active state of EGCII. Native PAGE analysis of EGCII shows two bands, and staining of the gel with ABP 9 confirms that the enzyme in both of the bands is active (**Figure 2.7d**). The analysis of the molecular weight of the eluted peaks with SEC-MALLS yields an M_w of 100 kDa for P1 and an M_w of 50 kDa for P2 (**Figure A1.2**), providing more evidence of a monomeric state and a dimeric state of the protein. Thus, it is concluded that EGCII is in equilibrium between monomeric and dimeric states in solution.

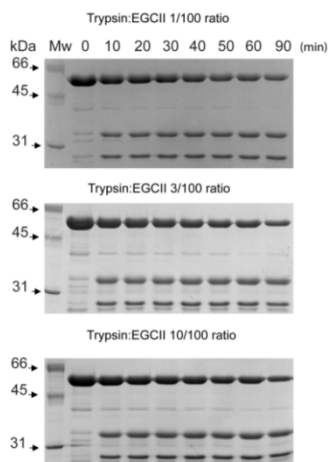


Figure 2.5: Tryptic digestion of EGCII at different ratios: Tryptic digestion of EGCII with trypsin from bovine pancreas (Sigma) with Trypsin: EGCII ratios 1:100, 3:100, 10:100 (by weight) in 150 mM McIlvaine's(citrate/phosphate) buffer pH 5.5 at 25°C.

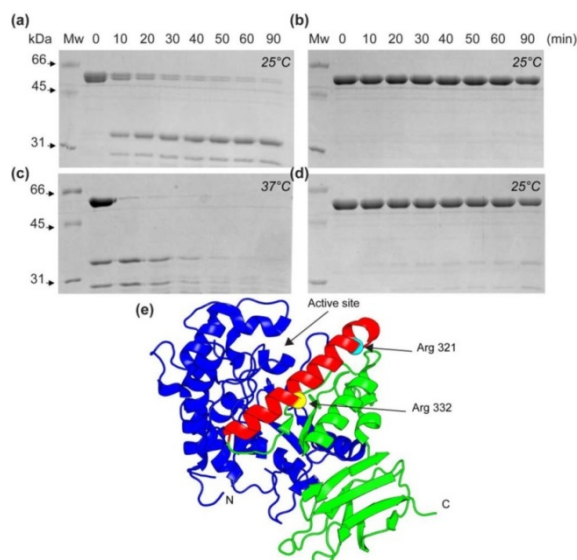


Figure 2.6. Time course of tryptic proteolysis of EGCII analyzed by SDS–PAGE. Tryptic proteolysis was performed at an E:S ratio of 1:100 (by weight) in 150 mM McIlvaine’s buffer (pH 5.5) at 25 °C **(a)**, at 25 °C in the presence of 1% lauryl glucoside **(b)**, at 37 °C **(c)**, and at 25 °C in the presence of 1% Triton X-100 **(d)**. Samples (5 µg) were taken from the reaction mixture every 10 min and analyzed via 10% SDS–PAGE followed by protein staining. **(e)** Major trypsin cleavage sites (Arg321 and Arg332 in the red helix) identified by mass spectrometry and depicted in EGCII 3D structure (PDB entry 2osw)¹⁹. N-Terminal and C-terminal protein fragments are colored blue and green, respectively.

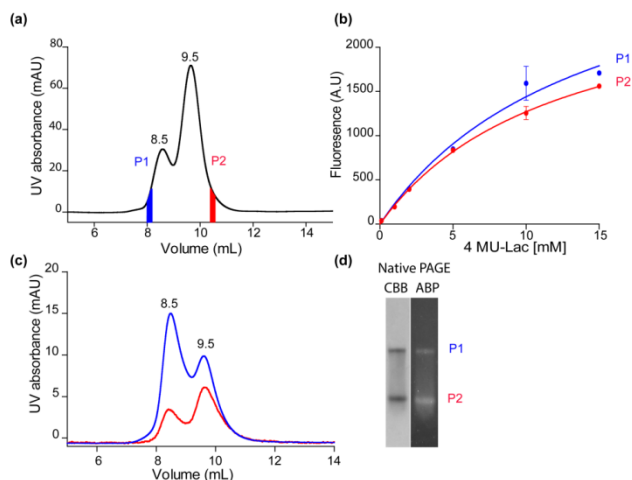


Figure 2.7. EGCII solution state analysis by size exclusion chromatography and native PAGE. **(a)** EGCII size exclusion chromatogram in 20 mM Tris-HCl and 150 mM NaCl (pH 7.6). The elution volumes of the peaks are indicated. **(b)** Enzymatic activity of eluted fractions P1 and P2 using 4MU-Lac as a substrate. The error bars represent the standard deviations of two experiments. **(c)** Size exclusion chromatograms of eluted fractions P1 (blue) and P2 (red). **(d)** Native gel analysis of the EGCII sample in Tris buffer, stained with Coomassie Brilliant Blue (CBB) and the activity-based probe (ABP) **9**.

EGCII complexed with *N*-alkyl azide-substituted cyclophellitol aziridine (compound **6**)

Because EGCII was found to irreversibly react with cyclophellitol aziridines, the impact of cyclophellitol derivatives on the biophysical properties of EGCII was studied. For this, compound **6** was used, an *N*-alkylated cyclophellitol aziridine functionalized with an azide. The effects of compound **6** on the thermodynamic properties of EGCII were investigated by measuring the apparent T_m of the complex. A pronounced increase in the apparent T_m of 12 °C was observed (**Figure 2.8a**). Such an increase is usually accompanied by changes in the protein structure and rigidity^{22,23}. The occurrence of conformational changes of EGCII upon complex formation was probed by comparing ¹⁵N-¹H TROSY spectra of the free and bound states. EGCII contains 38 leucine residues that were used as probes to detect conformational changes. In the free form, only a few resonances are observed (**Figure 2.8b**), which are very intense, suggesting that some leucine residues are in highly flexible regions whereas many others experience slower mobility, on the millisecond to microsecond time scale, which results in broadening of their resonances due to chemical exchange processes. For the EGCII-**6** complex, additional peaks with more spectral dispersion are observed, suggesting rigidification of regions of the enzyme. The effect of these conformational changes on the solvent-accessible hydrophobic surface of EGCII was monitored by ANSA, as an extrinsic fluorescence probe, which interacts with the exposed hydrophobic areas of the protein. The results show an 8-fold decrease in exposed protein hydrophobicity between the enzyme in the free form and that bound to compound **6**, as determined from the changes in ANSA fluorescence curve slopes (**Figure 2.8c**). The change in the accessible hydrophobic surface is accompanied by a shift in the protein equilibrium between the dimeric and monomeric state toward the monomeric state, as demonstrated by the single elution peak in SEC (**Figure 2.8d**). This suggests that the dimerization is due to intermolecular interactions between the exposed hydrophobic surfaces of the protein. Additionally, the effect of complex formation on EGCII flexibility was tested by trypsin digestion at 25 and 37 °C. At 25 °C, the EGCII-**6** complex is more resistant to proteolytic activity, compared to the protein free state, as shown by SDS-PAGE (**Figure 2.9a**). At 37 °C, the protein is still digested into two bands. However, these two bands persist during the incubation time (**Figure 2.9c**), contrary to what was observed for the free protein. This latter peptic profile resembles that seen in the free state at 25 °C. The peptic fragments were analyzed by Western blotting with an anti-His tag antibody against the C-terminal histidine tag of EGCII. The blot confirms that the lower band contains the C-terminal fragment of the protein (**Figure 2.9b**). The same peptic pattern is observed when the protein is labeled with activity-based probe **9**. The lower band is the part of the protein that contains covalently bound ABP **9**, presumably to the nucleophile Glu351 (**Figure 2.9d**). To investigate the EGCII-**6** complex peptic fragment, the trypsin-cleaved

and uncleaved EGCII samples were analyzed by SEC. Their chromatograms show the same elution volume for a single peak, and also single bands are observed via native gel electrophoresis (**Figure 2.9e,f**). These observations support the conclusion that after digestion the two protein fragments stick together forming a strong noncovalent complex. On SDS-PAGE, two bands were observed due to the dissociation of the complex under the denaturing conditions (**Figure 2.9f**). Therefore, it could be speculated that the hydrophobic interaction between the two nicked fragments is the main force that keeps the complex together. This hydrophobic interaction is likely enhanced by the aliphatic tail of the irreversible inhibitors. On the basis of these observations, it can be concluded that in its complexed state EGCII experiences pronounced conformational changes, as seen from its ^1H - ^{15}N HSQC-TROSY spectrum and the measured accessible hydrophobic solvent. Additionally, an increase in trypsin resistance was observed, although the trypsin cleavage site remains accessible. This conformation of the protein may represent a closed and rigid state that could be stabilized by the hydrophobic interaction between the aliphatic tail of the irreversible inhibitor and the hydrophobic part of the substrate binding site.

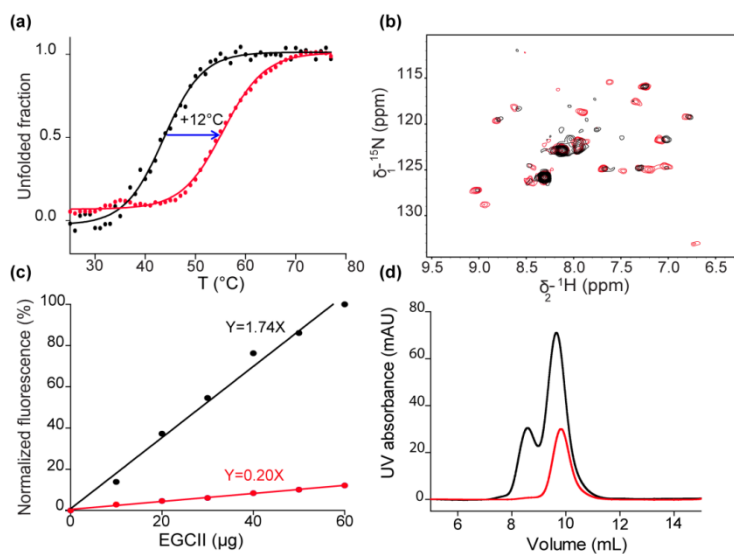


Figure 2.8. Effects of compound 6 on EGCII structure and thermal stability. **(a)** Thermal denaturation at pH 5.5 monitored by CD spectroscopy with a heating rate of 1 °C/min. The fitted apparent T_m values of the EGCII free state (black) and the EGCII-6 complex (red) were 43 and 55 °C, respectively. **(b)** ^{15}N - ^1H TROSY spectra of [^{15}N]-Leu-labeled EGCII in the free (black) and bound (red) states. **(c)** Relative solvent-accessible hydrophobic surface of EGCII free (black) and bound (red) states, determined by ANSA fluorescence. The lines represent a linear fit through the origin with the indicated fitted slopes. **(d)** Size exclusion chromatograms of EGCII free (black) and covalently bound (red) states.

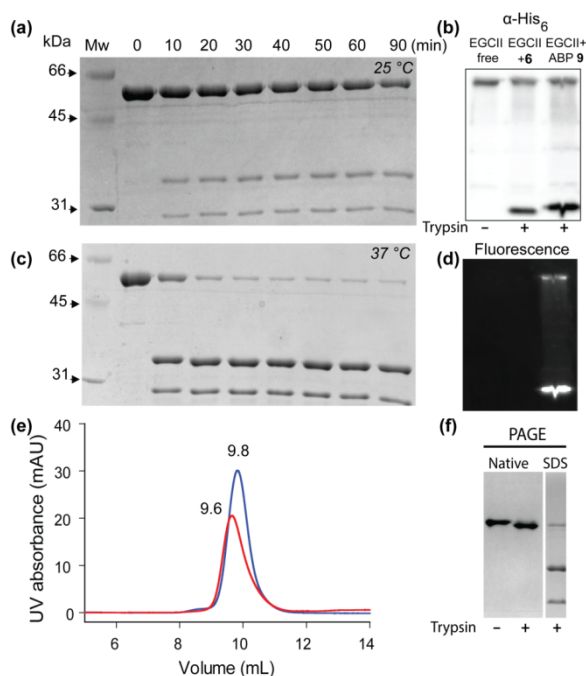


Figure 2.9. Rigidification of EGCI by compound **6**. EGCI-**6** complex peptic fragment pattern at 25 °C (a) and 37 °C (c) on 10% SDS–PAGE. (b) Anti- histidine tag Western blot membrane of digested EGCI in its free state and bound to compound **6** or ABP **9**. (d) Fluorescence image (Cy3) of the anti- histidine tag blot showing the fluorescence of ABP. (e) Size exclusion chromatograms of trypsin-treated (red) and untreated (blue) EGCI-**6** complex. The elution volumes of the peaks are indicated. (f) Untreated EGCI-**6** complex and EGCI-**6** treated with trypsin analyzed under native and denaturing electrophoresis conditions.

Correlation between EGCI stabilization and the lipophilic potential of cyclophellitols

A series of cyclophellitol aziridines *N*-alkylated or *N*-acylated with different lipophilic moieties (**Figure 2.10a**) were screened and the effects on EGCI melting temperature monitored by CD. Compounds **1** and **2** have no effect on the EGCI apparent T_m , in contrast to compounds **4-8**, for which an increase in the apparent T_m was observed with a maximal shift of 14.5 °C obtained with compound **8**, containing an adamantane moiety (**Figure 2.10b**). A correlation between the molecular lipophilic potential of the compounds and the increase in EGCI melting temperature is observed. This correlation can be explained by the more compact and rigid conformation adopted by the protein upon the interaction with the cyclophellitol aliphatic tags. Next, the solvent-accessible hydrophobic surfaces (SAHSs) of EGCI-cyclophellitol/cyclophellitol aziridine complexes were measured by ANSA (**Figure 2.10c**), and a decrease in EGCI SAHS was observed with an increase in inactivator lipophilicity. To highlight this correlation, the SAHS of the complexes is plotted against the theoretical “log *P*” of the compounds (**Figure 2.10d**). The plot suggests that with an increasing tag hydrophobicity, the protein

CHAPTER 2

adopts a more closed and compact conformation. An exception is observed for compound **3**, which could be due to its bulky aromatic ring that may cause steric hindrance in the narrow hydrophobic channel of the substrate binding pocket. On the basis of these results, it is concluded that the shape and length of the aliphatic tail, and therefore its molecular lipophilic potential, are key factors for rigidification and stabilization of EGCII.

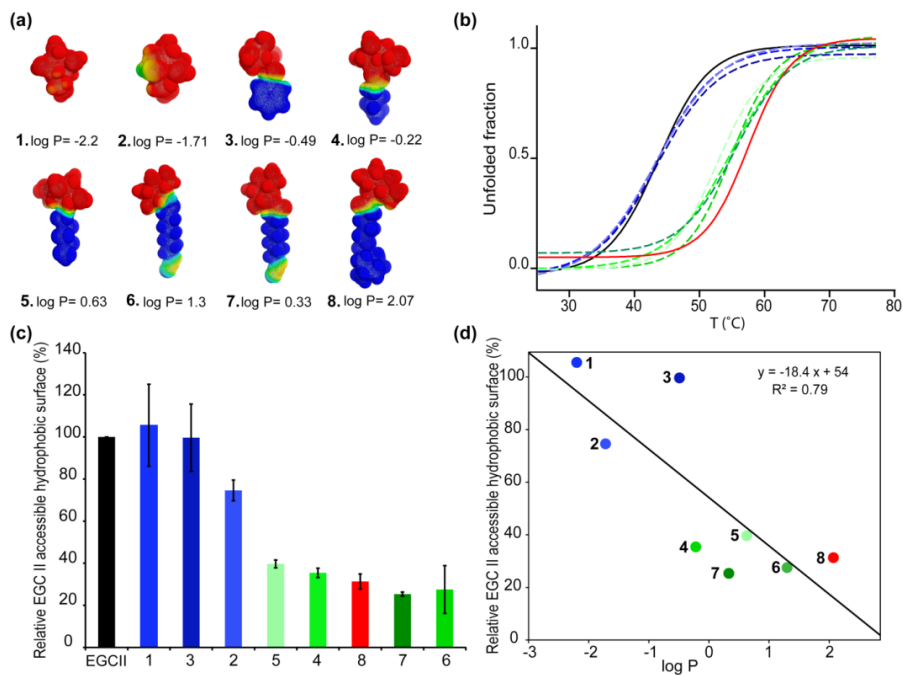


Figure 2.10. EGCII-cyclophellitol-aziridine derivative complexes. **(a)** Molecular lipophilic potential of cyclophellitol-aziridine derivatives as visualized using MLP Tools, a PyMOL plugin⁶⁰. **(b)** Fits of thermal denaturation curves of the different EGCII compound complexes, monitored by circular dichroism at pH 5.5 (the colors agree with those in panels c and d, and experimental data points were omitted for the sake of clarity). **(c)** Effect of the tested compounds on the relative EGCII solvent-accessible hydrophobic surface monitored by ANSA fluorescence. **(d)** Correlation between the calculated log P of the different tested compounds and the relative solvent-accessible hydrophobic surface of EGCII compound complexes. The free EGCII solvent-accessible hydrophobic surface was set to 100%.

Discussion

The interaction of a ligand binding protein with its cognate substrate usually induces changes in the protein thermal stability, resulting in a shift of the observed melting temperature (T_m). This phenomenon is widely exploited as a tool to identify potential binders for scientific and medicinal applications^{24,25}. For instance, this approach found successful application in the identification of target inhibitors in drug screening and for decrypting unknown protein functions. As an illustrative example, ligand-induced protein stabilization was used to identify inhibitors against human serine/threonine kinases. It was found that compounds that enhanced protein thermostability have a higher inhibition activity²⁶. Another example is the elucidation of a protein function of an essential gene from *Streptococcus pneumoniae* using a thermofluor screening assay²⁷. A library of 3000 compounds was screened against the unknown functional protein, and two hits were found to increase the protein thermal stability by 25 and 5 °C. The shifts of the protein melting temperature correlated with the ligand dissociation constant (K_d values of ≈ 50 pM and ≈ 2.5 μ M, respectively). The protein was identified as a nucleoside diphospho-keto-sugar aminotransferase²⁷. Ligand-induced protein stabilization can also be attained by changes of the protein conformational flexibility²⁸⁻³⁰. By studying the interaction between ANSA derivatives and BSA, Celej and co-workers found that binding of ligand to the protein induces an increase in protein conformational rigidity that correlates with thermostability³⁰. Rigidification upon ligand binding is used to screen for small compounds that assist protein refolding and prevent their aggregation³¹ or for specific active site binders that stabilize the folded state of a protein and improve its functionality³². The latter compounds are called pharmacological chaperones and have potential application in drug discovery for rescuing protein activity in several misfolding diseases³³⁻³⁶. As a representative example, a deficiency of GBA activity represents the etiology of Gaucher disease, the most common lysosomal storage disorder³⁷. This deficiency can be due to various point mutations, destabilizing the protein fold and disrupting cellular trafficking. It has been reported that active site binders restore to some extent the activity of lysosomal retaining β -glucosidase GBA mutants by stabilizing the folded conformation of the protein. For instance, IFG increased GBA thermal stability at neutral pH by 8.7 °C and improved protein trafficking of the N370S GBA mutant, resulting in an increase in GBA cellular levels in Gaucher patient tissues, including brain³⁸. Additionally, oral administration of IFG increased GBA L444P mutant activity in mice up to 5-fold⁷. Several lipophilic IFG derivatives proved to have a higher affinity and chaperoning activity toward GBA mutants³⁹⁻⁴². In connection to these findings, irreversible inhibitor cyclophellitol and its aziridine derivatives were also found to be effective mechanism-based ligands against retaining β -glucosidases⁴³⁻⁴⁵; therefore, they were used to study the kinetics and structural basis of β -glucosidase inhibition⁴⁶. In the

CHAPTER 2

work presented here, on the basis of the similarity of the structural topology between β -glucosidases GBA and EGCII as well as of their target of catalysis, the β -glucosidic linkage in glucosylceramide, it was speculated that cyclophellitol derivatives binding covalently to the catalytic nucleophile of GBA might also react with EGCII. The observation that EGCII is indeed irreversibly inhibited by cyclophellitol derivatives opened new possibilities for research on the enzyme. The factors influencing the conformational stability of EGCII were investigated with several biophysical and biochemical techniques, with emphasis on the effect of occupancy of the active site by cyclophellitols. This investigation led to a number of findings warranting further discussion. The thermostability study of EGCII by circular dichroism indicated that the protein has an apparent midpoint of the unfolding transition of 42 °C with an irreversible unfolding process, forming an aggregate as a final state. The isothermal denaturation of EGCII at 37 °C, which represents its optimal catalytic temperature, shows that the protein has a short half-life of 10 min, unlike what was observed at 25 °C where the protein shows a remarkable kinetic stability. These findings differ from those reported by Ito and co-workers. They found that the protein has a thermal stability of 60 min at 37 °C at the same pH¹. An explanation for this discrepancy is presently not available; the buffer conditions were not reported, so they may have deviated from the ones used here. The noted thermolability of EGCII could stem from its 3D structure containing several flexible regions without a well-packed hydrophobic core¹⁹. Analysis of EGCII flexibility in solution by proteolysis shows that the protein is susceptible to trypsin and has a major cleavage site localized in an α -helix in the crystal structure. It has been reported that protease cleavage sites for a variety of proteins of known 3D structure never occur in α -helices, but largely in loops⁴⁷. Therefore, it is speculated that this region in solution is either highly flexible or locally disordered. In the presence of detergents, this cleavage site becomes inaccessible to the trypsin and adopts a more structured conformation, as observed in the crystal structure of the protein. This local conformational flexibility, in combination with the high positive charge in this region, could play a crucial role in membrane association of EGCII, required to exert its enzymatic activity toward glycosphingolipids. The fact that EGCII processes a wide range of substrates²⁴, which requires a high flexibility and plasticity of the substrate binding site, may also explain its flexible behavior in solution. Protein flexibility may also be important in protein-protein complex formation. EGCII has an activator of 69 kDa that increases the catalytic activity of the enzyme against gangliosides in the absence of detergents under *in vitro* conditions⁴⁸. It could be that protein flexibility is necessary for protein-activator complex formation via an induced-fit mechanism. EGCII has a typical TIM (triose-phosphate isomerase) barrel folding pattern with a $(\beta/\alpha)_8$ N-terminal domain and a β -sheet C-terminal domain²⁷. The function of the β -sheet domain is unclear, even though it is highly conserved in different families of retaining β -glucosidases. The attempt to express only the catalytic domain to no avail, and all of the produced protein was found in inclusion bodies. This observation,

CHAPTER 2

combined with the high flexibility of the catalytic domain, supports the hypothesis that this domain not only is necessary for the stability of the catalytic domain but also may play a crucial role as an internal chaperone to guide the folding of the catalytic domain. The dramatic stabilization and rigidification of EGCII upon complex formation with the irreversible inhibitors are caused by the hydrophobic interaction with their aliphatic tail. A correlation between the molecular lipophilic potential of the tested compounds and the decrease in the solvent-accessible hydrophobic surface was observed. When accommodated into the enzyme binding pocket, the hydrophobic moieties of the compound appear to function as a “hydrophobic zipper”. This interaction makes the protein more rigid but with the preservation of the trypsin cleavage site. After cleavage, the two fragments were shown to stay together in a noncovalent complex, mediated by the hydrophobic interactions with the aliphatic tail of the irreversible inhibitor. A similar mechanism of binding pocket occupancy effects was observed for the complex between renin, an aspartic protease playing a key physiological role in the regulation of blood pressure, and a nonpeptidomimetic inhibitor, showing dramatic structural changes in renin. In this case, a movement of protein flexible loops of the binding pocket was observed and further changes in the protein around the bulky lipophilic substitutes of the inhibitors were seen. The lipophilic substitutes and hydrophobic side chains in renin act to form a new compact hydrophobic region within the protein⁴⁹. A stabilization and rigidification effect was also observed in the case of the covalent modification of the β -(1-4)-glycosidase Cex catalytic domain, from the soil bacterium *Cellulomonas fimi*, with the mechanism-based inhibitors 2,4-dinitrophenyl 2-deoxy-2-fluoro- β -cellobioside. The free state of the Cex catalytic domain was markedly stabilized upon formation of the glycosyl-enzyme intermediate with an increase in its T_m of 10.5 °C. This protein stabilization was accompanied by a distinct thermolysin proteolytic resistance, with no proteolysis of the glycosyl-enzyme complex occurring, even after incubation for 50 h at 50 °C⁵⁰.

Conclusion

In conclusion, EGCII was used as a research model to investigate the effects of occupancy of the active site by cyclophellitol analogues with variable lipophilic potential. The hydrophobic interaction plays a decisive role in the protein-inhibitor complex, promoting rigidification of the protein and conformational stability. In theory, endoglycoceramidases could be employed to treat a number of inherited glycosphingolipidoses caused by deficiency in a lysosomal exoglycosidase. Insight into factors influencing the conformational stability of endoglycoceramidases is one important prerequisite for their design as successful therapeutic agents.

Experimental procedures

General synthesis

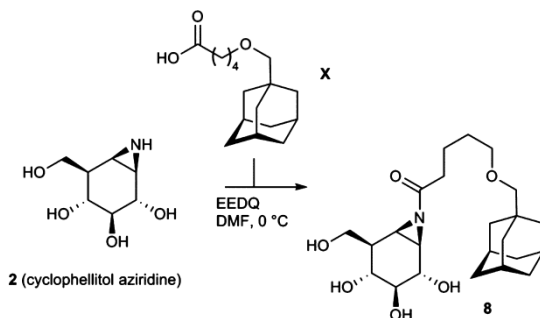
All reagents and solvents were of commercial grade and used as received unless stated otherwise. Tetrahydrofuran and dichloromethane were stored over flamedried 3 Å molecular sieves. All reactions were performed under an inert atmosphere unless stated otherwise. Solvents used for flash chromatography were of pro analysis quality. Reactions were monitored by TLC analysis using aluminum sheets precoated with silica gel 60 with detection by UV absorption (254 nm) and by spraying with a solution of $(\text{NH}_4)_6\text{Mo}_7\text{O}_{24} \cdot \text{H}_2\text{O}$ (25 g/L) and $(\text{NH}_4)_4\text{Ce}(\text{SO}_4)_4 \cdot \text{H}_2\text{O}$ (10 g/L) in 10% sulfuric acid, followed by charring at ~ 150 °C or by spraying with 20% sulfuric acid in ethanol followed by charring at ~ 150 °C. Column chromatography was performed using Screening Device silica gel in the indicated solvents. ^1H -nuclear magnetic resonance (NMR), ^{13}C NMR, COSY, and HSQC spectra were recorded on Bruker DMX-400 (400/100 MHz), Bruker AV-400 (400/100 MHz), and Bruker AVIII-600 (600/150 MHz) spectrometers in the given solvent. Chemical shifts are reported as δ values in parts per million relative to the chloroform residual solvent peak, tetramethylsilane (TMS) as an internal standard, or the deuterated solvent signal for CD_3OD . All given ^{13}C spectra were proton-decoupled. High-resolution mass spectra were recorded with an LTQ Orbitrap instrument (ThermoFinnigan). LC/MS analysis was performed on an LCQ Advantage Max (ThermoFinnigan) ion trap spectrometer (ESI+) coupled to a Surveyor high-performance liquid chromatography (HPLC) system (ThermoFinnigan) equipped with a C18 column (Gemini, 4.6 mm \times 50 mm, 3 μm particle size, Phenomenex) using buffers A (H_2O), B (acetonitrile in MeCN), and C (50mM NH_4OAc). For reverse phase HPLC purifications, an Agilent Technologies 1200 series instrument equipped with a semi preparative Gemini C18 column (10 mm \times 250 mm) was used. The applied buffers were 50 mM NH_4HCO_3 in H_2O (buffer A) and MeCN (buffer B). Compound **6** was synthesized according to a published report⁵¹. Compounds **1-5** and **7** and cyclophellitol-aziridine ABP **9** were prepared as described previously⁵².

Synthesis of compound 8

N-Ethoxycarbonyl-2-ethoxy-1,2-dihydroquinoline (EEDQ) (79 mg, 0.32 mmol) and 6-*O*-adamantanemethyl-6-hydroxyhexanoic acid X (85 mg, 0.32 mmol) were dissolved in anhydrous DMF (0.32 mL) and stirred at room temperature for 2 h (**Scheme 2.1**). The resulting dissolved mixed anhydride (160 μL) was added to cyclophellitol-aziridine **2**¹⁷ (35 mg, 0.2 mmol) in dry DMF (1.2 mL) at 0 °C and stirred for 30 min. At this time, an additional batch of mixed anhydride (160 μL) was added. The resulting mixture was stirred at 0 °C for 2 h. The reaction was quenched with MeOH (1 mL), and the mixture

was concentrated *in vacuo*. Then the crude product was purified by semipreparative reverse HPLC [linear gradient from 38 to 47% B in A, 12 min; solutions used, H₂O (A) and MeCN (B)], and the fractions were lyophilized yielding **8** as white powder (21 mg, 0.05 mmol, 25% yield): ¹H NMR (400 MHz, MeOD) δ 4.09 (d, J = 10.4, 4.4 Hz, 2H), 3.72–3.66 (m, 2H), 3.414 (t, J = 6.4 Hz, 2H), 3.23 (dd, J = 10.0, 8.0 Hz, 1H), 3.10–3.02 (m, 2H), 2.74 (d, J = 5.6 Hz, 1H), 2.55–2.51 (m, 2H), 2.01–1.95 (m, 4H), 1.77–1.66 (m, 8H); 1.64–1.56 (m, 8H); ¹³C NMR (100 MHz, MeOD) δ 188.5, 83.0, 79.1, 73.4, 72.2, 69.4, 63.6, 45.3, 42.4, 41.1, 40.8, 38.3, 36.6, 35.2, 30.1, 29.9, 29.8, 22.9; LC/MS t_R 7.87 min (linear gradient from 10 to 90% B in 15 min); ESI-MS m/z 424.4 (M + H)⁺; HRMS calcd for C₁₄H₁₇NO₄ (M + H)⁺ 424.26936, found 424.26921.

Scheme 2.1. Synthesis of Compound **8**



Production and purification of recombinant EGCII

The gene encoding EGCII from *Rhodococcus* sp. strain M777 lacking the N-terminal signal peptide sequence was subcloned into pET21a using NdeI/NotI restriction sites, introducing a C-terminal His tag. *Escherichia coli* BL21(DE3) pLysS cells were transformed with the obtained vector and cultured at 37 °C in lysogeny broth containing 50 μ g/mL ampicillin and 30 μ g/mL chloramphenicol. Gene expression was induced with 0.5 mM isopropyl β -D-1-thiogalactopyranoside (IPTG) when the culture reached an OD₆₀₀ of \approx 0.6, and the incubation was continued overnight at 20 °C. The cells were harvested by centrifugation, resuspended in extraction buffer [20 mM Tris-HCl, 150 mM NaCl, and 20 mM imidazole (pH 7.6)], and sonicated. The resulting EGCII 6-His supernatant was further purified by Ni(II) affinity chromatography to > 95%, as determined by sodium dodecyl sulfate-polyacrylamide gel electrophoresis (SDS-PAGE). All the purification steps were conducted at 4 °C. [¹⁵N]-Leucine isotope selective labeling of EGCII was started by culturing the transformed *E. coli* BL21(DE3) in a 50 mL culture in M9 medium overnight at 37 °C, supplemented with each amino acid (at 0.1 g/L) except leucine, as well as 125 mg/L adenosine, 125 mg/L guanosine, 125 mg/L cytosine, 50 mg/L thymine, 50 mg/L uracil, 50 mg/L nicotinic acid, and 2 g/L succinic acid. The next day, 0.5 L of this medium was inoculated with the overnight preculture and incubated at 37 °C until the OD₆₀₀ reached \approx 0.6. Fifteen minutes before induction, a mixture of 0.5 g of each unlabeled amino acid except leucine and 50 mg of [¹⁵N]-Leucine were added to the culture⁵³. Protein production was started by inducing gene expression with 0.5 mM

IPTG, and the culture was continued overnight at 20 °C. The purification procedure was as described above.

NMR spectroscopy

Two-dimensional ^{15}N - ^1H TROSY⁵⁴ spectra were recorded at 298 K on a Bruker Avance III HD 850 MHz spectrometer equipped with a TCI-Z-GRAD cryoprobe on a sample of 150-200 μM [^{15}N]-Leu EGCII in McIlvaine's buffer [110 mM Na_2HPO_4 and 40 mM citric acid (pH 5.5)] and 6% D_2O . Data were processed with Topspin (Bruker Biospin) and analyzed using the Sparky software package⁵⁵.

EGCII activity assay and cyclophellitol complex formation

The enzymatic activity of the purified enzyme was measured in the presence of the substrate 4-methylumbelliferyl- β -D-lactopyranoside (4MU-Lac) (Marker Gene Technologies, Inc.). The enzyme (153 nM) was incubated with different concentrations of 4MU-Lac for 1 h at 37 °C in McIlvaine's (citrate/phosphate) buffer and 0.1% BSA. The reaction was quenched by adding 2.5 mL of a 0.3 M glycine solution (pH 10.6). The reaction rates were monitored by measuring the fluorescence of the released 4MU at its emission wavelength of 445 nm on an LS55 fluorimeter. For each enzymatic reaction, a blank was used, in the absence of EGCII, to measure the spontaneous hydrolysis of 4MU-Lac, and this rate was subtracted from the enzymatically catalyzed reaction rate. For covalent complex formation, EGCII and the irreversible inhibitors were incubated at a ratio of 1:30 in McIlvaine's buffer for 3 h at 25 °C. Thereafter, the samples were incubated for 1 h at 37 °C as a final step to promote complex formation and to discard aggregated protein. The samples were centrifuged for 30 min at 16000g, and the excess of inhibitor was removed by buffer exchange. The samples were kept at 4 °C for further experiments.

Circular dichroism (CD) spectroscopy

The far-UV region (200–280 nm) CD spectra were recorded in a 0.1 cm path length quartz cuvette in a Jasco 810 CD spectrometer using a 5 μM protein solution. The spectra were recorded using four scans with a bandwidth and a wavelength step of 1 nm. The obtained spectra were background corrected and smoothed using Jasco Spectra Manager. The unfolding transition point (T_m) was measured by following the dichroic signal decay at 222 nm, by applying heating rates from 1 to 5 °C/min, over a temperature gradient from 20 to 80 °C in McIlvaine's buffer. The obtained CD ellipticity at each point (θ_i) was assumed to be the linear combination of the folded (θ_F) and unfolded (θ_U) ellipticity. At each point of the melting curve, the unfolded fraction was calculated using the formula $f_U = (\theta_i - \theta_F) / (\theta_U - \theta_F)$. The unfolding transition curves were plotted and fitted using GraphPad Prism, and the T_m was extracted from the obtained fits as the temperature for which $f_U = 0.5$.

Limited proteolysis

Proteolysis of free EGCII and EGCII complexes was conducted at 25 or 37 °C using a trypsin: EGCII ratio of 1:100 (by weight) in the absence and the presence of 1% Triton X-100 and lauryl glucoside. A time course analysis of the proteolytic events was conducted using SDS-PAGE, and the peptic fragments were further analyzed by in-gel

digestion LC-MS on a Thermo LTQ-orbitrap mass spectrometer following the described protocol⁵⁶. To analyze the mass of the produced EGCII tryptic fragments, the proteolytic reaction was quenched by adding phenylmethanesulfonyl fluoride (PMSF) after incubation for 10 min and analyzed on a SYNAPT G2-Si mass spectrometer (Waters).

EGCII solvent-accessible hydrophobic surface determination by 8-anilino-1-naphthalenesulfonic acid (ANSA)

Protein surface hydrophobicity was determined using ANSA according to the method described by Kato and Nakai⁵⁷. A stock solution of 10 mM ANSA was prepared in McIlvaine's buffer. A variable amount of EGCII or EGCII-inactivator complex was mixed with a 2 mM ANSA solution. The mixture was incubated for 30 min in the dark at room temperature. The fluorescence was measured using an LS55 fluorimeter. The excitation and emission slits were both 5 nm, and the excitation and emission wavelengths were set at and 366 and 490 nm, respectively. The fluorescence of a blank solution was subtracted from each protein sample. The slope of the net fluorescence intensity (percent) plotted versus the protein concentration was calculated by linear regression analysis with GraphPad Prism and used as an index of the protein surface hydrophobicity.

Size exclusion chromatography and multiangle laser light scattering

Size exclusion chromatography in conjunction with multiangle laser light scattering (SEC-MALLS) was used to determine the absolute molecular mass of EGCII samples. EGCII (1 mg/mL) in 20 mM Tris-HCl (pH 7.6) or McIlvaine's buffer was injected into the column. The refractive index and multiangle light scattering were measured simultaneously as the solute eluted from the size exclusion column. The concentration of the solute was determined from the refractive index, the excess Rayleigh scattering from the light scattering. These two parameters were entered into the Rayleigh-Gans-Debye approximation to determine the molar mass of the solute using SEC-MALLS Astra 473 software manager⁵⁸.

References

1. Ito, M., and Yamagata, T. (1986) A novel glycosphingolipid-degrading enzyme cleaves of the linkage between the oligosaccharide and ceramide of neutral and acidic glycosphingolipids. *J. Biol. Chem.* 261, 14278–14282.
2. Li, S.-C., Degasperis, R., Muldrey, J. E., and Li, Y.-T. (1986) A unique glycosphingolipid-splitting enzyme (ceramide-glycanase from leech) cleaves the linkage between the oligosaccharide and the ceramide. *Biochem. Biophys. Res. Commun.* 141, 346–352.
3. Li, Y.-T., Ishikawa, Y., and Li, S.-C. (1987) Occurrence of ceramide-glycanase in the earthworm, *Lumbricusterrestris*. *Biochem. Biophys. Res. Commun.* 149, 167–172.
4. Basu, M., Dastgheib, S., Girzadas, M. A., O'Donnell, P. H., Westervelt, C. W., Li, Z. X., Inokuchi, J., and Basu, S. (1998) Hydrophobic nature of mammalian ceramide glycanases: Purified from rabbit and rat mammary tissues. *Acta Biochim. Polym.* 45, 327–342.
5. Basu, M., Kelly, P., Odonell, P., Miguel, M., and Basu, S. (1998) Ceramide glycanase activities in human cancer cells. *Glycobiology* 8, 1129–1129.
6. Lieberman, R. L., Wustman, B. A., Huertas, P., Powe, A. C., Pine, C. W., Khanna, R., Schlossmacher, M. G., Ringe, D., and Petsko, G. A. (2007) Structure of acid [β]-glucosidase with pharmacological chaperone provides insight into Gaucher disease. *Nat. Chem. Biol.* 3, 101–107.
7. Khanna, R., Benjamin, E. R., Pellegrino, L., Schilling, A., Rigat, B. A., Soska, R., Nafar, H., Ranes, B. E., Feng, J., Lun, Y., Powe, A. C., Palling, D. J., Wustman, B. A., Schiffmann, R., Mahuran, D. J., Lockhart, D. J., and Valenzano, K. J. (2010) The pharmacological chaperone isofagomine increases the activity of the Gaucher disease L444P mutant form of β -glucosidase. *FEBS J.* 277, 1618–1638.
8. Koshland, D. E. (1953) Stereochemistry and the mechanism of enzymatic reactions. *Biol. Rev. Camb. Philos. Soc.* 28, 416–436.
9. Davies, G. J., Planas, A., and Rovira, C. (2012) Conformational Analyses of the Reaction Coordinate of Glycosidases. *Acc. Chem. Res.* 45, 308–316.
10. Atsumi, S., Umezawa, K., Iinuma, H., Naganawa, H., Nakamura, H., Iitaka, Y., and Takeuchi, T. (1990) Production, isolation and structure determination of a novel beta-glucosidase inhibitor, cyclo-phellitol, from *phellinus* sp. *J. Antibiot.* 43, 49–53.
11. Witte, M. D., Kallemeijn, W. W., Aten, J., Li, K.-Y., Strijland, A., Donker-Koopman, W. E., van den Nieuwendijk, A. M. C. H., Bleijlevens, B., Kramer, G., Florea, B. I., Hooibrink, B., Hollak, C. E. M., Ottenhoff, R., Boot, R. G., van der Marel, G. A., Overkleef, H. S., and Aerts, J. M. F. G. (2010) Ultrasensitive in situ visualization of active glucocerebrosidase molecules. *Nat. Chem. Biol.* 6, 907–913.
12. Li, K.-Y., Jiang, J., Witte, M. D., Kallemeijn, W. W., Donker-Koopman, W. E., Boot, R. G., Aerts, J. M. F. G., Codee, J. D. C., van der Marel, G. A., and Overkleef, H. S. (2014) Exploring functional cyclophellitol analogues as human retaining β -glucosidase inhibitors. *Org. Biomol. Chem.* 12, 7786–7791.
13. Kallemeijn, W. W., Li, K.-Y., Witte, M. D., Marques, A. R. A., Aten, J., Scheij, S., Jiang, J., Willems, L. I., Voorn-Brouwer, T. M., van Roomen, C. P. A. A., Ottenhoff, R., Boot, R. G., van den Elst, H., Walvoort, M. T. C., Florea, B. I., Codee, J. D. C., van der Marel, G. A., Aerts, J. M. F. G., and Overkleef, H. S. (2012) Novel Activity-Based Probes for Broad-Spectrum Profiling of Retaining beta-Exoglucosidases In Situ and In Vivo. *Angew. Chem., Int. Ed.* 51, 12529–12533.
14. Grabowski, G. A., Osiecki-Newman, K., Dinur, T., Fabbro, D., Legler, G., Gatt, S., and Desnick, R. J. (1986) Human acid β -glucosidase. Use of conduritol B epoxide derivatives to investigate the catalytically active normal and Gaucher disease enzymes. *J. Biol. Chem.* 261, 8263–8269. Brumshtein, B., Greenblatt, H. M., Butters, T. D., Shaaltiel, Y.,
15. Aviezer, D., Silman, I., Futerman, A. H., and Sussman, J. L. (2007) Crystal Structures of Complexes of N-Butyl- and N-Nonyl-Deoxyojir-imycin Bound to Acid β -Glucosidase: Insights into the mechanism of chemical chaperone action in gaucher disease. *J. Biol. Chem.* 282, 29052–29058.
16. Ito, M., and Yamagata, T. (1989) Purification and characterization of glycosphingolipid-specific endoglycosidases (endoglycoceramidas) from a mutant strain of *rhodococcus* sp evidence for 3 molecular-species of endoglycoceramidase with different specificities. *J. Biol. Chem.* 264, 9510–9519.
17. Hubbard, S. J., Eisenmenger, F., and Thornton, J. M. (1994) Modelling studies of the change in conformation required for cleavage of limited proteolytic sites. *Protein Sci.* 3, 757–768.
18. Zhang, N., and Li, L. (2004) Effects of common surfactants on protein digestion and matrix-assisted laser desorption/ionization mass spectrometric analysis of the digested peptides using two-layer sample preparation. *Rapid Commun. Mass Spectrom.* 18, 889–896.

CHAPTER 2

19. Caines, M. E. C., Vaughan, M. D., Tarling, C. A., Hancock, S. M., Warren, R. A. J., Withers, S. G., and Strynadka, N. C. J. (2007) Structural and mechanistic analyses of endo-glycosylceramidase II, a membrane-associated family 5 glycosidase in the Apo and GM3 ganglioside-bound forms. *J. Biol. Chem.* 282, 14300–14308.
20. Corbett, R. J. T., and Roche, R. S. (1984) Use of high-speed size-exclusion chromatography for the study of protein folding and stability. *Biochemistry* 23, 1888–1894.
21. Uversky, V. N., and Pitsyn, O. B. (1994) Partly folded state, a new equilibrium state of protein molecules-4-state guanidinium chloride induced unfolding of beta-lactamase at low-temperature. *Biochemistry* 33, 2782–2791.
22. Zavodszky, P., Kardos, J., Svingor, A., and Petsko, G. A. (1998) Adjustment of conformational flexibility is a key event in the thermal adaptation of proteins. *Proc. Natl. Acad. Sci. U. S. A.* 95, 7406–7411.
23. Hajdu, I., Bothe, C., Szilagyí, A., Kardos, J., Gal, P., and Zavodszky, P. (2008) Adjustment of conformational flexibility of glyceraldehyde-3-phosphate dehydrogenase as a means of thermal adaptation and allosteric regulation. *Eur. Biophys. J.* 37, 1139–1144.
24. Thompson, P. A., Wang, S., Howett, L. J., Wang, M.-M., Patel, R., Averill, A., Showalter, R. E., Li, B., and Appleman, J. R. (2008) Identification of Ligand Binding by Protein Stabilization: Comparison of ATLAS with Biophysical and Enzymatic Methods. *Assay Drug Dev. Technol.* 6, 69–81.
25. Senisterra, G., Chau, I., and Vedadi, M. (2012) Thermal Denaturation Assays in Chemical Biology. *Assay Drug Dev. Technol.* 10, 128–136.
26. Fedorov, O., Marsden, B., Pogacic, V., Rellos, P., Müller, S., Bullock, A. N., Schwaller, J., Sundström, M., and Knapp, S. (2007) A systematic interaction map of validated kinase inhibitors with Ser/Thr kinases. *Proc. Natl. Acad. Sci. U. S. A.* 104, 20523–20528.
27. Carver, T. E., Bordeau, B., Cummings, M. D., Petrella, E. C., Pucci, M. J., Zawadzke, L. E., Dougherty, B. A., Tredup, J. A., Bryson, J. W., Yanchunas, J., Doyle, M. L., Witmer, M. R., Nelen, M. I., Desjarlais, R. L., Jaeger, E. P., Devine, H., Asel, E. D., Springer, B. A., Bone, R., Salemme, F. R., and Todd, M. J. (2005) Decrypting the Biochemical Function of an Essential Gene from *Streptococcus pneumoniae* Using Thermo-Fluor® Technology. *J. Biol. Chem.* 280, 11704–11712.
28. Teague, S. J. (2003) Implications of protein flexibility for drug discovery. *Nat. Rev. Drug Discovery* 2, 527–541.
29. Gonzalez, M., Bagatolli, L. A., Echabe, I., Arrondo, J. L. R., Argarana, C. E., Cantor, C. R., and Fidelio, G. D. (1997) Interaction of biotin with streptavidin - Thermostability and conformational changes upon binding. *J. Biol. Chem.* 272, 11288–11294.
30. Celej, M. S., Montich, C. G., and Fidelio, G. D. (2003) Protein stability induced by ligand binding correlates with changes in protein flexibility. *Protein Sci.* 12, 1496–1506.
31. Vedadi, M., Niesen, F. H., Allali-Hassani, A., Fedorov, O. Y., Finerty, P. J., Wasney, G. A., Yeung, R., Arrowsmith, C., Ball, L. J., Berglund, H., Hui, R., Marsden, B. D., Nordlund, P., Sundstrom, M., Weigelt, J., and Edwards, A. M. (2006) Chemical screening methods to identify ligands that promote protein stability, protein crystallization, and structure determination. *Proc. Natl. Acad. Sci. U. S. A.* 103, 15835–15840.
32. Andreotti, G., Monticelli, M., and Cubellis, M. V. (2015) Looking for protein stabilizing drugs with thermal shift assay. *Drug Test. Anal.* 7, 831–834.
33. Chaudhuri, T. K., and Paul, S. (2006) Protein-misfolding diseases and chaperone-based therapeutic approaches. *FEBS J.* 273, 1331–1349.
34. Andreotti, G., Citro, V., Correr, A., and Cubellis, M. V. (2014) A thermodynamic assay to test pharmacological chaperones for Fabry disease. *Biochim. Biophys. Acta, Gen. Subj.* 1840, 1214–1224.
35. Parenti, G., Fecarotta, S., Marca, G. I., Rossi, B., Ascione, S., Donati, M. A., Morandi, L. O., Ravaglia, S., Pichiecchio, A., Ombrone, D., Sacchini, M., Pasanisi, M. B., Filippi, P. D., Danesino, C., Della Casa, R., Romano, A., Mollica, C., Rosa, M., Agovino, T., Nusco, E., Porto, C., and Andria, G. (2014) A Chaperone Enhances Blood Alpha-Glucosidase Activity in Pompe Disease Patients Treated with Enzyme Replacement Therapy. *Mol. Ther.*, DOI: 10.1038/mt.2014.138.
36. Andreotti, G., Cabeza de Vaca, I., Poziello, A., Monti, M. C., Guallar, V., and Cubellis, M. V. (2014) Conformational Response to Ligand Binding in Phosphomannomutase2: Insights into inborn glycosylation disorder. *J. Biol. Chem.* 289, 34900–34910.
37. Jmoudiak, M., and Futerman, A. H. (2005) Gaucher disease: pathological mechanisms and modern management. *Br. J. Haematol.* 129, 178–188.
38. Lieberman, R. L., Wustman, B. A., Huertas, P., Powe, A. C., Pine, C. W., Khanna, R., Schlossmacher, M. G., Ringe, D., and Petsko, G. A. (2007) Structure of acid β -glucosidase with pharmacological chaperone provides insight into Gaucher disease. *Nat. Chem. Biol.* 3, 101–107.

CHAPTER 2

39. Sawkar, A. R., Cheng, W. C., Beutler, E., Wong, C. H., Balch, W. E., and Kelly, J. W. (2002) Chemical chaperones increase the cellular activity of N370S β -glucosidase: A therapeutic strategy for Gaucher disease. *Proc. Natl. Acad. Sci. U. S. A.* 99, 15428–15433.
40. Abian, O., Alfonso, P., Velazquez-Campoy, A., Giraldo, P., Poci, M., and Sancho, J. (2011) Therapeutic Strategies for Gaucher Disease: Miglustat (NB-DNJ) as a Pharmacological Chaperone for Glucocerebrosidase and the Different Thermostability of Velaglucerase Alfa and Imiglucerase. *Mol. Pharmaceutics* 8, 2390–2397.
41. Sawkar, A. R., Adamski-Werner, S. L., Cheng, W. C., Wong, C. H., Beutler, E., Zimmer, K. P., and Kelly, J. W. (2005) Gaucher disease-associated glucocerebrosidases show mutation-dependent chemical chaperoning profiles. *Chem. Biol.* 12, 1235–1244.
42. Tong, M. K., and Ganem, B. (1988) A potent new class of active-site-directed glycosidase inactivators. *J. Am. Chem. Soc.* 110, 312–313.
43. Caron, G., and Withers, S. G. (1989) Conduritol aziridine: A new mechanism-based glucosidase inactivator. *Biochem. Biophys. Res. Commun.* 163, 495–499.
44. Nakata, M., Chong, C., Niwata, Y., Toshima, K., and Tatsuta, K. (1993) A family of cyclophellitol analogs: Synthesis and evaluation. *J. Antibiot.* 46, 1919–1922.
45. Gloster, T. M., Madsen, R., and Davies, G. J. (2007) Structural basis for cyclophellitol inhibition of a β -glucosidase. *Org. Biomol. Chem.* 5, 444–446.
46. Kokkinidis, M., Glykos, N. M., and Fadoulglou, V. E. (2012) Protein flexibility and enzymatic catalysis. In *Advances in Protein Chemistry and Structural Biology* (Christov, C., and Karabencheva Christova, T., Eds.) Vol. 87, pp 181–218, Elsevier, Amsterdam. 10.1016/B978-0-12-398312-1.00007-X.
47. Fontana, A., Polverino de Lauro, P., DeFilippis, V., Scaramella, E., and Zamboni, M. (1997) Probing the partly folded states of proteins by limited proteolysis. *Folding Des.* 2, R17–R26.
48. Ito, M., Ikegami, Y., and Yamagata, T. (1991) Activator proteins for glycosphingolipid hydrolysis by endoglycoceramidase: Elucidation of biological functions of cell-surface glycosphingolipids *in situ* by endoglycoceramidase made possible using these activator proteins. *J. Biol. Chem.* 266, 7919–7926.
49. Oefner, C., Binggeli, A., Breu, V., Bur, D., Clozel, J. P., D'Arcy, A., Dorn, A., Fischli, W., Gruninger, F., Guller, R., Hirth, G., Marki, H. P., Mathews, S., Muller, M., Ridley, R. G., Stadler, H., Vieira, E., Wilhelm, M., Winkler, F. K., and Wostl, W. (1999) Renin inhibition by substituted piperidines: a novel paradigm for the inhibition of monomeric aspartic proteinases? *Chem. Biol.* 6, 127–131.
50. Poon, D. K. Y., Ludwiczek, M. L., Schubert, M., Kwan, E. M., Withers, S. G., and McIntosh, L. P. (2007) NMR spectroscopic characterization of a β -(1,4)-glycosidase along its reaction pathway: Stabilization upon formation of the glycosyl-enzyme intermediate. *Biochemistry* 46, 1759–1770.
51. Jiang, J., Beenakker, T. J. M., Kallemeijn, W. W., van der Marel, G. A., van den Elst, H., Codec, J. D. C., Aerts, J. M. F. G., and Overkleeft, H. S. (2015) Comparing Cyclophellitol N-Alkyl and N-Acyl Cyclophellitol Aziridines as Activity-Based Glycosidase Probes. *Chem. Eur. J.* 21, 10861–10869.
52. Li, K. Y., Jiang, J. B., Witte, M. D., Kallemeijn, W. W., van den Elst, H., Wong, C. S., Chander, S. D., Hoogendoorn, S., Beenakker, T. J. M., Codec, J. D. C., Aerts, J., van der Marel, G. A., and Overkleeft, H. S. (2014) Synthesis of Cyclophellitol, Cyclophellitol Aziridine, and Their Tagged Derivatives. *Eur. J. Org. Chem.* 2014, 6030–6043.
53. Senn, H., Eugster, A., Otting, G., Suter, F., and Wüthrich, K. (1987) ¹⁵N-labeled P22 c2 repressor for nuclear magnetic resonance studies of protein-DNA interactions. *Eur. Biophys. J.* 14, 301–306.
54. Pervushin, K., Riek, R., Wider, G., and Wüthrich, K. (1997) Attenuated T2 relaxation by mutual cancellation of dipole-dipole coupling and chemical shift anisotropy indicates an avenue to NMR structures of very large biological macromolecules in solution. *Proc. Natl. Acad. Sci. U. S. A.* 94, 12366–12371.
55. Goddard, T. D., and Kneller, D. G. (2007) SPARKY 3, University of California, San Francisco.
56. Shevchenko, A., Tomas, H., Havlis, J., Olsen, J. V., and Mann, M. (2007) In-gel digestion for mass spectrometric characterization of proteins and proteomes. *Nat. Protoc.* 1, 2856–2860.
57. Kato, A., and Nakai, S. (1980) Hydrophobicity determined by a fluorescence probe method and its correlation with surface-properties of proteins. *Biochim. Biophys. Acta, Protein Struct.* 624, 13–20.
58. Knobloch, J. E., and Shaklee, P. N. (1997) Absolute molecular weight distribution of low-molecular-weight heparins by size-exclusion chromatography with multiangle laser light scattering detection. *Anal. Biochem.* 245, 231–241.
59. Ye, Y., and Godzik, A. (2003) Flexible structure alignment by chaining aligned fragment pairs allowing twists. *Bioinformatics* 19, ii246–ii255.

CHAPTER 2

60. Oberhauser, N., Nurisso, A., and Carrupt, P.-A. (2014) MLP Tools: a PyMOL plugin for using the molecular lipophilicity potential in computer-aided drug design. *J. Comput.-Aided Mol. Des.* 28, 587–596.

CHAPTER 3

Stabilization of Glucocerebrosidase by Active Site Occupancy

Abstract

Gluocerebrosidase (GBA) is a lysosomal β -glucosidase that degrades glucosylceramide. Its deficiency results in Gaucher disease (GD). The effects of active site occupancy of GBA on its structural stability were examined. For this, cyclophellitol-derived activity-based probes (ABPs) that bind irreversibly to the catalytic nucleophile (E340) were used in conjunction with the potent reversible inhibitor isofagomine, for comparison. It is demonstrated that cyclophellitol ABPs improve the stability of GBA *in vitro*, as revealed by thermodynamic measurements (T_m increase by 21 °C), and introduce resistance to tryptic digestion. The stabilizing effect of cell-permeable cyclophellitol ABPs is also observed in intact cultured cells containing wild-type GBA, N370S GBA (labile in lysosomes), and L444P GBA (exhibits impaired ER folding): all show marked increases in lysosomal forms of GBA molecules upon exposure to ABPs. The same stabilization effect is observed for endogenous GBA in the liver of wild-type mice injected with cyclophellitol ABPs. Stabilization effects similar to those observed with ABPs were also noted at high concentrations of the reversible inhibitor isofagomine. In conclusion, evidence is provided that the increase in cellular levels of GBA by ABPs and by the reversible inhibitor is in part caused by their ability to stabilize GBA folding, which increases the resistance of GBA against breakdown by lysosomal proteases. These effects are more pronounced in the case of the amphiphilic ABPs, presumably due to their high lipophilic potential, which may promote further structural compactness of GBA through hydrophobic interactions. This study provides further rationale for the design of chaperones for GBA to ameliorate Gaucher disease.

This work was published as: Ben Bdira, F., et al., Stabilization of Glucocerebrosidase by Active Site Occupancy. *ACS Chemical Biology*, 2017. **12**(7): p. 1830-1841.

All of the cell biology studies were conducted by: Kallemeijn, W. W., Oussoren, S. V., Scheij, S., Bleijlevens, B., Florea, B. I., van Roomen, C. P. A. A., Ottenhoff, R., van Kooten, M. J. F. M., Walvoort, M. T. C., Witte, M. D., Boot, R. G. at the Department of Medical Biochemistry Academic Medical Center, University of Amsterdam, Amsterdam (The Netherlands).

Introduction

Lysosomal β -glucosidase glucocerebrosidase (GBA) cleaves glucosylceramide, an essential step in the turnover of cellular glycosphingolipids^{1,2}. GBA is co-translationally translocated into the ER, where it acquires four N-linked glycans³. After removal of its signal peptide, the 495-amino acids polypeptide completely folds and subsequently binds to the triple helical structure in the apical region of the integral membrane protein LIMP-2 (lysosome integral membrane protein 2, encoded by the *Scarb2* gene), which contains trafficking information in its cytoplasmic tail^{4,5}. Complexed to LIMP2, GBA is transported through the Golgi apparatus, where its N-linked glycans are converted into complex-type structures⁶. The GBA–LIMP2 complex is routed to late endosomes/lysosomes, where GBA dissociates as a result of local acid pH^{5,7}. GBA belongs to family 30 of glycoside hydrolase clan A (www.cazy.org); its structural topology displays a typical $(\alpha/\beta)_8$ TIM barrel fold that forms the catalytic domain, a β -sheets domain, and an immunoglobulin-like domain. The catalytic domain contains several loops located in the proximity of the enzyme's active site⁸. These seem to adopt multiple conformations, indicating their structural flexibility and presumably reflecting their crucial role in the enzyme's conformational stability and/or its substrate turnover⁹. Inspection of the GBA crystal structure in complex with N-nonyldeoxynojirimycin (NN-DNJ) (PDB code: 2V3E) shows that the binding site of the enzyme is formed by a hydrophilic glycon binding pocket, where the sugar ring of the inhibitor is accommodated, forming multiple hydrogen bonds with its surrounding residues. Also, an aglycon binding pocket is present, formed by a narrow hydrophobic channel in which the aliphatic tail of the inhibitor forms a cluster of hydrophobic interactions with residues Leu241, Phe246, Tyr313, Leu314, and Tyr244 (**Figure 3.2d**)¹⁰. Deficiency of GBA results in Gaucher disease¹¹. At present, more than 200 mutations in the *gba1* gene have been linked with GD, and next to truncations and splicing defects, several hundred amino acid substitutions in GBA have been shown to cause GD¹². Substitutions in the GBA polypeptide chain distant from the catalytic site destabilized GBA's structure, decreasing its half-life in the cell. For instance, the L444P substitution in GBA causes faulty folding of most of its molecules in the ER, followed by subsequent proteasomal degradation¹³. Homozygosity for L444P GBA nearly always leads to a severe neuronopathic course of GD, albeit with great individual variability in onset and progression¹¹. Premature degradation may also occur in the case of GBA molecules with mutations in the catalytic domain. In fact, many of the documented mutations in GBA lead to defective folding and reduced transport to lysosomes¹⁴. An exception is the N370S GBA substitution, which is the most prevalent *gba1* mutation among caucasian GD patients. This amino acid substitution is in a loop close to the catalytic pocket and was found to affect the enzyme's pH optimum and its kinetic

parameters such as affinity for substrates and inhibitors¹⁵⁻¹⁹. Notably, the intralysosomal stability of N370S GBA is also reduced^{15,16,19}. The survival of wild-type GBA within lysosomes is already relatively short ($t_{1/2} \sim 24-36$ h), at least in cultured cells, where its intralysosomal proteolytic breakdown is supposedly mediated by cysteine proteases, as suggested by inhibition studies with leupeptin²⁰. The major symptoms of GD are predominantly caused by the abnormal accumulation of glucosylceramide in lysosomes of tissue macrophages^{21,22}. Lysosomal accumulation of glucosylceramide induces a multisystem disorder with various symptoms such as hepatosplenomegaly, cytopenia, and bone disease¹¹. Severely affected GD patients also develop neurological symptoms, and GBA abnormalities have been recognized as a risk factor for developing α -synucleinopathies²³. Enzyme replacement therapy (i.e., chronic intravenous administration of macrophage-targeted recombinant human GBA²⁴) markedly improves visceral symptomatology in GD patients, but the inability of the infused enzyme to pass the blood-brain barrier prohibits the prevention and correction of neurological manifestations²⁵. An alternative treatment might be offered by so-called pharmacological chaperones that promote the folding and stability of (mutant) GBA through interacting with its catalytic site²⁶⁻²⁹. These, preferably brain-permeable, small compounds should promote the folding of (mutant) GBA in the endoplasmic reticulum, resulting in increased transport of GBA to the lysosome²⁶⁻²⁹. Additionally, pharmacological chaperones might also stabilize GBA intra-lysosomally¹⁵. Whether the latter is clinically beneficial is debated since pharmacological chaperones that interact with the active site of GBA will intrinsically also inhibit its enzymatic activity. Among pharmacological chaperone candidates, one of the best studied is the iminosugar isofagomine (IFG **1**). IFG **1** increased the thermal stability of GBA at neutral pH by 8.7 °C and improved the trafficking of the N370S GBA mutant, resulting in an increase of cellular GBA levels in Gaucher patient tissues, including the brain³⁰. Additionally, oral administration of IFG **1** increased GBA L444P mutant activity in mice up to 5-fold³¹. Nevertheless, IFG **1** has exhibited poor performance when tested in humans, which could be due to its high hydrophilicity. Therefore, several other lipophilic derivatives have been tested and shown to have a higher affinity and chaperoning activity toward GBA mutants. For example, the GBA inhibitors N-butyldeoxyojirimycin (NB-DNJ, Miglustat) and NN-DNJ have been applied to GD cells with relative success: NN-DNJ has been used to restore protein levels of the N370S GBA variant in fibroblasts and NN-DNJ has been shown to lead to a significant increase in the protein level of several GBA mutants in cells, with a moderate enhancement in their thermal stability *in vitro*^{17,32}. The crystal structures of GBA bound to IFG **1**, NB-DNJ, and NN-DNJ have provided insights into the interactions in GBA-inhibitor complexes^{10,30}. However, these crystalline states did not provide a clear correlation between the induced conformational changes in GBA upon complex formation and the mechanism by which the inhibitors stabilized GBA folding in solution. Therefore, it is aimed to elucidate this mechanism using reversible and irreversible

glycomimetic ligands with different lipophilic properties *in vitro* and to verify the findings *in vivo*. Moreover, it is aimed to address the question of whether the occupancy of the binding pocket of GBA promotes its protection against proteolytic degradation in lysosomes. In the present study, first the stabilizing effects of cyclophellitol-type activity-based probes (ABPs; **Figure 3.1a**) were examined, which permanently bind to the E340 catalytic nucleophile, on pure, recombinant GBA by utilizing its double-displacement mechanism (**Figure 3.1b**). The ABPs are β -glucose-configured cyclophellitols with a spacer possessing hydrophobic green or red fluorescent BODIPY moieties (MDW933 **4** and MDW941 **5**; **Figure 3.1a**) attached to C6^{33,34}. Also conduritol β -epoxide (CBE **2**) was used as a small hydrophilic covalent inhibitor that is supposed to occupy only the glycon binding pocket of GBA. By trapping GBA in its intermediate state by forming an adduct complex with the aforementioned mechanism-based inhibitors, the contribution of the different moieties to the structural stabilization of GBA through binding site occupancy was dissected. The effect of 2-deoxy-2-fluoro- β -D-glucopyranosyl-N-phenyltrifluoroacetimidate (fluoro **3**; **Figure 3.1a**)³⁵, which forms a transient glycosyl-enzyme intermediate (**Figure 3.1c**), on GBA was also examined. For comparison, the effect of the potent reversible competitive GBA inhibitor IFG **1**, which has an *in vitro* IC₅₀ of ~ 30 nM at pH 5.2 and 5 nM at pH 7.0²⁷ was studied. The various investigations are described herein, and their implications are discussed.

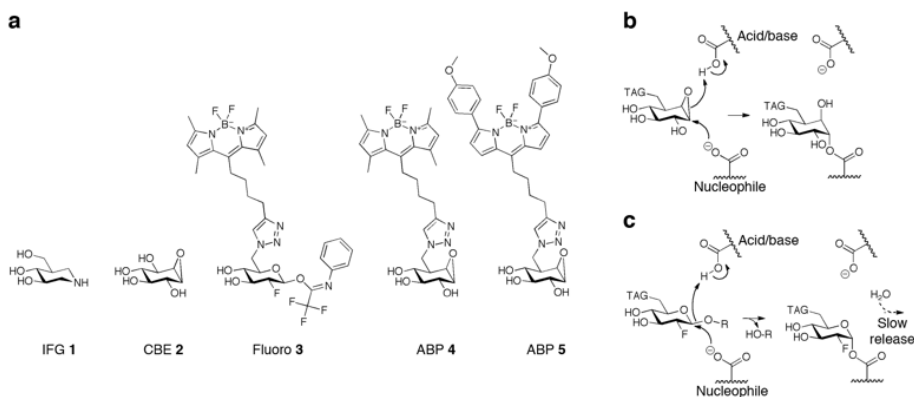


Figure 3.1. Inhibitors and reaction mechanism. (a) Structural formulas of competitive, reversible inhibitor isofagomine (IFG **1**), irreversible inhibitors conduritol β -epoxide (CBE **2**), semi-irreversible inhibitor-2-deoxy-2-fluoro- β -D-glucopyranosyl-N-phenyltrifluoroacetimidate³³ (fluoro**3**), cyclophellitol β -epoxide type ABP **4** (MDW933, green fluorescent), and β -epoxide-type ABP **5** (MDW941, red fluorescent)³⁵. (b) Irreversible binding mechanism of GBA via its double-displacement mechanism. (c) Hydrolysis of fluoro **3** and temporary trapping of the glycosylated nucleophile adducts of GBA.

Results

Structural Stability and Flexibility of GBA: Impact of pH and

Temperature

During its life cycle, GBA is exposed to a broad range of pH values: from neutral pH in the ER to an increasingly acidic pH in endosomes and lysosomes (pH 6.5 to >pH 4.5-5.0). Therefore, the effect of both acidic and neutral pH on the structural stability of purified recombinant GBA (rGBA, imiglucrase) was first investigated, by monitoring its thermal unfolding using circular dichroism. The dependence of the secondary structure of rGBA on temperature was recorded by monitoring the emission rGBA at a helical ellipticity wavelength (222 nm) while gradually heating it from 30 to 80°C (1 °C/min; see **Figure 3.2a**). The melting curve obtained for rGBA at pH 7.4 shows an apparent T_m value of 57 °C, and its melting temperature at pH 5.2 increased by 4 °C to an apparent T_m value of 61 °C. The increase in T_m at acidic pH is in agreement with previously reported measurements using differential scanning calorimetry (DSC)^{15,32}. Next, the effect of neutral and acidic pH on the activity of rGBA was investigated in a time-dependent manner at 37 °C. For this purpose, rGBA was first incubated for different lengths of time at 37 °C in 150 mM McIlvaine's buffer at a pH of 5.2 or 7.4. The residual activity of rGBA was measured with the 4MU- β -D-Glc substrate in 150 mM McIlvaine buffer at pH 5.2 (**Figure 3.2b**). The data indicate that the activity of rGBA is preserved under acidic conditions, whereas at pH 7.4, its activity is lost in a time dependent manner, with a half-life of 30 min. The noted loss in rGBA activity at pH 7.4 could be due to a loss of the enzyme's native fold, apparently due to an irreversible process since the remaining activity was measured at pH 5.2. To substantiate this explanation, a limited proteolysis reaction using trypsin was performed to probe the effects of pH on the rigidity of rGBA. Here, rGBA was digested with trypsin in 150 mM McIlvaine buffer at pH 5.2 or 7.4, and the tryptic events were analyzed every 10 min by SDS-PAGE (**Figure 3.2c**). At pH 5.2, rGBA shows resistance to tryptic digestion over the course of 90 min, whereas at pH 7.4, rGBA is more sensitive to trypsin digestion, with about 40% degraded within 60 min. The activity of trypsin at pH 5.2 and 7.4 on endoglucosylceramidase (EGCII) was checked and found it to be similar (**Figure 3.3**). Of note, a tryptic fragment of approximately 34 kDa appears during proteolysis that persists over the course of the experiment, which may point to a structured and rigid domain of rGBA (**Figure 3.2c**, arrow). Mass spectrometry was used to tentatively identify the trypsin cleavage site in GBA. The results suggest that the cleavage site position could be after lysine 233 (UniProt: P04062) within the polypeptide sequence VNGK_GSL, located in a loop close to the active site (**Tables A2.1** and **A2.2**). In addition, this cleavage site seems to be more

accessible to trypsin digestion at neutral pH and more protected at acidic pH (**Figure 3.2d**).

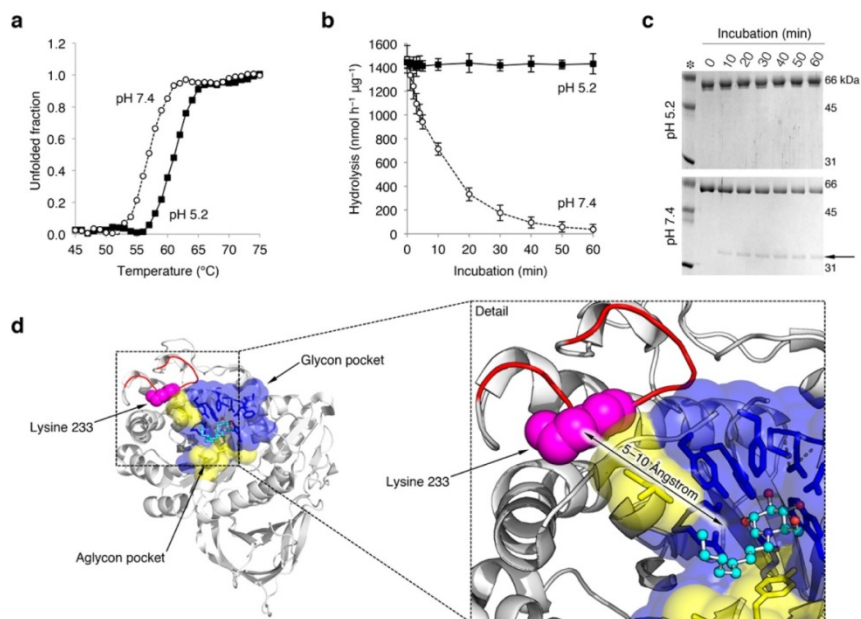


Figure 3.2. pH affects the structure of rGBA. **(a)** rGBA melting curve at pH 5.2 (closed squares) and pH 7.4 (open circles) as determined by circular dichroism. **(b)** Time-dependent decay of rGBA activity at pH 5.2 (closed squares) and pH 7.4 (open circles), as determined by hydrolysis of 4MU- β -D-Glc substrate at pH 5.2. Data are averages of duplicate values \pm SD. **(c)** Coomassie brilliant blue staining of the time-dependent tryptic digestion of rGBA with a trypsin/rGBA ratio of 1/10 (w/w) at pH 5.2 and 7.4 (top and bottom, respectively). The 35 kDa tryptic fragment is highlighted by an arrow. **(d)** Trypsin cleavage site at lysine 233 (pink spheres) present on the flexible outer loop (red) shown on the crystal structure of GBA in complex with NN-DNJ (PDB code: 2V3E), with NN-DNJ shown using a ball and stick model. Amino acid residues of the glycan binding pocket of GBA are shown in blue, and residues of the aglycon site are shown in yellow. A detail view of the rendered structure is shown to the right.

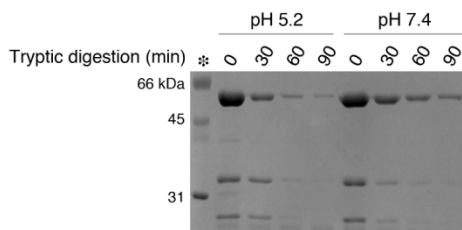


Figure 3.3. Coomassie brilliant blue staining of time-dependent, tryptic digestion of endoglycosidase EGCII with an optimum trypsin/EGCII ratio of 1/100 (w/w) at pH 5.2 and 7.4 (left, right, respectively).

Thermal Stability of rGBA: Impact of Glycomimetic Ligands

The effects of the competitive inhibitor IFG **1**, the semi-irreversible inhibitor fluoro **3**, and the irreversible inhibitors CBE **2** and lipophilic ABPs **4/5** on the thermal stability of rGBA were investigated at pH 5.2, mimicking lysosomal conditions. For this purpose, rGBA was incubated with saturating concentrations of inhibitors for 1 h at 37 °C and then gradually heated while monitoring tryptophan fluorescence^{36,38}, which decays as a result of tertiary structure unfolding. As depicted in **Figure 3.4a**, IFG **1** increased the T_m of rGBA (55.2 °C) by +5.6 °C, irreversible inhibitor **2**, by +14.1°C, **3**, by +12.9 °C, and ABPs **4** and **5**, by +21.0 and +21.7 °C, respectively. Another analysis of biophysical stability was performed by circular dichroism³⁷. rGBA without inhibitors was compared to the enzyme saturated with **2** and β -epoxide **4** (**Figure 3.4b**). The calculated melting temperatures of rGBA preparations follow a similar trend as that observed using tryptophan fluorescence decay. Again, β -epoxide **4** is found to exert the most prominent stabilization of rGBA.

Glycomimetic Ligands Influence the Intrinsic Fluorescence of GBA

The 12 tryptophan residues present in GBA were exploited to probe the effects of ligand binding on the general folding of GBA. Notably, Trp178 and Trp381 are in close proximity to the substrate binding pocket, and residue Trp348 (loop2) and Trp393 (loop3) reside on the protein surface; the other Trp residues are buried in the hydrophobic core of the protein⁹. rGBA emission spectra were acquired by exciting tryptophan residues at 295 nm and recording the emission by scanning from 300 to 450 nm in the presence or absence of various irreversible inhibitors (**Figure 3.3c**). In its free form, rGBA exhibits a maximum emission of 336.5 nm (similar to a previously reported value³⁸). A slight 2 nm blue shift in the spectrum was observed upon complex formation with CBE **2**, with a maximum emission at 334.5 nm, reflective of a more hydrophobic environment of the tryptophan residues within the complex state (**Figure 3.3d**). rGBA exhibits a slightly larger blue shift when bound to ABPs **4** and **5**, with emission maxima of 333 nm. These data suggest that CBE **2** and ABPs **4/5** cause changes in the folding of rGBA, with the stronger effects of the latter ABPs presumably being promoted by their lipophilic tails. Serendipitously, the blue shifts induced by ABP **4** and **5** were concomitant with fluorescence quenching. As ABPs **4** and **5** contain a BODIPY fluorescence moiety (green and red fluorescent, respectively), it was speculated that part of the intrinsic GBA tryptophan emitted fluorescence is transferred to these fluorophores through an intrinsic FRET (iFRET) mechanism³⁹. To test this, the fluorescence spectra of ABP **4** and ABP **5**-labeled rGBA were acquired by exciting at 295 nm and extending the scanning range to 700 nm. Indeed, two peaks appear (515 and 610 nm) at maximum emission, which represent the maximum emission for both ABP- incorporated BODIPYs (**Figure 3.3d**).

This iFRET mechanism is also supported by the overlap between the emission spectra of rGBA and ABPs (**Figure 3.5**).

Glycomimetic Ligands Variably Rigidify the Structure of GBA

Protein stabilization by ligands is generally paired with protein rigidification due to new hydrogen bonds formation or due to the formation of new clusters of hydrophobic interactions⁴⁰. From the data presented above, it is speculated that there is a correlation between the ligand-induced conformational changes in GBA and its thermodynamic stabilization. Next it was investigated whether interactions with (ir)reversible inhibitors stabilize GBA by rigidification *in vitro*; the effect of these inhibitors on the ability of trypsin to digest rGBA was analyzed. As depicted in **Figure 3.4e,f**, only ~10% of rGBA in its free form remains after 90 min of incubation, and two major fragments are formed (~35 and ~40 kDa), which remain mostly intact over the course of the experiment. The trypsin cleavage site of the 35 kDa fragment was previously identified to be after Lys233 (**Tables A2.1** and **A2.2**). The presence of hydrophilic compounds IFG **1** or CBE **2** increased the resistance of rGBA against tryptic digestion, with 50% of rGBA remaining intact, and cleavage site of rGBA in its free state by trypsin was preserved (**Figure 3.4 e,f**). Fluoro **3** and ABPs **4** and **5** exert prominent effects on the sensitivity of rGBA to tryptic digestion (**Figure 3.4 e,f**) such that within 90 min no degradation was observed. These ABPs have long hydrophobic tails of 15-18 Å, giving them a high lipophilic potential. After binding to the nucleophile of GBA, the ABPs' hydrophobic tails further rigidify GBA through hydrophobic interactions that shield its hydrophobic core and lock into place the flexible loop that contains the trypsin cleavage site. Altogether, these observations match the incremental increases in the melting temperature of rGBA between CBE **2** and ABPs **4** and **5** (**Figure 3.4a,b**). Of note, amphiphilic inhibitors **4** and **5** also show the lowest IC₅₀ values regarding the inhibition of GBA's enzymatic activity, reflecting a correlation between their stabilization effects and their high binding affinity for the catalytic pocket (**Table 3.1**).

Table 3.1. Apparent IC₅₀ of Inhibitors^a

compound	apparent IC ₅₀ (nM)
IFG 1	31.4 at pH 5.2; 5.8 at pH 7.2
CBE 2	9497 ± 42.8
fluoro 3	5458 ± 130
ABP 4	1.24 ± 0.04
ABP 5	1.94 ± 0.08

^aValues determined toward rGBA using artificial 4MUβ-D-Glc substrate, as described earlier⁵⁴.

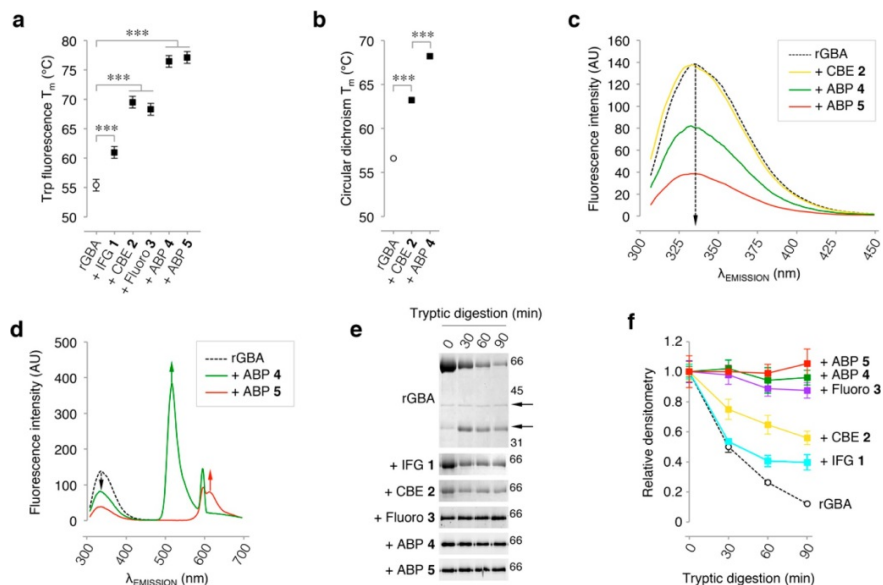


Figure 3.4. rGBA conformational changes monitored by intrinsic fluorescence and tryptic digestion. **(a)** Melting temperature (T_m) determined by tryptophan fluorescence of rGBA in the absence (control) or presence of saturating concentrations of inhibitors IFG 1, CBE 2, fluoro 3, or β -epoxide ABPs 4 and 5. Statistical analysis of $n = 3$ experiments, two-way ANOVA (***, $p < 0.001$). **(b)** T_m determined by circular dichroism of rGBA in the absence or presence of saturating concentrations of inhibitors 2 and 4. Statistical analysis of $n=2$, two-way ANOVA (***, $p < 0.001$). **(c)** rGBA fluorescence spectra at λ_{EX} 295 nm in the absence of additives (black dashed line) with a maximum λ_{EM} of 335 nm, in complex with CBE 2 (yellow) with a maximum λ_{EM} of 333 nm, with ABP 4 (green) with a maximum λ_{EM} of 332 nm, and with ABP 5 (red) with a maximum λ_{EM} of 331 nm. **(d)** rGBA fluorescence spectra showing fluorescence quenching by ABP 5 (red) with the appearance of an emission peak at 610 nm and ABP 4 (green) with the emergence of an emission peak at 515 nm. All measurements were done in 10 mM phosphate buffer, 150 mM NaCl, pH 7.4. **(e)** Time-resolved analysis of the tryptic digestion of rGBA in complex with IFG 1, CBE 2, fluoro 3, ABP 4, or ABP 5. **(f)** Quantification of rGBA band densitometry during tryptic digestion in the absence (black dashed line) and presence of ABP 5 (red), ABP 4 (green), fluoro 3 (magenta), CBE 2 (yellow), or IFG 1 (cyan). Duplicate quantifications \pm SD.

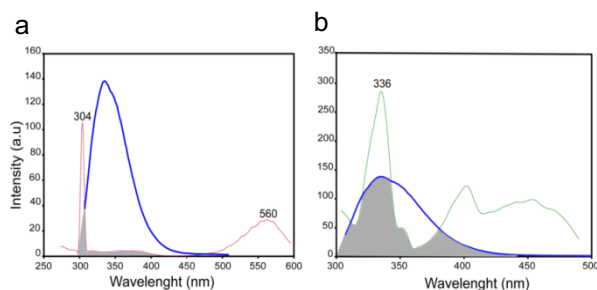


Figure 3.5: Absorption spectra of free ABPs 4 and 5 versus the emission spectrum of unlabeled rGBA. **(a)** Overlay of unlabeled rGBA emission spectrum (blue) excited at 295 nm and ABP 5 absorption spectrum (red dashed line) with a maximum absorption at 304 and 560 nm. Overlap between the spectra is highlighted in grey. **(b)** Overlay of unlabeled rGBA emission spectrum (blue) with ABP 4 absorption spectrum (green dashed line) with a maximum absorption at 336 nm. Overlap between the spectra is highlighted in grey.

Lipophilic ABPs 4 and 5 Stabilize GBA in Macrophages and Living Mice

As ABPs **4** and **5** exerted the strongest effect on the stability of rGBA *in vitro*, their influence on the enzyme *in situ* was assessed. Hence, human monocyte-derived macrophages were cultured with 100 nM ABP **5**, completely labeling all active GBA molecules (in situ IC₅₀ ~10 nM). After a continuous pulse for up to 192 h (8 days), *in situ* ABP **5**-labeled GBA was detected by fluorescence scanning (**Figure 3.6a**). ABP **5** labeled various molecular weight forms of GBA in the range 58-66 kDa, stemming from modifications in the enzyme's N-linked glycans⁴¹. Earlier investigations revealed that the 58 kDa form of GBA is formed inside lysosomes as a result of N-linked glycans being trimmed by local glycosidases⁴¹. As seen in **Figure 3.6a**, the mature 58 kDa form of GBA accumulates when the enzyme is labeled with **5**. This finding suggests that ABP labeling stabilizes GBA against proteolytic degradation in lysosomes and does not prohibit N-glycan modifications by lysosomal glycosidases.

To further examine the stabilizing effect of ABPs on GBA *in situ*, the fate of exogenous unlabeled rGBA and the same enzyme prelabeled with ABP **4** following uptake by human monocyte-derived macrophages (**Figure 3.6b**) was analyzed. The ABP **4**-labeled enzyme was stable after uptake for at least 48 h, in sharp contrast with the rapid breakdown of unlabeled rGBA (**Figure 3.6b**). The *in situ* stabilizing effect was also visualized and verified through fluorescence microscopic analyses, showing stable ABP **4**-rGBA in monocyte-derived macrophages 48 h after uptake compared to cells loaded with rGBA (**Figure 3.6c**). Next, mice were infused intravenously with 1 nanomole of ABP **4**, which subsequently labeled endogenous GBA in various tissues^{34,35,54}. In the livers of treated animals, sacrificed 6 weeks post ABP administration, **4**-labeled GBA could still be detected (**Figure 3.6d**). The amount was around ~35% of that in the livers of animals that were sacrificed 24 h after infusion of an identical dose of ABP **4** (**Figure 3.6d**, with quantification in **e**). This suggests again that ABP labeling markedly stabilizes GBA *in vivo*, since the half-life of unlabeled GBA is reported to be around 32-48 h^{18,20}.

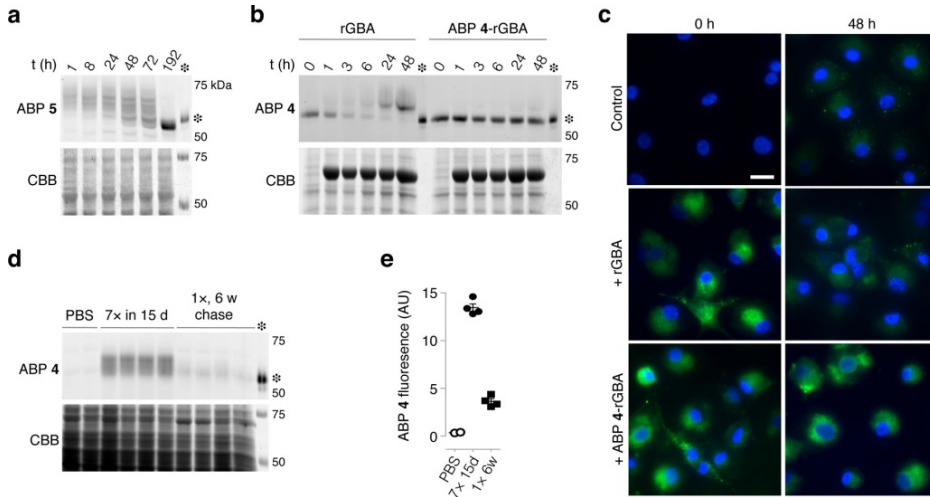


Figure 3.6. *In situ* labeling of GBA with cyclophellitol ABPs **4** and **5**. **(a)** Continuous labeling of human monocyte-derived macrophage GBA with ABP **5** (top) and Coomassie brilliant blue (CBB) staining of protein input (bottom). **(b)** Chase of ABP **4** (pre-) labeled rGBA (imglucerase) taken up by CBE **2** pretreated human monocyte-derived macrophages (top) and CBB staining (bottom). **(c)** Fluorescence micrographs of macrophages in **(b)**: control (top) and cells treated with unlabeled rGBA (middle) and ABP 4-labeled rGBA (bottom) after 0 and 48 h (left and right, respectively). Unlabeled rGBA was detected by labeling for 30 min with 10 nM ABP **4** prior to fixation. Scale bar represents 25 μ m. **(d)** Chase of murine hepatic (endogenous) GBA of animals treated either with vehicle, ABP **4** for 15 days (7 injections), or a single dose 6 weeks prior to sacrifice (top) and CBB staining (bottom). **(e)** Densitometry of ABP **4**-emitted fluorescence from **(d)**, normalized using CBB, with no treatment (open circles) or treated with repeated doses of ABP **4** (closed diamonds) or a single dose (closed squares); data are the mean of duplicate quantifications \pm SEM. All gels contain 50 fmol of equimolar ABP **4**- and **5**-labeled \sim 59 kDa imglucerase (asterisk) as a positive control.

Lipophilic ABPs **4** and **5** Increase GBA in Fibroblasts by Protection against Lysosomal Proteolysis

To assess whether the accumulation of ABP **4**-labeled 58 kDa GBA stems from a reduced susceptibility to lysosomal proteases, confluent human control fibroblasts were treated for 3, 5, 7, 9, or 12 days with the cysteine-cathepsin inhibitor leupeptin¹⁸. After harvesting the cells, GBA in the lysates of control cells and leupeptin-exposed cells was labeled with excess ABP **4** *in vitro*. As shown in **Figure 3.7a**, the amount of green fluorescent **4**-labeled GBA in untreated control cells increased slightly with culture time (top row). The incubation of the cells with Leupeptin caused a prominent accumulation of \sim 58 kDa active GBA over time (second row)¹⁸. Next, cells were incubated with red fluorescent ABP **5**. The inhibitor treatment induced a prominent time-dependent accumulation of ABP-labeled GBA (third row, **Figure 3.7a**). The increase in *in situ* ABP 5-labeled GBA was slightly further enhanced in cells co-incubated with leupeptin (fourth row), suggesting that **5**-labeled GBA is still prone to some degree of proteolysis within lysosomes (**Figure 3.7a**).

The quantification of ABP-labeled GBA is shown in **Figure 3.7b**, indicating that the *in situ* stabilization of GBA by leupeptin and ABP **5** at least partially overlap.

Lipophilic ABPs **4** and **5** Increase Mutant GBA Molecules in GD Fibroblasts

In fibroblasts from a homozygous N370S GBA Gaucher patient and a homozygous L444P GBA Gaucher patient, similar stabilizing effects of ABP on the enzyme were observed (**Figure 3.7c**). Both fibroblast cell lines contained a lower amount of active GBA compared to the control fibroblasts. Incubation of the cells with leupeptin and ABP **5** resulted in the stabilization of GBA, which was more prominent (6-8-fold) compared to that seen for GBA in wild-type cells (about 3-fold) (compare **Figure 3.7**, panels **b** and **d**). Exposure of both Gaucher fibroblast cell lines to the combination of ABP **5** and leupeptin further increased the stabilizing effect, which again partially overlapped (**Figure 3.7d**). Total GBA protein in cell lysates was also visualized by western blotting using the GBA-specific 8E455 antibody (**Figure 3.7e,g**, with corresponding quantification in **Figure 3.7f,h**). Again, a prominent stabilization of ~58 kDa GBA was noted with ABP **5** and/or leupeptin in the case of wild-type cells and N370S GBA Gaucher fibroblasts (**Figure 3.7**, panels **f** and **h**, respectively). Unfortunately, comparable analysis of L444P GBA Gaucher fibroblasts was not reliable due to their very low quantities of GBA protein. Overall, these findings suggest that the stabilizing effect of ABP **5** is partially caused by protection against breakdown by lysosomal proteases. This effect is specific since the lysosomal glycosidases processing GBA to its 58 kDa form do not appear to be inhibited. The reversible inhibitor IFG **1** and semi-irreversible inhibitor **3** were found to augment GBA in fibroblasts to a lesser extent. Confluent wild-type and homozygous N370S GBA fibroblasts were treated for 12 days with 0-100 μ M **1**. After harvesting, cell lysates were labeled with excess green ABP **4** to visualize residual active GBA molecules (**Figure 3.8a,b**). A stabilizing effect of IFG **1** became evident only at concentrations greater than 10 μ M, being maximal at 100 μ M (the highest concentration tested). Western blot analysis of the same experiment rendered a similar result (**Figure 3.8c,d**). The semi-irreversible inhibitor **3** comparably augmented GBA in wild-type and N370S/N370S GD fibroblasts (**Figure 3.9a,b**). The findings from treating fibroblasts with **3** were confirmed by western blot analysis (**Figure 3.9c,d**).

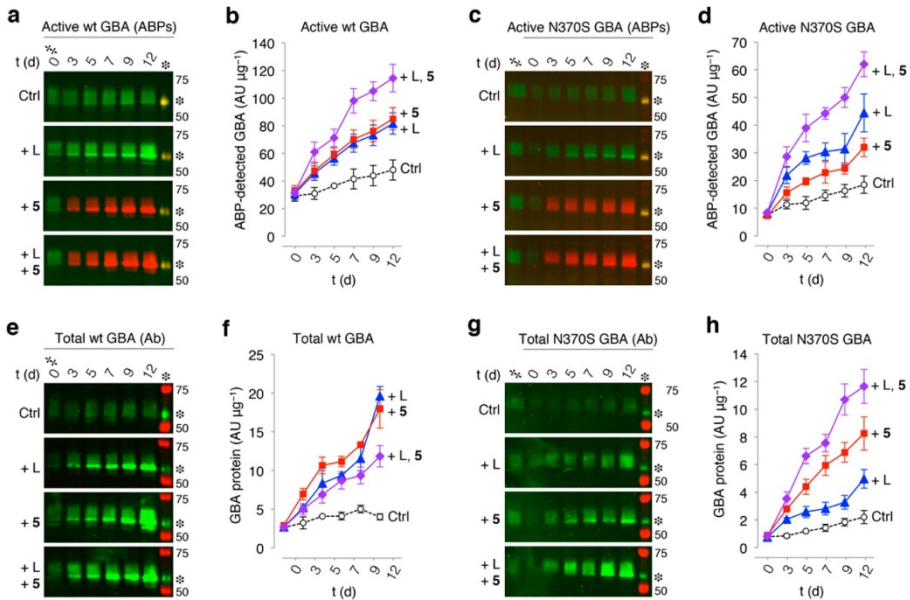


Figure 3.7. *In situ* stabilization of GBA by ABP 5 and leupeptin. Wild-type GBA fibroblasts were incubated with leupeptin, ABP 5 (red), or both for the indicated lengths of time. **(a)** GBA levels in untreated fibroblasts (top row) and cells incubated with leupeptin (second row), visualized *in vitro* with ABP 4 (green). Labeling of GBA in cells *in situ* with ABP 5 (red, third row) and in combination with leupeptin (bottom row). Equal green and red fluorescence yields a yellow overlay; fluorescence was calibrated with 50 fmol of equimolar green ABP 4- and red ABP 5-labeled imiglucerase present in each SDS-PAGE gel (asterisk). **(b)** Quantification of ABP-emitted fluorescence from *in vitro* ABP 4-labeled controls (open black circles), cells treated with leupeptin only (blue triangles), cells treated with *in situ* ABP 5-labeled GBA (red squares), and cells treated with a combination of ABP 5-labeled GBA and leupeptin (purple diamonds). Data are the mean of $n = 2 \pm \text{SD}$. **(c)** GBA levels in N370S/N370S fibroblasts treated in the same manner as wild-type GBA fibroblasts in panel a, *vide supra*. **(d)** Quantifications of ABP fluorescence in N370S/N370S fibroblasts. **(e)** Detection of total GBA protein in wild-type fibroblasts (green) by western immunoblotting of gels depicted in panel a (molecular weight ladder is in red). **(f)** Quantification of total GBA protein from *in vitro* ABP 4-labeled controls (open black circles), cells treated with leupeptin only (blue triangles), cells treated with *in situ* ABP 5-labeled GBA (red squares), and cells treated with a combination of ABP 5-labeled GBA and leupeptin (purple diamonds). Data are the mean of $n = 2 \pm \text{SD}$. **(g)** Total GBA protein in N370S/N370S fibroblasts treated in the same manner as wild-type GBA fibroblasts in panel a, *vide supra*. **(h)** Quantifications of ABP fluorescence in N370S/N370S fibroblasts. All data are expressed as average of $n = 2 \pm \text{SD}$.

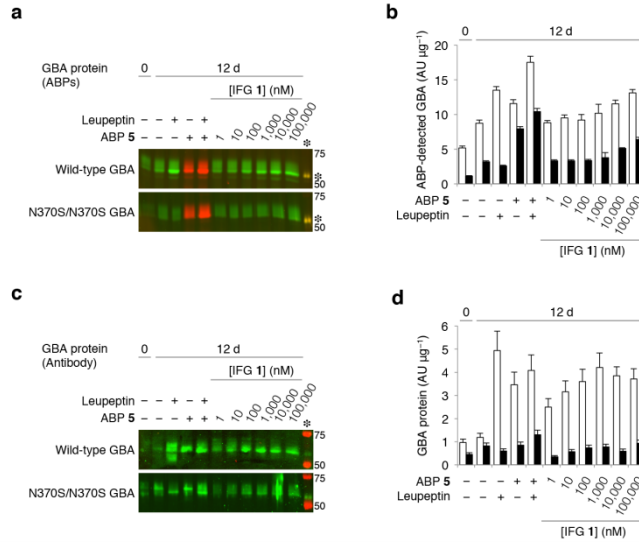


Figure 3.8: *In situ* GBA stabilization by IFG 1. Wild-type GBA (open columns) and N370S GBA (closed columns) fibroblasts were grown for 12 days in the absence or presence of incubated with leupeptin, red fluorescent ABP 5, both, or 0.001–100 μ M IFG 1. **(a)** Gel depicts *in situ* labeling of active GBA wild type (top) and N370S variant (bottom) by ABP 5 in the presence and absence of IFG 1 and/or leupeptin. **(b)** Quantification of ABP-emitted fluorescence from *in vitro* ABP 4-labeled controls, leupeptin and IFG 1-treated cells, compared to fluorescence of *in situ* ABP 5-labeled GBA. **(c)** Total GBA protein in wild type (top) and N370S variant (bottom) fibroblasts lysates visualized by Western blot using GBA-specific antibody 8E4 and its densitometry quantification **(d)** in the presence and absence of IFG 1, leupeptin and/or ABP 5. All data expressed as average of $n = 2$, \pm SD.

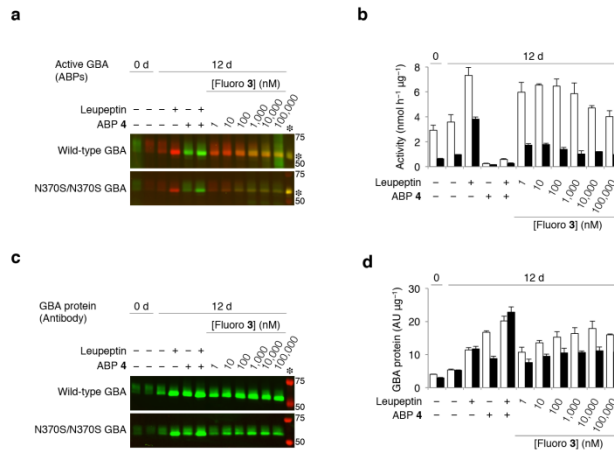


Figure 3.9: *In situ* GBA stabilization by fluoro 3. Wild-type GBA (open columns) and N370S GBA (closed columns) fibroblasts were grown for 12 days in the absence or presence of incubated with leupeptin, green fluorescent ABP 4, both, or 0.001–100 μ M fluoro 3. **(a)** Gel depicts *in situ* labeling of active GBA wild type (top) and N370S variant (bottom) by ABP 4 in the presence and absence of fluoro 3 and/or leupeptin. **(b)** GBA activity towards artificial substrate in lysates shown in a. **(c)** Total GBA protein in wild type (top) and N370S variant (bottom) fibroblasts lysates visualized by Western blot using GBA-specific antibody 8E4 and its densitometry quantification **(d)** in the presence and absence of fluoro 3, leupeptin and/or ABP 4. All data expressed as average of $n = 2$, \pm SD.

Discussion

In recent years, attention has been paid to the design and synthesis of chemical chaperones for GBA. Reviews by Benito et al.²⁸ and Jung et al.²⁹ cover some of the classes of glycomimetics currently under investigation as GBA chaperones. Many of these are reversible competitive, or mixed-type, inhibitors of GBA. The most well-studied chemical chaperone so far has been IFG **1**, which was the subject of several preclinical studies as well as a clinical study that did not fully meet expectations. Ambroxol⁴²⁻⁴⁵, a weak, mixed-type inhibitor of GBA, has been found to augment the enzyme in cultured GD patient cells, and following oral administration to patients, an impressive reduction in spleen and liver volumes was observed. The beneficial effects of chemical chaperones on GBA in cultured cells are generally attributed to improved chaperone-assisted folding of GBA in the endoplasmic reticulum. The present investigation suggests an additional beneficial mode of action of inhibitors, i.e., the contribution of hydrophobic interactions in the GBA aglycon binding pocket to its structural stability and protection against intralysosomal proteolytic degradation.

The evidence for this notion stems from *in vitro* and *in vivo* experiments testing GBA stabilization by inhibitors. Thermodynamic measurements with pure recombinant GBA suggested that all tested inhibitors stabilized the enzyme to a degree that correlates with the strength of the inhibition. A modest stabilization of GBA was observed for small hydrophilic compounds IFG **1** and conduritol β -epoxide **2**. The lipophilic fluoro **3** and β -epoxides **4/5** equipped with hydrophobic fluorophores cause a more dramatic increase in the melting temperature of rGBA up by 21 °C. Upon complex formation with CBE **2**, GBA presents a slight shift toward the blue region of its fluorescence spectra, an indication of a conformational change, possibly resulting from orientation adjustments of its indole groups toward a more hydrophobic environment. A higher shift toward the blue region was observed when the protein was in complex with lipophilic ABPs **4** and **5**. Presumably, their lipophilic tails cause further conformational changes in which the indole groups of a tryptophan experience extra hydrophobicity. Of note, equipping cyclophellitol and cyclophellitol-aziridine with hydrophobic fluorophore tags markedly increases their affinity for GBA^{33,34}. Along the same line, Vocadlo and co-workers developed an elegant fluorescence-quenched substrate for GBA by exploiting the fact that GBA accommodates the hydrophobic ceramide moiety of glucosylceramide, as it is known that GBA could tolerate a hydrophobic modification in the 6-position of glucose⁴⁶. The designed high-affinity fluorescence-quenched substrate harbors a fluorophore attached at C6 of glucose and the hydrophobic quencher attached to the anomeric site; to a certain extent, it mimics fluoro **3** and ABPs **4** and **5**. This successful substrate design indicates again that the catalytic pocket of GBA accommodates substrates possessing a hydrophobic modification. At present, no crystal structure of GBA has been solved in the presence of the fluoro **3** or ABPs **4** and **5**. However, the crystal structure of GBA in complex with a lipophilic ligand

CHAPTER 3

(NN-DNJ, PDB code: 2V3E) shows that GBA loops **1** and **2** become structured and undergo interactions with the aliphatic tails of NN-DNJ¹⁰. Similarly, upon complex formation with **3**, **4**, and **5**, GBA becomes extremely protected against tryptic digestion, providing strong evidence of its structural rigidification, presumably by the formation of clusters of hydrophobic interactions between the tails of the ABPs and the flexible loops in the entrance of the catalytic site of GBA. Therefore, it is presumed that the observed differences of the stabilization mechanisms between the tested compounds are mainly due to differences in their lipophilic potential. The predominant trypsin cleavage site in GBA's free state is located in a loop (residues 223-241, UniProt: P04062) close to the active site. In solution, this loop appears to be accessible for trypsin digestion by adopting a flexible conformation that fits within the protease catalytic site. Protease cleavage sites almost never occur in rigid secondary structures; they occur largely in flexible loops.⁴⁷ Interestingly, within this protein region, 16 mutations have been reported. These have been described to dramatically decrease GBA stability and activity, leading to severe GD symptoms. For instance, the L224F substitution decreases GBA activity to 4% and markedly increases its susceptibility to proteolytic degradation⁴⁸. Mutation V230E dramatically affects GBA activity, leading to type 1 GD disease⁴⁹. Along this line, the G232E mutation was identified in GD patients as well as patients suffering from Parkinson's disease, with the mutation markedly reducing GBA activity (~7%) and causing severe type 2 GD⁵⁰. Moreover, substitution of G234E in GBA's sequence has severe effects on the stability and catalytic activity of the enzyme⁵¹. The position of the latter mutation overlaps with what it is described here as a major trypsin cleavage site. On the basis of those observations, this particular region is plausibly essential for maintaining the correct fold of GBA's catalytic domain. Upon complex formation with lipophilic ABPs, this site becomes protected against proteolytic degradation. Recently similar stabilization mechanism for another retaining β -glucosidase, endoglycoceramidase II (EGCII) from *Rhodococcus* sp⁵² was noticed. The stability of EGCII was found to be improved by the formation of covalent complexes with cyclophellitols substituted with hydrophobic moieties. The tested compounds induced a more compact conformation of the flexible protein structure, revealed by an increased EGCII melting temperature, resistance against tryptic digestion, changes in its NMR spectrum, and a decrease of its exposed hydrophobic surface to the solvent, as determined by 8-anilino-1-naphthalenesulfonic acid fluorescence. Stabilization of the conformation of EGCII was correlated with the shape and hydrophobicity of the cyclophellitols substituents. The structural comparison between GBA and EGCII showed a remarkable overlap of their glycon and aglycon binding pockets⁵². Therefore, the EGCII study supports the proposed stabilization mechanism of inhibitors on the structure of GBA. Following the observed *in vitro* stabilization of GBA by inhibitors, This study was extended to living cells and mice. It is consistently noted that exposing cells (monocyte-derived macrophages and skin fibroblasts) and mice to cyclophellitol ABP **4** or **5** resulted in the

accumulation of GBA with a molecular weight of approximately 58 kDa, suggestive of lysosomal localization. Co-incubation of fibroblasts with ABPs and leupeptin, a broad lysosomal cysteine protease inhibitor known to inhibit the proteolytic breakdown of GBA, indicated that the stabilizing effect could indeed be partly ascribed to reduced lysosomal breakdown. Of note, the beneficial action of catalytic pocket occupancy by amphiphilic inhibitors on the stability and proteolytic resistance of GBA was also observed for N370S and L444P, two common mutations in GD. Clearly, irreversible covalent inhibitors **4** and **5** are of no use in the treatment of GD. However, they are valuable tools to establish the contribution of hydrophobic interactions to GBA stabilization and to selectively label the active form of GBA within living cells and laboratory animals. Fluoroglucosides, designed by Withers and co-workers⁵³, in theory may be more attractive as chaperones since they initially covalently bind to the catalytic nucleophile of a retaining glycosidase but are ultimately released. Therapeutic application of such compounds in patients will, however, offer the major challenge of dosing the inhibitor adequately to reach concomitant beneficial effects in all tissues: under-dosing in a tissue will be without effect and overdosing will cause undesired loss of degradative capacity in addition to GBA activity inhibition. It should also be mentioned that the natural substrate glucosylceramide may assist in the stabilization of GBA in lysosomes. In that case, intralysosomal GBA levels would be higher during high substrate flux, and the prolonged absence of substrate would promote the degradation of the enzyme. It will be of interest to examine whether a reduction of glycosphingolipids in cells by inhibition of glucosylceramide synthase activity is associated with increased lysosomal turnover of GBA.

In conclusion, GBA is significantly stabilized by the dual occupancy of its glycon and aglycon binding pockets by amphiphilic inhibitors, likely in part by promoting a global structural compactness of the enzyme associated with reduced susceptibility for proteolytic cleavage by lysosomal proteases. The findings of this study reveal new insights into the mechanism of stabilization by pharmacological chaperones that could be further exploited in the design of new compounds to rescue GBA proteostasis in GD patients.

Material and Methods

General Methods

Isofagomine **1**, fluoro **3**, and ABPs **4** and **5** were synthesized as described previously^{34,35,54}. Chemicals were obtained from Sigma-Aldrich if not otherwise indicated. Recombinant GBA (rGBA, imiglucerase) was obtained from Genzyme (Cambridge, MA, USA). Gaucher patients were diagnosed on the basis of reduced GBA activity and demonstration of an abnormal genotype. Fibroblasts were obtained with consent from donors. Cell lines were cultured in Ham's F12/DMEM (Invitrogen) supplemented with 10% (v/v) FBS. Monoclonal anti-human GBA antibody 8E4 was produced from hybridoma cells as described earlier⁵⁵. Buffy coats were purchased at Sanquin Bloodbank (Amsterdam).

Cerezyme Purification

rGBA (imiglucerase) was supplied as a sterile white lyophilized powder in the presence of mannitol and polysorbate 80 NF as stabilizer substances. Thorough purification of rGBA from its additives was conducted by affinity chromatography using a Concanavalin A-Sepharose column, eluting with a 30-min gradient of 0-1 M mannoside in 150 mM McIlvaine buffer (citric acid- Na_2HPO_4 , pH 5.2). Next, an additional purification step was performed on pooled fractions using size-exclusion chromatography (Superdex 75), and elution occurred either with 150 mM McIlvaine buffer (citric acid- Na_2HPO_4 , pH 5.2) or with 20 mM Tris-HCl, pH 7.4, supplemented with 150 mM NaCl. rGBA was concentrated using Amicon Ultra-4 centrifugal filter devices (30 kDa cutoff) and kept at 4 °C for further experiments.

Limited Proteolysis

Tryptic digestion of purified rGBA with or without reversible or irreversible inhibitors was performed at 37 °C either in 150 mM McIlvaine's buffer (pH 5.2 or 7.4) or in 20 mM Tris-HCl, pH 7.4, supplemented with 150 mM NaCl, using a trypsin/rGBA ratio of 1/10 (w/w) as the optimum conditions for proteolysis. Digestions were stopped with cracking buffer (50 mM Tris-HCl, pH 6.8, supplemented with 1% (w/v) SDS, 25% (v/v) glycerol, 1% (v/v) β -mercaptoethanol, and 0.05% (w/v) bromophenol blue), immediately followed by heating for 10 min at 100 °C. The tryptic digestion products (1.5-5 μg) were separated by SDS-PAGE and analyzed by Coomassie staining or, where stated, by fluorescence scanning (see below). To check the effect of acidic and neutral pH on trypsin activity, we used EGCII as a control. The same proteolysis conditions (see above) were applied with an optimum trypsin/EGCII ratio of 1/ 100 (w/w).

Tryptophan Fluorescence

rGBA (50 μM) was preincubated with 1 mM IFG **1** or fluoro **3**, 10 mM conduritol β -epoxide **2**, or 100 μM cyclophellitol ABP **4** or **5** in 150 mM McIlvaine's buffer (citric acid- Na_2HPO_4 , pH 5.2, supplemented with 0.2% (w/v) sodium taurocholate and 0.1% (v/v) Triton X-100) for 3 h at 37 °C. Fluorescence decay curves were obtained by diluting the rGBA-inhibitor complex to 1 μM in Nanopure H_2O , followed by determination of tryptophan fluorescence (λ_{EX} 295 nm, slit width 5 nm; λ_{EM} 345 nm, slit width 5 nm) while the sample temperature was increased at a rate of 1.5 °C per minute. Sample temperature was controlled via a PTP-1 Fluorescence Peltier system (PerkinElmer). We defined the inflection point of the temperature-induced decrease in tryptophan fluorescence intensity as the melting temperature (T_m). This value was determined by taking the minimum value of the first-derivative of the slope, at which the negative slope is maximal, using GraphPad Prism 5.1. Tryptophan emission fluorescence spectra were mapped using λ_{EX} 295 nm (slit width 5 nm) and scanning emission at λ_{EM} 300–470 (slit width 5 nm; Cary Eclipse fluorescence spectrophotometer, Agilent Technologies). Samples were composed of 5 μM purified rGBA with or without **2**, **4**, or **5** in 10 mM potassium phosphate buffer (K_2HPO_4 - KH_2PO_4 , pH 7.4) supplemented with 150 mM NaCl. Spectral backgrounds were corrected and smoothed using Cary Eclipse fluorescence spectrophotometer software. To obtain the different protein-inhibitor complexes, purified rGBA was preincubated with inhibitors in excess for 3 h at 37 °C in 150 mM McIlvaine buffer. After labeling, excess irreversible inhibitor was removed via buffer exchange into 10 mM potassium phosphate buffer using Centrprep filter devices (30 kDa cutoff).

Circular Dichroism

Spectra were recorded on a Chirascan CD spectrometer (Applied Photophysics). Far-UV CD spectra were recorded from 180 to 300 nm in a 1 mm path length quartz cuvette (Hellma) at 20 °C at a concentration of ca. 10 μ M. Spectra were collected for 0.5 s per data point at a 0.5 nm step size (spectral bandwidth was 1 nm) and were corrected for background signals. A Peltier element was used to control the sample temperature and allow the temperature to be ramped at 1 °C per minute. The intensity of the CD signal was monitored at various wavelengths (204, 215, and 235nm). The unfolding transition point (T_m) of free purified rGBA at different pH values (5.2 or 7.4) was measured by following the ellipticity signal decay at 222 nm by applying a heating rate of 1 °C per minute over a temperature gradient from 30 to 80 °C in 10 mM potassium phosphate buffer (K_2HPO_4 - KH_2PO_4 , pH 5.2 or 7.4), supplemented with 150 mM NaCl. The melting curves were fitted, and the T_m 's were calculated using GraphPad Prism 5.1.

Enzyme Activity Assays

The residual β -glucosidase activity associated with GBA was assayed at 37 °C by incubating samples with 3.75 mM 4-methylumbelliferyl- β -D-glucopyranoside (4MU- β -D-Glc) as substrate in 150 mM McIlvaine buffer, pH 5.2, supplemented with 0.1% (w/v) BSA, 0.2% (w/v) sodium taurocholate, and 0.1% (v/v) Triton X-100.56 The half-maximal inhibitory concentrations (IC_{50}) of compounds 1-5 were measured as published previously⁵⁴. The time-dependent decay of rGBA activity was assessed by incubating rGBA for 0-60 min at 37 °C, and at various time points, the residual rGBA activity was assessed by adding substrate. Assays were stopped with excess NaOH-glycine (pH 10.3), and fluorescence was measured with a LS30/LS55 fluorimeter (PerkinElmer) using λ_{EX} 366 nm and λ_{EM} 445 nm.

Isolation and Maturation of Macrophages.

Buffy coats were diluted into PBS supplemented with 0.1% (w/v) BSA and heparin, subsequently layered on top of a Lymphoprep gradient (Stemcell Technologies), and centrifuged at 1000g for 15 min at room temperature (RT). After washing the peripheral blood mononuclear cell pellets with PBS supplemented with 0.1% (w/v) BSA, cells were centrifuged at 750g for 10 min at RT and rinsed, and this was repeated at 500g for 5 min. Hereafter, the pellet was washed with aforementioned PBS and centrifuged at 250g for 10 min at RT. Then, monocytes were separated on a Percoll gradient. The resulting pellet was resuspended in 2.5 mL of 60% (w/v) SIP, layered with 5 mL of 45% (w/v) SIP and 2.0 mL of 34% (w/v) SIP, and centrifuged at 1750 g for 45 min at RT. The upper interface containing monocytes was washed thrice with the aforementioned PBS, centrifuged at 500g for 10 min, and then centrifuged twice at 500g for 5 min. The cell fraction was then resuspended in RPMI medium supplemented with 1% (w/v) human serum; the monocytes were counted with trypan blue staining, and 106 monocytes were seeded per well. After 1 h at 37 °C in a 5% (v/v) CO_2 atmosphere, non-adherent nonmonocyte cells were washed away with the aforementioned PBS and the adherent monocytes were cultured in RPMI medium supplemented with 10% (v/v) human serum for 7 days prior to experiment initiation.

Continuous β -Epoxide ABP 5 Pulse in Human Monocyte-Derived Macrophages

Human monocyte-derived macrophages were switched to X-VIVO 15 medium (Lonza) lacking human serum and continuously pulsed with 100 nM β -epoxide ABP 5. After 0-192 h (8 days), cells were washed extensively with PBS and lysed by scraping them in 25 mM potassium phosphate buffer (pH 6.5, supplemented with 0.1% (v/v) Triton X-100 and protease inhibitor cocktail (Roche)). Protein concentrations were determined, and 10 μ g of total protein (20 μ L) was denatured with 5 \times Laemmli buffer (50% (v/v) 1 M Tris-HCl, pH 6.8, 50% (v/v) glycerol, 10% (w/v) DTT, 10% (w/v) SDS, 0.01% (w/v) bromophenol blue), boiled for 4 min at 100 $^{\circ}$ C, and separated by electrophoresis on a 7.5% (w/v) SDS-PAGE gel running continuously at 90 V.^{34,35,54-56} Wet slab gels were scanned for fluorescence using a Typhoon variable mode imager (Amersham Biosciences) using λ_{EX} 488 nm and λ_{EM} 520 nm (band pass filter 40 nm) for green fluorescent fluoro ABP 3 and β -epoxide ABP 4 and λ_{EX} 532 nm and λ_{EM} 610 nm (band pass filter 30 nm) for red fluorescent β -epoxide ABP 5. ABP-emitted fluorescence was quantified using ImageJ software (NIH, Bethesda, USA) and verified in-gel by the presence of 50 fmol of equimolar green β -epoxide ABP 4- and red ABP 5-labeled imiglucerase. After fluorescence scanning, SDS-PAGE gels were fixed (50/40/10 MeOH/H₂O/HAC) for 1 h, stained for total protein (50/40/10 with 1% (w/v) CBB-G250), and destained (45/45/10). Coomassie brilliant blue-stained gels were scanned on a flatbed scanner.

Determination of *in Situ* IC₅₀.

Confluent human skin control fibroblasts with wild-type GBA were incubated with 0-100 μ M IFG 1, 0-10 μ M fluoro ABP 3, or 0-100 nM β -epoxide ABP 4 for 2 h at 37 $^{\circ}$ C, and GBA-associated β -glucosidase activity was subsequently determined by incubating them in the presence or absence of 250 μ M fluorescein-di- β -D-glucopyranoside (FDG) for 1 h at 37 $^{\circ}$ C. Next, cells were suspended by trypsinization, fixed in 3% (w/v) *p*-formaldehyde, and analyzed by FACS using the FL1 channel (λ_{EX} 488 nm) of a FACSCalibur (BD Biosciences). In the case of reversible inhibitor 1, all procedures, including washing with PBS, occurred in the presence of 1 at the concentration employed during the *in situ* incubation.

Pulse-Chase of Exogenous GBA

rGBA (imiglucerase, 50 μ M) was incubated with(out) 100 μ M ABP 4 for 1 h in 150 mM McIlvaine buffer, pH 5.2, supplemented with 0.2% (w/v) sodium taurocholate and 0.1% (v/v) Triton X-100, at 37 $^{\circ}$ C and cleaned three times over a 30 kDa cutoff filter with PBS. Mature human monocyte-derived macrophages were incubated with 300 μ M 2 for 2 h; cells were washed extensively with PBS, incubated with 100 nM rGBA (control) or 4-labeled rGBA with for 30 min at 37 $^{\circ}$ C, and again washed extensively; the medium was then refreshed. After 0-48 h, cells were again washed extensively with PBS and lysed by scraping in 25 mM potassium phosphate buffer (pH 6.5, supplemented with 0.1% (v/v) Triton X-100 and protease inhibitor cocktail (Roche)). Protein concentrations were determined in the lysates, and of the control rGBA-treated cells, 10 μ g of total protein was labeled *in vitro* with 1 μ M β -epoxide ABP 4 in McIlvaine buffer, pH 5.2, and with supplements, for 1 h at 37 $^{\circ}$ C. Finally, samples were denatured, and 4-labeled proteins were visualized by fluorescence scanning of the SDS-PAGE slab gels. ABP-emitted fluorescence was quantified using ImageJ software (NIH, Bethesda, USA), *vide supra*.

Pulse-Chase of GBA in Living Animals.

The appropriate ethics committee for animal experiments approved all experimental procedures. C57BL/6J mice were obtained from Charles River (Wilmington, MA, USA) and fed a commercially available lab diet (CRM(E), Special Diet Services, UK). Two male C57BL/6J mice were injected intravenously via the tail vein with a single dose of 100 μ L of PBS, four were injected with 100 μ L of PBS containing 100 pmol of ABP **4** (\sim 2 μ g kg^{-1}) 6 weeks prior to sacrifice, and four mice received the same dose every 48 h for 15 days prior to sacrifice. At the termination of the experiment, the mice were anesthetized with FFM mix (25/25/50 fentanyl citrate/midazolam/ H_2O) and then perfused via the heart into the aortic root with PBS, flowing at 3.0 mL min^{-1} , using a syringe pump (Harvard apparatus, Holliston, MA, USA). The liver was collected and directly frozen in liquid nitrogen. Homogenates were made in 25 mM potassium phosphate buffer, pH 6.5, supplemented with 0.1% (v/v) Triton X-100, and ABP 4-labeled GBA in 10 μ g of total protein was analyzed via SDS-PAGE. After fluorescence scanning, SDS-PAGE gels were fixed and stained with CBB, *vide supra*.

Pulse-Chase of Normal and Gaucher Patient Skin Fibroblasts

Confluent human skin fibroblasts homozygous for wild-type, N370S, or L444P GBA were cultured with medium supplemented with 100 nM ABP **5**, 100 μ M leupeptin, or both components. Medium was completely refreshed every fortnight, and after 0-12 days, cells were lysed by scraping in 25 mM potassium phosphate buffer (pH 6.5, supplemented with 0.1% (v/v) Triton X-100 and protease inhibitor cocktail (Roche). After determination of the protein concentration, 10 μ g of total protein was incubated with 100 nM ABP **4** (if fibroblasts were not treated by β -epoxide ABP **5** *in situ*) dissolved in 150 mM McIlvaine buffer (pH 5.2, supplemented with 0.2% (w/v) sodium taurocholate, 0.1% (v/v) Triton X-100, and protease inhibitor cocktail (Roche) for 1 h at 37 °C. Finally, samples were analyzed by SDS- PAGE on two gels: one for fluorescence scanning followed by CBB staining and one for western blotting; this was accomplished by transferring the protein in the gel to a membrane for 1 h at 12 V, followed by blocking the membrane with 2% (w/v) BSA in TBST buffer (50 mM Tris-HCl, pH 7.4, 150 mM NaCl, 0.1% (v/v) Tween-20), incubating the membrane with a 1:1000 diluted primary mouse α -human GBA monoclonal antibody (8E4, 2% (w/v) BSA in TBST), washing with TBST for 20 min (repeated 6 times), incubating with a 1:10000 diluted secondary rabbit α -mouse IRD680 antibody (Cell Signaling, 2% (w/v) BSA in TBST), subsequent washing with TBST for 20 min (repeated 6 times), and reading the signal on an Odyssey infrared scanner (LI-COR). Fluorescence emitted by either ABP-labeled proteins or antibodies was quantified using ImageJ software (NIH, Bethesda, MD, USA), *vide supra*.

***In Situ* Treatment with IFG 1 or Fluoro 3.**

Confluent human skin fibroblasts homozygous for wild-type, N370S, or L444P GBA were incubated for 12 days with 100 nM ABP **5**, 100 μ M leupeptin, or both or with 0.001-100 μ M IFG **1** or fluoro **3**. Medium was completely refreshed every fortnight, and samples were treated as described earlier, *vide supra*.

References

1. Brady, R. O., Kanfer, J. N., Bradley, R. M., and Shapiro, D. (1966) Demonstration of a deficiency of glucocerebrosidase in Gaucher's disease. *J. Clin. Invest.* 45, 1112–1115.
2. Patrick, A. D. (1965) A deficiency of glucocerebrosidase in Gaucher's disease. *Biochem. J.* 97, 17C–18C.
3. Berg-Fussman, A., Grace, M. E., Ioannou, Y., and Grabowski, G.A. (1993) Human acid β -glucosidase. N-glycosylation site occupancy and the effect of glycosylation on enzymatic activity. *J. Biol. Chem.* 268, 14861–14866.
4. Reczek, D., Schwake, M., Schröder, J., Hughes, H., Blanz, J., Jin, X., Brondyk, W., Van Patten, S., Edmunds, T., and Saftig, P. (2007) LIMP-2 is a receptor for lysosomal mannose-6-phosphate-independent targeting of beta-glucocerebrosidase. *Cell* 131, 770–783.
5. Zunke, F., Andresen, L., Wessler, S., Groth, J., Arnold, P., Rothaug, M., Mazzulli, J. R., Krainc, D., Blanz, J., Saftig, P., and Schwake, M. (2016) Characterization of the complex formed by β -glucocerebrosidase and the lysosomal integral membrane protein type- 2. *Proc. Natl. Acad. Sci. U. S. A.* 113, 3791–3796.
6. Aerts, J. M., Schram, A. W., Strijland, A., van Weely, S., Jonsson, L. M., Tager, J. M., Sorrell, S. H., Gimms, E. I., Barranger, J. A., and Murray, G.J. (1988) Glucocerebrosidase, a lysosomal enzyme that does not undergo oligosaccharide phosphorylation. *Biochim. Biophys. Acta, Gen. Subj.* 964, 303–308.
7. Saftig, P., and Klumperman, J. (2009) Lysosome biogenesis and lysosomal membrane proteins: trafficking meets function. *Nat. Rev. Mol. Cell Biol.* 10, 623–635. Dvir, H., Harel, M., McCarthy, A. A., Tokar, L., Silman, I., Futerman, A. H., and Sussman, J. L. (2003) X-ray structure of human acid- β -glucosidase, the defective enzyme in Gaucher disease. *EMBO Rep.* 4, 704–709.
8. Dvir, H., Harel, M., McCarthy, A. A., Tokar, L., Silman, I., Futerman, A. H., and Sussman, J. L. (2003) X-ray structure of human acid- β -glucosidase, the defective enzyme in Gaucher disease. *EMBO Rep.* 4, 704–709.
9. Lieberman, R. L. (2011) A Guided Tour of the Structural Biology of Gaucher Disease: Acid- β -Glucosidase and Saposin C. *Enzyme Res.* 2011, 973231.
10. Brumshtein, B., Greenblatt, H. M., Butters, T. D., Shaaltiel, Y., Aviezer, D., Silman, I., Futerman, A. H., and Sussman, J. L. (2007) Crystal Structures of Complexes of N-Butyl- and N-Nonyl- Deoxynojirimycin Bound to Acid β -Glucosidase: Insights into the mechanism of chemical chaperone action in gaucher disease. *J. Biol. Chem.* 282, 29052–29058.
11. Beutler, E., and Grabowski, G. A. (2001) Glucosylceramide Lipidosis-Gaucher Disease. In *The Metabolic and Molecular Bases of Inherited Diseases* (Scriver, C. R., Beaudet, A., Sly, W. S., and Valle, D., Eds.) 8th ed., McGraw-Hill, New York.
12. Hruska, K. S., LaMarca, M. E., Scott, C. R., and Sidransky, E. (2008) Gaucher disease: mutation and polymorphism spectrum in the glucocerebrosidase gene (GBA). *Hum. Mutat.* 29, 567–583.
13. Tan, Y. L., Genereux, J. C., Pankow, S., Aerts, J. M., Yates, J. R., 3rd, and Kelly, J. W. (2014) ERdj3 Is an Endoplasmic Reticulum Degradation Factor for Mutant Glucocerebrosidase Variants Linked to Gaucher's Disease. *Chem. Biol.* 21, 967–976.
14. Schmitz, M., Alfalah, M., Aerts, J. M., Naim, H. Y., and Zimmer, K. P. (2005) Impaired trafficking of mutants of lysosomal glucocerebrosidase in Gaucher's disease. *Int. J. Biochem. Cell Biol.* 37, 2310–2320.
15. Wei, R. R., Hughes, H., Boucher, S., Bird, J. J., Guziewicz, N., Van Patten, S. M., Qiu, H., Pan, C. Q., and Edmunds, T. (2011) X-ray and Biochemical Analysis of N370S Mutant Human Acid beta-Glucosidase. *J. Biol. Chem.* 286, 299–308.
16. van Weely, S., van den Berg, M., Barranger, J. A., Sa Miranda, M.C., Tager, J. M., and Aerts, J. M. (1993) Role of pH in determining the cell-type-specific residual activity of glucocerebrosidase in type 1 Gaucher disease. *J. Clin. Invest.* 91, 1167–1175.
17. Sawkar, A. R., Cheng, W. C., Beutler, E., Wong, C. H., Balch, W. E., and Kelly, J. W. (2002) Chemical chaperones increase the cellular activity of N370S beta -glucosidase: a therapeutic strategy for Gaucher disease. *Proc. Natl. Acad. Sci. U. S. A.* 99, 15428–15433.
18. Grace, M. E., Graves, P. N., Smith, F. I., and Grabowski, G. A. (1990) Analyses of catalytic activity and inhibitor binding of human acid beta-glucosidase by site-directed mutagenesis. Identification of residues critical to catalysis and evidence for causality of two Ashkenazi Jewish Gaucher disease type 1 mutations. *J. Biol. Chem.* 265, 6827– 6835.
19. Ohashi, T., Hong, C. M., Weiler, S., Tomich, J. M., Aerts, J. M., Tager, J. M., and Barranger, J. A. (1991) Characterization of human glucocerebrosidase from different mutant alleles. *J. Biol. Chem.* 266,

CHAPTER 3

- 3661–3667.
20. Jonsson, L. M., Murray, G. J., Sorrell, S. H., Strijland, A., Aerts, J. F. G. M., Ginns, E. I., Barranger, J. A., Tager, J. M., and Schram, A. W. (1987) Biosynthesis and maturation of glucocerebrosidase in Gaucher fibroblasts. *Eur. J. Biochem.* 164, 171–179.
 21. Ferraz, M. J., Kallemeijn, W. W., Mirzaian, M., Herrera Moro, D., Marques, A., Wisse, P., Boot, R. G., Willems, L. I., Overkleeft, H. S., and Aerts, J. M. (2014) Gaucher disease and Fabry disease: new markers and insights in pathophysiology for two distinct glyco- sphingolipidoses. *Biochim. Biophys. Acta, Mol. Cell Biol. Lipids* 1841, 811–825.
 22. Dekker, N., van Dussen, L., Hollak, C. E., Overkleeft, H., Scheij, S., Ghauharali, K., van Breemen, M. J., Ferraz, M. J., Groener, J. E., Maas, M., Wijburg, F. A., Speijer, D., Tylki-Szymanska, A., Mistry, P. K., Boot, R. G., and Aerts, J. M. (2011) Elevated plasma glucosylsphingosine in Gaucher disease: relation to phenotype, storage cell markers, and therapeutic response. *Blood* 118, e118–127.
 23. Siebert, M., Sidransky, E., and Westbroek, W. (2014) Glucocerebrosidase is shaking up the synucleinopathies. *Brain* 137, 1304–1322.
 24. Barton, N. W., Brady, R. O., Dambrosia, J. M., Di Bisceglie, A. M., Doppelt, S. H., Hill, S. C., Mankin, H. J., Murray, G. J., Parker, R. I., Argoff, C. E., et al. (1991) Replacement therapy for inherited enzyme deficiency macrophage-targeted glucocerebrosidase for Gaucher's disease. *N. Engl. J. Med.* 324, 1464–1470.
 25. Desnick, R. J., and Schuchman, E. H. (2012) Enzyme replacement therapy for lysosomal diseases: lessons from 20 years of experience and remaining challenges. *Annu. Rev. Genomics Hum. Genet.* 13, 307–335.
 26. Zechel, D. L., Boraston, A. B., Gloster, T., Boraston, C. M., Macdonald, J. M., Tilbrook, D. M., Stick, R. V., and Davies, G. J. (2003) Iminosugar glycosidase inhibitors: structural and thermodynamic dissection of the binding of isofagomine and 1-deoxynojirimycin to β -glucosidases. *J. Am. Chem. Soc.* 125, 14313–14323.
 27. Steet, R. A., Chung, S., Wustman, B., Powe, A., Do, H., and Kornfeld, S. A. (2006) The iminosugar isofagomine increases the activity of N370S mutant acid β -glucosidase in Gaucher fibroblasts by several mechanisms. *Proc. Natl. Acad. Sci. U. S. A.* 103, 13813–13818.
 28. Benito, J. M., García Fernández, J. M., and Ortiz Mellet, C. (2011) Pharmacological chaperone therapy for Gaucher disease: a patent review. *Expert Opin. Ther. Pat.* 21, 885–903.
 29. Jung, O., Patnaik, S., Marugan, J., Sidransky, E., and Westbroek, W. (2016) Progress and potential of non-inhibitory small molecule chaperones for the treatment of Gaucher disease and its implications for Parkinson disease. *Expert Rev. Proteomics* 13, 471–479.
 30. Lieberman, R. L., Wustman, B. A., Huertas, P., Powe, A. C., Pine, C. W., Khanna, R., Schlossmacher, M. G., Ringe, D., and Petsko, G. A. (2007) Structure of acid beta-glucosidase with pharmacological chaperone provides insight into Gaucher disease. *Nat. Chem. Biol.* 3, 101–107.
 31. Khanna, R., Benjamin, E. R., Pellegrino, L., Schilling, A., Rigat, B. A., Soska, R., Nafar, H., Ranes, B. E., Feng, J., Lun, Y., Powe, A. C., Palling, D. J., Wustman, B. A., Schiffmann, R., Mahuran, D. J., Lockhart, D. J., and Valenzano, K. J. (2010) The pharmacological chaperone isofagomine increases the activity of the Gaucher disease L444P mutant form of β -glucosidase. *FEBS J.* 277, 1618–1638.
 32. Abian, O., Alfonso, P., Velazquez-Campoy, A., Giraldo, P., Pocovi, M., and Sancho, J. (2011) Therapeutic Strategies for Gaucher Disease: Miglustat (NB-DNJ) as a Pharmacological Chaperone for Glucocerebrosidase and the Different Thermostability of Velaglycerase Alfa and Imiglycerase. *Mol. Pharmaceutics* 8, 2390–2397.
 33. Walvoort, M. T., Kallemeijn, W. W., Willems, L. I., Witte, M. D., Aerts, J. M., van der Marel, G. A., Codec, J. D., and Overkleeft, H. S. (2012) Tuning the leaving group in 2-deoxy-2-fluoroglucoside results in improved activity-based retaining β -glucosidase probes. *Chem. Commun. (Cambridge, U. K.)* 48, 10386–10388.
 34. Li, K. Y., Jiang, J., Witte, M. D., Kallemeijn, W. W., van den Elst, H., Wong, C. S., Chander, S. D., Hoogendoorn, S., Beenakker, T. J. M., Codec, J. D. C., van der Marel, G. A., Aerts, J. M. F. G., and Overkleeft, H. S. (2014) Synthesis of cyclophellitol, cyclophellitol aziridine and their tagged derivatives. *Eur. J. Org. Chem.* 2014, 6030–6043.
 35. Kallemeijn, W. W., Li, K. Y., Witte, M. D., Marques, A. R., Aten, J., Scheij, S., Jiang, J., Willems, L. I., Voorn-Brouwer, T. M., van Roomen, C. P., Ottenhoff, R., Boot, R. G., van den Elst, H., Walvoort, M. T., Florea, B. I., Codec, J. D., van der Marel, G. A., Aerts, J. M., and Overkleeft, H. S. (2012) Novel activity-based probes for broad-spectrum profiling of retaining β -exoglucosidases in situ and in vivo. *Angew. Chem., Int. Ed.* 51, 12529–12533.
 36. Lasch, J., Bessmertnaya, L., Kozlov, L. V., and Antonov, V. K. (1976) Thermal stability of immobilized enzymes circular dichroism, fluorescence and kinetic measurements of α -chymotrypsin attached to soluble carriers. *Eur. J. Biochem.* 63, 591–598.
 37. Michell, S. (1950) A photo-electric method for measuring circular dichroism. *Nature* 166, 434–435.

CHAPTER 3

38. Qi, X., and Grabowski, G. A. (1998) Acid β -glucosidase: intrinsic fluorescence and conformational changes induced by phospholipids and saposin C. *Biochemistry* 37, 11544–11554.
39. Kim, J. H., Sumranjit, J., Kang, H. J., and Chung, S. J. (2014) Discovery of coumarin derivatives as fluorescence acceptors for intrinsic fluorescence resonance energy transfer of proteins. *Mol. Biosyst.* 10, 30–33.
40. Celej, M. S., Montich, G. G., and Fidelio, G. D. (2003) Protein stability induced by ligand binding correlates with changes in protein flexibility. *Protein Sci.* 12, 1496–1506.
41. Van Weely, S., Aerts, J. M. F. G., Van Leeuwen, M. B., Heikoop, J. C., Donker-Koopman, W. E., Barranger, J. A., Tager, J. M., and Schram, A. W. (1990) Function of oligosaccharide modification in glucocerebrosidase, a membrane-associated lysosomal hydrolase. *Eur. J. Biochem.* 191, 669–677.
42. Maegawa, G. H., Tropak, M. B., Buttner, J. D., Rigat, B. A., Fuller, M., Pandit, D., Tang, L., Kornhaber, G. J., Hamuro, Y., Clarke, J. T., and Mahuran, D. J. (2009) Identification and characterization of ambroxol as an enzyme enhancement agent for Gaucher disease. *J. Biol. Chem.* 284, 23502–23516.
43. Babajani, G., Tropak, M. B., Mahuran, D. J., and Kermode, A. R. (2012) Pharmacological chaperones facilitate the post-ER transport of recombinant N370S mutant β -glucocerebrosidase in plant cells: evidence that N370S is a folding mutant. *Mol. Genet. Metab.* 106, 323–329.
44. Zimran, A., Altarescu, G., and Elstein, D. (2013) Pilot study using ambroxol as a pharmacological chaperone in type 1 Gaucher disease. *Blood Cells, Mol., Dis.* 50, 134–137.
45. Bendikov-Bar, I., Maor, G., Filocamo, M., and Horowitz, M. (2013) Ambroxol as a pharmacological chaperone for mutant glucocerebrosidase. *Blood Cells, Mol., Dis.* 50, 141–145.
46. Yadav, A. K., Shen, D. L., Shan, X., He, X., Kermode, A. R., and Vocadlo, D. J. (2015) Fluorescence-quenched substrates for live cell imaging of human glucocerebrosidase activity. *J. Am. Chem. Soc.* 137, 1181–1189.
47. Fontana, A., de Laureto, P. P., Spolaore, B., Frare, E., Picotti, P., and Zamboni, M. (2004) Probing protein structure by limited proteolysis. *Acta. Biochim. Polym.* 51, 299–321.
48. Liou, B., Kazimierczuk, A., Zhang, M., Scott, C. R., Hegde, R. S., and Grabowski, G. A. (2006) Analyses of Variant Acid β -Glucosidases: effects of gaucher disease mutations. *J. Biol. Chem.* 281, 4242–4253.
49. Micić, S., Filocamo, M., Dominissini, S., Montalvo, A. L. E., Vlahoviček, K., Deganuto, M., Mazzotti, R., Cariati, R., Bembi, B., and Pittis, M. G. (2005) Identification and functional characterization of five novel mutant alleles in 58 Italian patients with Gaucher disease type 1. *Hum. Mutat.* 25, 100–100.
50. Neumann, J., Bras, J., Deas, E., O’Sullivan, S. S., Parkkinen, L., Lachmann, R. H., Li, A., Holton, J., Guerreiro, R., Paudel, R., Segarane, B., Singleton, A., Lees, A., Hardy, J., Houlden, H., Revesz, T., and Wood, N. W. (2009) Glucocerebrosidase mutations in clinical and pathologically proven Parkinson’s disease. *Brain* 132, 1783–1794.
51. Grace, M. E., Desnick, R. J., and Pastores, G. M. (1997) Identification and expression of acid beta-glucosidase mutations causing severe type 1 and neurologic type 2 Gaucher disease in non-Jewish patients. *J. Clin. Invest.* 99, 2530–2537.
52. Ben Bdira, F., Jiang, J., Kallemeijn, W., de Haan, A., Florea, B. I., Bleijlevens, B., Boot, R., Overkleeft, H. S., Aerts, J. M., and Ubbink, M. (2016) Hydrophobic Interactions Contribute to Conformational Stabilization of Endoglycosidase II by Mechanism-Based Probes. *Biochemistry* 55, 4823–4835.
53. Rempel, B. P., Tropak, M. B., Mahuran, D. J., and Withers, S. G. (2011) Tailoring the specificity and reactivity of a mechanism-based inactivator of glucocerebrosidase for potential therapeutic applications. *Angew. Chem., Int. Ed.* 50, 10381–10383.
54. Witte, M. D., Kallemeijn, W. W., Aten, J., Li, K. Y., Strijland, A., Donker-Koopman, W. E., van den Nieuwendijk, A. M., Bleijlevens, B., Kramer, G., Florea, B. I., Hooibrink, B., Hollak, C. E., Ottenhoff, R., Boot, R. G., van der Marel, G. A., Overkleeft, H. S., and Aerts, J. M. (2010) Ultrasensitive in situ visualization of active glucocerebrosidase molecules. *Nat. Chem. Biol.* 6, 907–913.
55. Aerts, J. M. F. G., Donker-Koopman, W. E., Murray, G. J., Barranger, J. A., Tager, J. M., and Schram, A. (1986) A procedure for the rapid purification in high yield of human glucocerebrosidase using immunoaffinity chromatography with monoclonal antibodies. *Anal. Biochem.* 154, 655–663.
56. Aerts, J. M. F. G., Donker-Koopman, W. E., van der Vliet, M. K., Jonsson, L. M., Ginns, E. I., Murray, G. J., Barranger, J. A., Tager, J. M., and Schram, A. W. (1985) The occurrence of two immunologically distinguishable beta-glucocerebrosidases in human spleen. *Eur. J. Biochem.* 150, 565–574

CHAPTER 4

Exploring the Conformational Landscape and the Dynamics of GH11 xylanases During Catalysis

Abstract

GH11 xylanases are a family of β -glycosidases involved in the degradation of hemicellulose, one of the major components of renewable biomass. This family of enzymes has attracted increased attention due to their potential industrial applications, especially in biofuel production. To explore the conformational landscape and the dynamics of GH11 xylanases during catalysis, *Bacillus circulans* (BCX) xylanase was used as a model. By combining paramagnetic NMR spectroscopy with Carr-Purcell-Meiboom-Gill relaxation dispersion (CPMG RD) techniques, the millisecond dynamics and conformational changes of BCX in each step of its catalytic reaction were studied. To study the Michaelis-Menten complex a catalytically inactive variant of BCX was used in the presence of xylohexaose (X6); the glycosyl-enzyme intermediate was trapped using a novel epoxide compound, epoxy-Xylobiose (epoxyX2) that forms a stable adduct with the nucleophilic residue. The last step of the reaction, the product release, was studied in the presence of xylobiose (X2). In the free state, the protein adopts a ground state that resembles its crystal conformation showing millisecond dynamics in its “fingers” and “thumb” regions. Substrate binding to BCX follows an induced fit mechanism as revealed from the NMR titration data. The exchange rate between the open bound and the closed bound protein conformations is in the range of its substrate turnover rate, suggesting a role for such movement in the enzymatic reaction. Both of the enzyme bound states conformations are different from the one of the free state, as revealed by PCS data. Structural differences are located within the β -strands and the thumb that sculpture the enzyme binding cleft. X6 binding induces a global enhancement of the protein millisecond dynamics for the same regions that experience conformational changes. Such millisecond dynamics enhancement might reflect the role played by the protein motion in substrate positioning and sugar rings distortion.

In the covalent glycosyl-enzyme complex dynamics in the millisecond timescale is similar to that of the free enzyme. Nevertheless, covalent complex formation causes significant conformational changes located in the thumb and in the vicinity of the catalytic residues, as revealed by chemical shift perturbations and PCSs. In the product enzyme complex, the protein experiences subtle conformational changes compared to its free state, yet significant changes of its dynamic behaviour are observed. It is hypothesised that the protein motion in its product complex is playing a role in product dissociation from the catalytic site.

The protein ground states in the Michaelis-Menten and in the product complexes sample excited states that share a similar conformation with the glycosyl-enzyme complex ground state, which is suggested by the correlations between the chemical shift changes derived from the CPMG RD data fits and the chemical shifts of the intermediate state.

CHAPTER 4

In summary, BCX samples at least five ground states during catalysis and the rate limiting step of the reaction is possibly due to the high energy barrier that separates the adopted conformations in the Michaelis-Menten complex. The protein ground states are connected by an excited state that resembles the intermediate state conformation.

Introduction

Chemical reactions in living organisms occur at an ominously higher rate than their spontaneous counterparts as a result of a decrease of the transition state energy of the reaction by highly sophisticated catalysts called enzymes. In the past decades, understanding enzyme function has been revolutionized by determining snapshots of their 3D structures at an atomic resolution using X-ray crystallography, paving the way for describing their structure/function relationships. Despite this great triumph, the obtained static structures cannot always explain the elusive catalytic function of enzymes. Later on, it became evident that proteins in general, including enzymes, are dynamic entities that sample a large ensemble of conformations around an average structure. The time scale of these structural fluctuations in combination to their amplitudes and directions have proven to be the missing piece of the puzzle necessary to achieve a better understanding of enzyme function. The conformational space that can be explored by a protein is referred to its “energy landscape” in which its native conformation populates a low-energy state called “ground states”, which is in a continuous exchange with higher energy conformations called “excited states”^{1, 2}. The exchange kinetics between the protein conformers is dictated by the amplitude of the energy barrier that separates the different states. Excited states that are separated by a high energy barrier, interconvert on the microsecond to millisecond time scale or longer. Those “excited states” have been associated with enzyme molecular function, including ligand binding^{3, 4} and catalysis^{5, 6}.

NMR spectroscopy and X-ray crystallography are the techniques of choice to determine the protein ground state structures. However, each technique has its limitations and challenges, for instance structure calculation by NMR spectroscopy remains a laborious method limited by the protein size and the quality of its NMR spectra. X-ray crystallography does not always capture the in-solution conformation of the ground state, due to crystal packing artefacts. Moreover, in the presence of their ligands, enzymes can experience conformational changes in solution that may not be visible in the crystalline state. Recently, paramagnetic NMR spectroscopy has emerged as an approach that bridges both techniques by providing structural restraints in solution that can be used to validate protein conformations in the crystalline state⁷. For instance, pseudocontact shifts (PCSs) provide long range restraints. They are caused by magnetic susceptibility anisotropy of a paramagnetic metal ion, described by a tensor, the $\Delta\chi$ -tensor⁷. PCSs have been used in crystal structure refinement⁸ and also exploited to determine the structure of a short-lived enzyme intermediate state⁹. These advanced applications of PCSs in the field of structural biology benefit from rigid lanthanide tags such as CLaNP-5¹⁰. On the other hand, the characterisation of the excited state conformers and the understanding of their interconversion mechanisms with the enzyme ground-state remains a challenge, due

CHAPTER 4

to their short lifetime and their lowly populated fraction compared to the ground state. By virtue of the recent development of NMR spectroscopy techniques it is possible now to probe those “invisible” states and characterize their thermodynamics and kinetics properties. One of the most successful techniques is the Carr-Purcell-Meiboom-Gill relaxation dispersion (CPMG RD)^{11, 12}. It has been applied to dissect the energy landscape of enzymes during catalysis in combination with lower resolution techniques¹³⁻¹⁵. However, the most successful RD studies profited from the availability of enzyme conformations of consecutive steps of catalysis captured in the crystalline state, a situation that is not accessible for most enzymes^{13, 15}.

One of the prominent enzyme classes in nature are glycosyl hydrolases (GHs), which are classified in more than 140 families in *Cazy* the database¹⁶. GH11 xylanases are GHs able to hydrolyse the endo β -1-4-glycosidic link of xylan polymers, the main components of hemicellulose and the second most abundant renewable biomass material¹⁷. This family of enzymes attracted an increasing attention in the last decades due to their potential applications in industry and, especially, in biofuel production¹⁸. Therefore, the quest to find the optimum conditions for their large-scale industrial applications has boosted research to understand their structure/function relationship. GH11 xylanases have a characteristic fold, a β -jelly roll fold with a highly conserved amino acid sequence for the residues lining the binding site. The superposition of more than forty available crystal structures from different organisms revealed a remarkable conservation of the β -jelly roll domain topology as indicated by the small C α atom RMSD ($<1.5 \text{ \AA}$)¹⁹. The overall shape of the GH11 fold is often compared to a right-hand fist. It includes β -strands A which are nearly planar and distorted at the end to form a “hand palm” and “fingers”, and β -strands B perpendicular to β -strands A, sculpting the binding cleft and including the “thumb” region. The two sides of the cleft are connected by a long loop called the “cord”. The fold includes a single α -helix, sitting under the β -strands B structure (**Figure 4.1a**). The topographical properties of the catalytic cleft of GH11 xylanases are highly conserved with an approximate depth of 9 \AA , a width of 4 \AA and length of 25 \AA . The position of the catalytic dyad in the middle of catalytic cleft is in agreement with their endo catalytic mechanism. The thumb region displays a well-structured classical hairpin, containing a type I β -turn with six internal hydrogen bonds. Among GH11 members the primary structure of this loop is conserved, suggesting a key role for function²⁰. One of the best characterized GH11 xylanases member is the endo β -1-4 xylanase from *Bacillus circulans* (BCX). This enzyme has been extensively studied by X-ray crystallography²¹ and NMR spectroscopy²² due to its low molecular weight (20 kDa, like other GH11 members) and its apparently rigid and globular structure. The binding cleft of BCX has at least three (-) subsites (glycon binding site) and three (+) subsites (aglycon binding sites) according to the nomenclature of Davies et al.²³. The glycosidic bond hydrolysis of xylan

polymer takes place between the -1/+1 subsites with a substrate binding in at least the -2/-1 and +1 subsites in accordance with the protein endo catalytic mechanism.

BCX, like other GH11 members, employs the “Koshland” double displacement mechanism with a catalytic nucleophile and acid/base for catalysis²⁴. After substrate binding within the enzyme binding cleft (**ES** complex), a nucleophilic attack by the catalytic amino acid to the anomeric carbon of the glycosidic substrate occurs. Concomitantly, a proton transfer from the acid/base residue followed by departure of the leaving group from the aglycon site takes place during the first catalytic phase, from which an enzyme-glycoside covalent intermediate results (**EI** complex). In the next phase, an activated water molecule acts as a nucleophile with the assistance of the general acid/base to deglycosylate the catalytic residue through an oxocarbenium ion transition state. The final step is the product release from the enzymatic pocket (**EP** complex) (**Figure 4.1b**). The chemistry behind this hydrolysis function is widely accepted. Although several studies, mainly based on molecular dynamics calculations²⁵⁻²⁷ have provided some insights, a complete understanding of the conformational changes and dynamics of BCX during catalysis is still lacking. For instance, molecular dynamics simulations have suggested the opening of the thumb loop to induce the product dissociation²⁵⁻²⁸. The only evidence of a full opening of the thumb was observed in the case of a xylanase mutant from *B. subtilis* in the crystalline state²⁹. A recently published study of GH11 xylanase millisecond time scale dynamics using the CPMG RD technique showed that the protein in its free form experiences a millisecond motion for multiple residues localized within the binding site³⁰. In the presence of its substrate (**ES**), an enhancement of the millisecond (ms) time scale motion was observed³⁰. This study has provided the first evidence of such dynamics behaviour in GH11 family enzymes. A thorough MD investigation on GH11 family enzymes was undertaken in XYNII from *Trichoderma reesei*.³¹ By combining the different crystal structures of the enzyme, it was proposed that the protein samples three sequential substates during its catalytic reaction. First, the protein adopts an open state to accommodate the substrate in the cleft. Substrate binding induces a closed conformation necessary for positioning the substrate into the correct configuration for glycosidic bond hydrolysis. The last state is a loose structure from which the product is released. The study provided a first model for the enzyme catalytic cycle based on the available crystal structures, which still needs to be validated with in solution studies.

In the present work, paramagnetic NMR and CPMG RD techniques were combined to characterize GH11 xylanases in each step of their catalytic cycle using BCX as a model. First, the in-solution average conformations of the enzyme in its **E_{free}** as well as **ES**, **EI** and **EP** forms were studied by PCSs. To characterize the **ES** complex, a silenced version of the enzyme was generated by substituting the E78 nucleophile with a glutamine in the presence of xylohexose (X6). The **EI** complex was trapped by a novel compound epoxyxylobiose (epoxyX2) that mimics closely the intermediate state of the reaction and forms a covalent adduct complex with the enzyme. The **EP** ground state conformation was

studied in the presence of xylobiose (X2) that appears to bind only to the -1/-2 subsites, thus emulating the last step of the reaction. The dynamic behaviour of each complex, separately, was also studied using CPMG RD, aiming to uncover the link between the ground and excited states. The implications for BCX catalytic function are discussed.

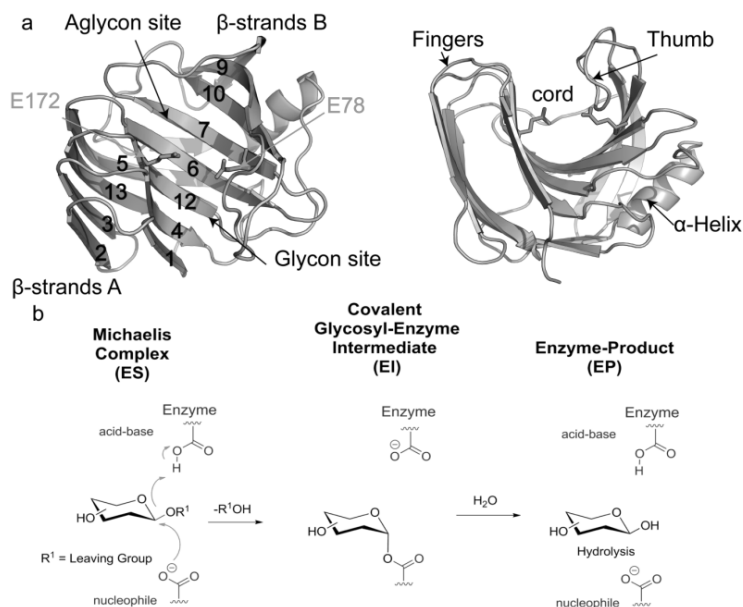


Figure 4.1. GH11 fold and catalytic mechanism. **(a)** β -jelly roll fold of *Bacillus circulans* xylanase with β -strands numbering. Glycon and aglycon binding sites of BCX binding cleft are indicated in arrows. The catalytic dyad in the middle of the binding cleft are shown in sticks. **(b)** General retaining β -glycosidases mechanism.

Results

BCX free state (E_{free}) in solution conformation

To investigate BCX conformational state in solution with an atomic resolution, pseudocontact shifts (PCSs) were used. BCX PCSs were obtained by preparing diamagnetic and paramagnetic NMR samples through the attachment of Lu-CLaNP-5 and Yb-CLaNP-5 to ^{15}N labelled BCX T109C/T111C double mutant, respectively. The choice of the double mutations positions was based on the rigidity of the region and its exposure to the surface, as suggested by the protein crystal structure³². Positions for which the distance between the C α atoms was between 8 to 10 Å, in accordance with the standard for CLaNP5⁴² were selected, to warrant correct attachment of the lanthanide tag to the protein. A few double cysteines mutants at different positions were generated and tested for expression yield and stability and the optimal one was identified to be T109C/T111C (**Figure 4.2**).

The backbone nuclei of the diamagnetic and paramagnetic spectra were assigned using the wild type assignment²⁴. By calculating the chemical shift differences between the paramagnetic and diamagnetic spectra 127 PCSs were obtained (**Figure 4.3a**). The experimental PCSs were used to determine the position of the lanthanoid ion and the size and the orientation of the $\Delta\chi$ tensor. The data was fitted to BCX crystal structure (PDB ID: 2bv or 1bcx)³² and the lanthanoid position was $\sim 8 \text{ \AA}$ from the C α atoms of both cysteines, which is in agreement the previously reported distances¹⁰. The magnitudes of the axial and rhombic parts of the tensor were determined to be $8.3 \pm 0.1 \times 10^{-32} \text{ m}^3$ and $2.1 \pm 0.1 \times 10^{-32} \text{ m}^3$, respectively. A correlation between the experimental and the predicted PCSs from BCX crystal structure was observed with a low Q factor value equal to 0.021 including all data (**Figure 4.3b**). Exceptions are residues G139, W58 and T44 which show slight deviations from predicted values. Overall, the PCSs are consistent with prior studies that revealed BCX is indeed globular and compact, mainly due the extensive hydrogen bonds network between its backbone amide groups^{21, 22}. The compact conformation of BCX is also supported by study of the pico-nanosecond dynamics³³. The protein exhibits restricted motion on the probed time scale. Nevertheless, these observations do not exclude the possibility of a slower protein motion, on the millisecond time scale.

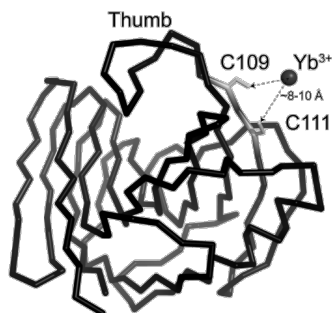


Figure 4.2. Locations of engineered Cys residue for CLaNP-5 attachment and the lanthanoid position on the BCX surface, depicted on the crystal structure (PDB ID:2bv). BCX is shown in black C α trace, cysteines in grey sticks and the lanthanoid in black sphere. The distances between the cysteines side chains and the lanthanoid are indicated.

E_{free} dynamics

To follow the millisecond time scale dynamics of BCX a relaxation dispersion TROSY-CPMG experiment at 293 K was performed. Forty-three residues show relaxation dispersion profiles ($R_{\text{ex}} > 1 \text{ s}^{-1}$) clustered within the fingers, thumb and palm regions and in loops connecting β -strands 6 and 7 and the ones connecting β -strand 12 to the α -helix (**Figure 4.3c, d**). A global two-site exchange fit of 27 residues with $R_{\text{ex}} \geq 1.8 \text{ s}^{-1}$ yields an exchange rate (k_{ex}) between the ground and excited states of $2.5 (\pm 0.09) \times 10^3 \text{ s}^{-1}$ with an excited fraction (p_{B}) equal to 0.78 %, suggesting a lowly populated excited state with local ms time scale dynamics (**Figure 4.4a**).

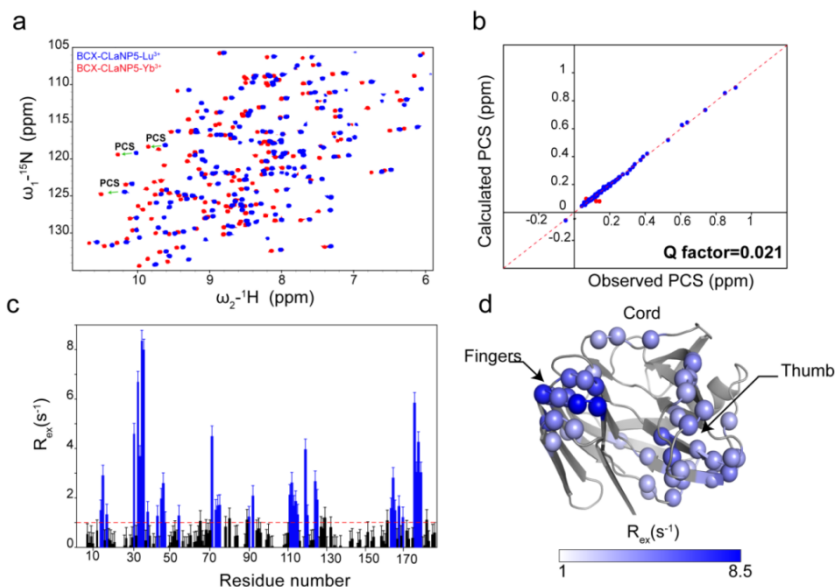


Figure 4.3. BCX free state conformation and dynamics in solution. **(a)** Overlay between BCX free state diamagnetic (BCX T09C/T111C-CLaNP-5-Lu³⁺, blue) and paramagnetic (BCX T09C/T111C-CLaNP-5-Yb³⁺, red) spectra. Three PCSs are highlighted with green arrows. **(b)** Plot of the observed vs. calculated PCSs after fitting to the BCX crystal structure (PDB ID:2bvj)³². Blue circles indicate PCSs of with high correlation factor (PCS deviation < 0.02) and red circles indicate PCSs of outliers (PCS deviation > 0.02). The dashed line represents a perfect correlation. **(c)** Plot of R_{ex} vs. residue numbers of BCX free state. Residues with $R_{ex} \geq 1 \text{ s}^{-1}$ are shown in blue bars. The error bars represent the estimated error based on a duplicate measurement of different ν_{CPMG} frequencies. **(d)** Amides with $1 \text{ s}^{-1} \leq R_{ex} \leq 8.5 \text{ s}^{-1}$ shown in spheres on the BCX crystal structure (PDB ID: 2bvj) and coloured with a white/blue gradient. Residues with $R_{ex} \leq 1 \text{ s}^{-1}$ are shown in grey cartoon.

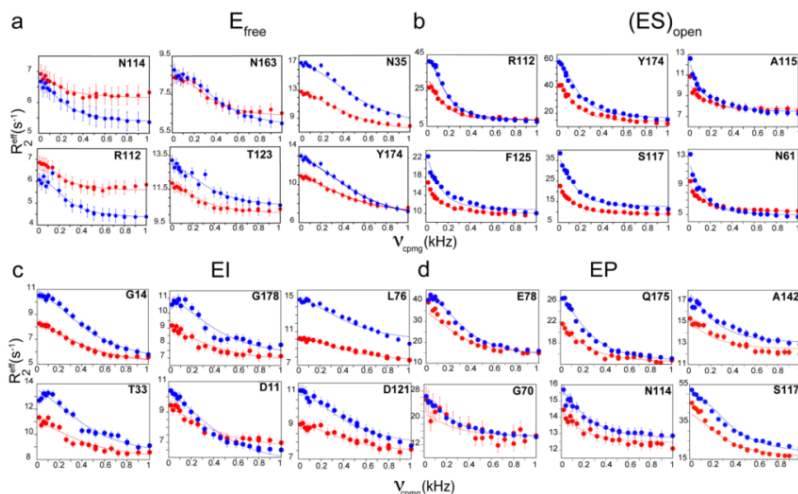


Figure 4.4: Global fit of CPMG RD data to a two-state chemical exchange model acquired on two static fields (red at 600 MHz and blue at 850 MHz) for **(a)** E_{free} ; **(b)** $(ES)_{open}$; **(c)** EI ; **(d)** EP . Six residues with the best global fit profiles are shown for each state. Residue names are indicated.

BCX substrate complex (ES)

Michaelis-Menten binding

The first step of any enzymatic reaction is the formation of the Michaelis-Menten complex between the enzyme and its cognate substrate. GH11 xylanases binding sites are formed by multiple subsites that accommodate at least six sugar units of xylan polymer. The subsites are named -1/-2/-3 and +1/+2/+3 for the glycon and the aglycon binding cavities, respectively. BCX is able to hydrolyse the glycosidic link (between -1/+1 subsites) of at least three xylose units, where two of them have to be accommodated within the -1/-2 subsites and the remaining one in the +1 subsite.

To avoid substrate hydrolysis while investigating the Michaelis-Menten complex of BCX, the nucleophile residue E78 was substituted by a Q. ^1H - ^{15}N heteronuclear single quantum correlation spectroscopy (HSQC) was used to monitor the titration of the inactive enzyme with xylohexaose (X6). The single amino acid substitution did not induce major changes of the protein HSQC spectrum, so the mutant assignment was performed using the wild peak list and curated by PCSs. Twelve titration points were acquired by increasing X6 concentration from 0 to 20 mM. Throughout the titration, significant line broadening (**Figure 4.5a**) in conjunction to diverse chemical exchange regimes of the side-chain and backbone amides were observed. Line broadening reflects an increase of the global tumbling time, which could be due to the changes of the buffer viscosity or due to weak self-association induced by X6. Similar observations were made when titrating the enzyme with X4³⁴.

Residues N54, A55, N141 and W185 exhibited a fast exchange behaviour ($k_{\text{ex}} \gg \Delta\omega$) with progressive chemical changes and significant $\Delta\delta_{\text{avg}}$ (up to 0.4 ppm) (**Figure 4.6.a,c**). Those residues are located in the “knuckles” of the hand-like protein previously identified as a secondary binding site (SBS) of the substrate (**Figure 4.6d**)³⁴. Peak shape analysis of the SBS residues revealed a $K_d = 2.8 (\pm 0.01)$ mM and a $k_{\text{off}} = 5.7 (\pm 0.12) \times 10^3 \text{ s}^{-1}$. At 3.5 mM of X6 concentration, several secondary peaks start to appear in a slow exchange regime ($k_{\text{ex}} < \Delta\omega$) some of them appear in the vicinity of the amides primary peaks (**Figure 4.6b**). Among those secondary peaks, 32 were identified to be located within the enzyme binding cleft (primary binding site) and others scattered over the protein backbone. For instance, residues N8, G12 and K40 of the fingers and residues D119, G120, Y166 and V168 located within the thumb loop and its surrounding at the -1/ -2 /-3 subsites which exhibit clear splitting of their peaks. Moreover, residues of the +1/+2 subsites, such as Y65 and V81, experience the same phenomena. Variability in the linewidth of the secondary peaks was observed (**Figure 4.5b**). By performing a peak shape analysis of the titration data and fitting 16 backbone amides with a secondary peak to the “induced fit binding model”, a correlation between the predicted versus the experimental peaks positions was obtained (**Figure 4.6b**). The k_d of the binding process

CHAPTER 4

is equal to $1.9 (\pm 0.015)$ mM and the $k_{\text{off}} = 1.3 (\pm 0.03) \times 10^3 \text{ s}^{-1}$. The fit suggests that the ligand binds to the protein through an induced fit mechanism where the **ES** complex is in equilibrium between two conformations ($\mathbf{E}_{\text{free}} + \text{S} \rightarrow (\mathbf{ES})_{\text{open}} \leftrightarrow (\mathbf{ES})_{\text{closed}}$) with a k_{open} and k_{closed} equal to 11 and 9 s^{-1} , respectively. Additionally, residues distal from the enzyme binding cleft exhibit also chemical perturbations in the intermediate exchange regime ($k_{\text{ex}} \approx \Delta\omega$) such as A152 and S155 of the α -helix with respective $\Delta\delta_{\text{avg}} = 0.3$ and 0.18 ppm. The calculation of the average chemical shift perturbations ($\Delta\delta_{\text{avg}}$) between the backbone amides of the $(\mathbf{ES})_{\text{open}}$ and \mathbf{E}_{free} confirmed the location of the amides with secondary peaks in the enzyme binding cleft (**Figure 4.6c,e**). The most important $\Delta\delta_{\text{avg}}$ are for residues located within the thumb and the finger regions. Residues of the α -helix such as A152 and S155 experience also large $\Delta\delta_{\text{avg}}$ in the $(\mathbf{ES})_{\text{open}}$ state despite their remote position from the primary and secondary binding sites which might suggest changes of the α -helix conformation upon ligand binding.

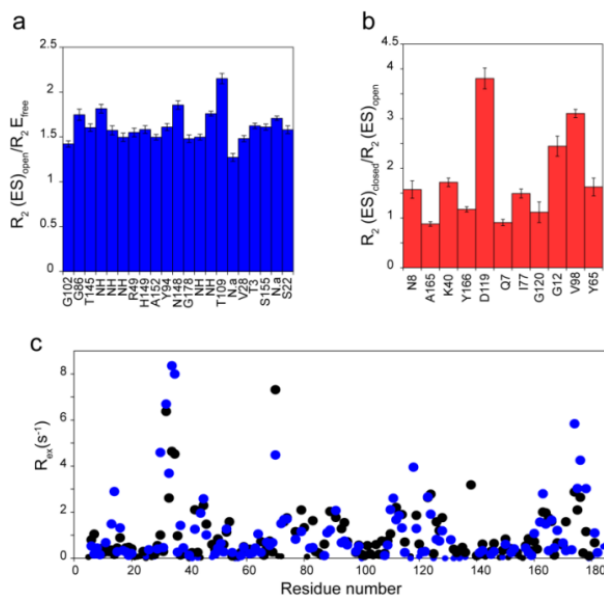


Figure 4.5: BCX E78Q NMR titration with X6 and its ms relaxation. **(a)** General line broadening of the BCX E78Q upon titration with X6. The ratios between R_2 values, predicted from the 2D peak shape analysis with TITAN, in the absence and the presence of 20 mM X6 from amides peaks that do not shift during titration. NH indicate side chain amides. N.a indicate non-assigned backbone amides. **(b)** the ratios between the $(\mathbf{ES})_{\text{open}}$ and $(\mathbf{ES})_{\text{closed}}$ R_2 values of the backbone amides in the slow exchange regime ($k_{\text{ex}} \ll \Delta\omega$). **(c)** Overlay between the R_{ex} values of the BCX WT (blue) and the BCX E78Q (black).

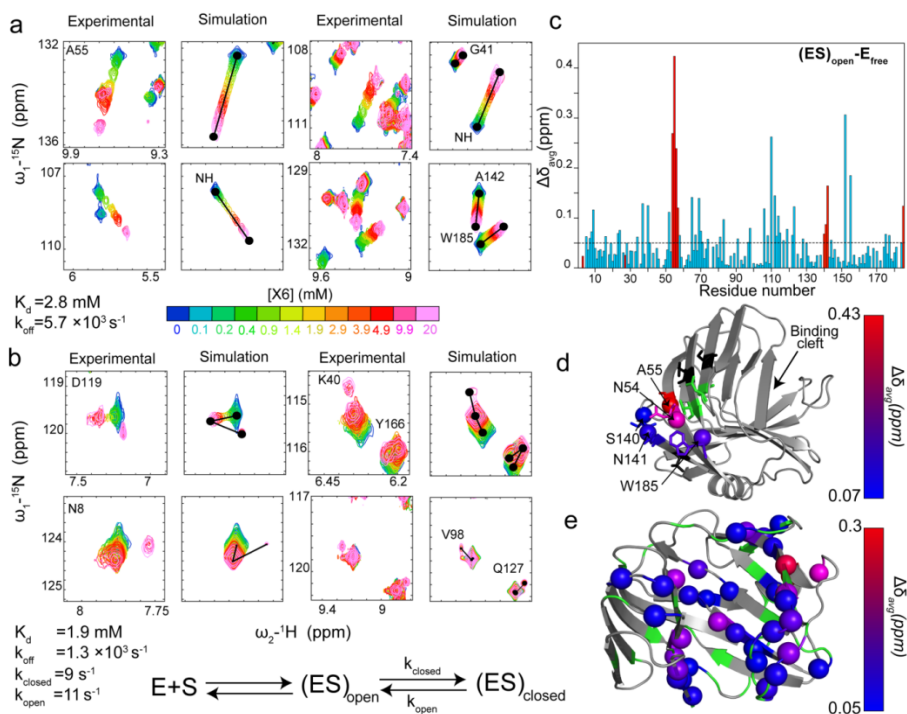


Figure 4.6. BCX E78Q titration with X6 (ES complex). (a) Experimental versus simulated chemical shift perturbations of backbone and side chain amides (NH) in the fast exchange regime ($k_{ex} \gg \Delta\omega$) that belong to the secondary binding site. The simulation was performed using TITAN^{3.5} software and the binding kinetics parameters are indicated. (b) Experimental chemical shift perturbations of BCX E78Q backbone amides with slow chemical regime ($k_{ex} < \Delta\omega$) versus their simulated chemical shift perturbations using an induced fit binding model. The kinetic parameters are indicated with a scheme of the enzyme-substrate interaction. (c) $\Delta\delta_{avg}$ between the $(ES)_{open}$ and the E_{free} plotted versus residue numbers. $\Delta\delta_{avg}$ of the secondary binding site amides are shown in red bars. (d) Amide groups of the secondary binding sites with $\Delta\delta_{avg} > 0.05$ ppm mapped on the BCX crystal structure (PDB ID: 1bcx)²⁷ in spheres and sticks and coloured by the amplitude of the $\Delta\delta_{avg}$ using a blue/red colour gradient. Residues for which no data were obtained are coloured in green and the ones with $\Delta\delta_{avg} < 0.05$ ppm in black. (e) Amide groups of the binding cleft with $\Delta\delta_{avg} > 0.05$ ppm, including amides with a secondary peak, mapped on the BCX crystal structure (PDB ID: 1bcx) in spheres and coloured by the amplitude of the calculated $\Delta\delta_{avg}$ using a blue/red colour gradient. Residues for which no data were obtained are coloured in green and the ones with $\Delta\delta_{avg} < 0.05$ ppm in grey.

ES conformations

To interrogate the conformational changes of BCX in the **ES** complex an X6 titration of the protein was performed using diamagnetic and paramagnetic NMR samples (¹H-¹⁵N BCX E78Q T109C/T111C tagged with CLaNP5). Similar chemical exchange regimes during titration were observed as for BCX E78Q. The chemical shift differences between the paramagnetic and diamagnetic NMR spectra of the protein in the presence of 20 mM X6 were calculated and 105 PCSs were obtained for the $(ES)_{open}$. Ten PCSs were also calculated for $(ES)_{closed}$. Fitting of the PCS data vs. the crystal structure of the free protein yielded small variations between the tensors obtained for the E_{free} and $(ES)_{open}$ states

(**Figure 4.7**), suggesting that the lanthanoid moves slightly or the tensor reorients. As the structure of the (**ES**)_{open} state is not available, it was decided that the PCSs were best compared using the structure of the free enzyme and the tensor obtained for that state. Thus, observed PCSs of the (**ES**)_{open} were compared to the PCSs predicted from BCX crystal structure (PDB ID:2bvv) using the tensor parameters of the **E**_{free} state. Eighty-seven PCSs show a good fit with the protein crystal and multiple outliers were observed ($Q=0.115$), which suggests conformational differences between the **E**_{free} and (**ES**)_{open} states (**Figure 4.8a**). When mapped on the protein structure, the amides outliers are seen to be located within the thumb, the α -helix and the finger regions (**Figure 4.8b**).

The PCSs differences (Δ PCSs) between the (**ES**)_{open} and **E**_{free} were calculated and plotted vs. residue numbers (**Figure 4.9.c**). It reveals that at least five regions of the protein backbone experience significant changes of their conformation ($|\Delta\text{PCS}| > 0.02$ ppm) upon substrate binding and they are approximately clusters between W9-N20 and T33-N35 in the fingers; Y65-Y69 in the middle of hand palm close, to the nucleophile catalytic residue E78; A115-S117 in the thumb and A165-G173 in the hand palm, which accommodates the acid/base catalytic residue. When mapped on the protein crystal structure, those regions are spanned all over the protein β -jelly roll fold including the fingers, the thumb, the cord, the α -helix and the palm-hand (**Figure 4.9d**). This suggest that upon substrate association, the protein experiences a global conformational change. Additionally, by comparing the 10 experimental PCSs of the (**ES**)_{open} and with their counterparts in the (**ES**)_{closed}, three of them show weak structural correlation between the two states (**Figure 4.8c**). Those residues include D119 located on the tip of the thump loop and I107 and V168 positioned deep in the binding cleft (**Figure 4.8d**). Thus, (**ES**)_{open} and (**ES**)_{closed} conformations might be also different at least within the thumb and hand palm regions.

Sanson-Flamsteed Equivalent Projection

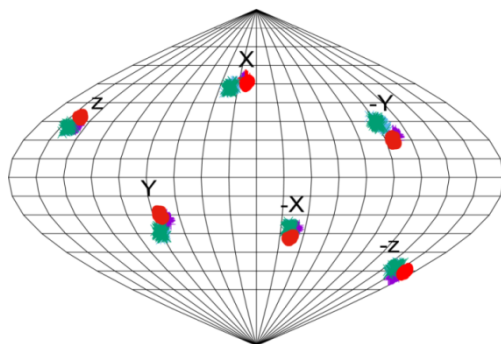


Figure 4.7: \mathbf{E}_{free} , $(\mathbf{ES})_{\text{open}}$, \mathbf{EI} and \mathbf{EP} tensors parameters and precision. One hundred $\Delta\chi$ tensors generated from jackknife analysis within Numbat for \mathbf{E}_{free} (cyan), $(\mathbf{ES})_{\text{open}}$ (purple), \mathbf{EI} (red) and \mathbf{EP} (green) placed at the center of a sphere. The locations where the X, Y, and Z components pierce the sphere are indicated. The surface of the sphere is shown as a Sanson-Flamsteed equivalent projection with gridlines at every 20° (vertical) and 10° (horizontal).

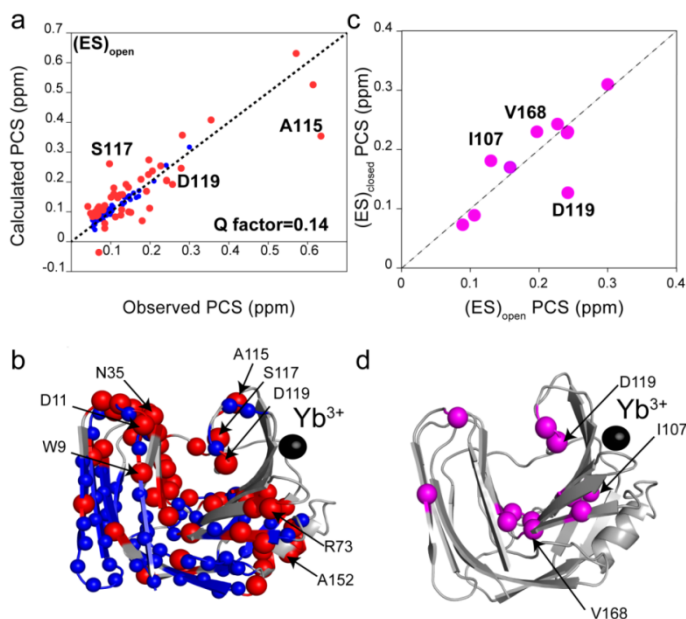


Figure 4.8. ES conformational states in solution probed by PCSs. (a) Plot of the $(\mathbf{ES})_{\text{open}}$ observed vs. calculated PCSs after fitting to the BCX crystal structure (PDB ID:2bv). Blue circles indicate PCSs with high correlation (PCS deviation < 0.02) and red circles indicate PCSs of outliers (PCS deviation > 0.02). The dashed line represents a perfect correlation. (b) $(\mathbf{ES})_{\text{open}}$ observed PCSs mapped on the BCX crystal structure (PDB ID:2bv) shown in spheres. Blue spheres indicate amide residues with high correlation to the back calculated PCSs and red spheres represent outliers. Residues with no observed PCSs are shown in grey cartoon. (c) Plot of observed PCSs of the $(\mathbf{ES})_{\text{open}}$ vs. the $(\mathbf{ES})_{\text{closed}}$ states. The dashed line represents a perfect correlation. (d) Amides for which the $(\mathbf{ES})_{\text{closed}}$ PCS could be measured mapped on the BCX crystal structure (PDB ID:2bv). The black spheres indicate the position of the lanthanide (Yb^{3+}).

ES millisecond dynamics

To investigate the dynamics of BCX in the **ES** complex, its ms time scale motions were probed. Previous study has shown a local change of a BCX protein homologue backbone dynamics when substituting the nucleophile with Ala³⁰. In the present study, the substitution E78 by Q did not cause significant changes of the protein dynamics behaviour (**Figure 4.5c**). Thereafter, a TROSY-CPMG experiment of BCX E78Q in the presence of 20 mM X6 (> 90% saturation of the primary binding site) was acquired. By analysing the relaxation dispersion profiles of the backbone amides of the (**ES**)_{open}, a remarkable enhancement of the chemical exchange was observed, as can be concluded from a comparison of R_{ex} values between the (**ES**)_{open} and **E**_{free} states (**Figure 4.9a**). Multiple protein regions experience such exchanges located mainly between W6-D11; N31-T43; N54-T72; M169-S176 of the fingers and between residues I77-V81 of the hand palm, including residue Q78 and T111-S130, covering the thumb region. All of these regions are spanning the binding cleft of the enzyme, including both the glycon (-1/-2/-3 subsites) and the aglycon (+1/+2/+3 subsites) sites (**Figure 4.9b**). A two-site exchange global fit of 30 dispersion profiles ($R_{ex} > 2 \text{ s}^{-1}$) yielded a $k_{ex} = 741 (\pm 9) \text{ s}^{-1}$ and an excited state fraction $p_B = 9.2 (\pm 0.2) \%$ (**Figure 4.4b**). The residues with enhanced R_{ex} are located in regions that experience conformational changes in the (**ES**)_{open} compared to **E**_{free}, as is revealed by the paramagnetic NMR study. For instance, the observed dynamics enhancement in the thumb regions is concomitant with pronounced Δ PCSs between the (**ES**)_{open} to the **E**_{free} states. The same observation is for the fingers, hand palm and the α -helix (**Figure 4.9d**).

The binding of the substrate may enhance the exchange effects already observed for **E**_{free} by lowering the free energy of the excited state, thus increasing its population. This is in line with the observations for the **EP** state (*vide infra*). Exchange effects could also be caused by the association and dissociation of the substrate and the underlying chemical shift perturbations of the **E**_{free} and (**ES**)_{open} states, however at 20 mM X6, the k_{ex} for the primary and secondary binding sites are 1.3 and $5.7 \cdot 10^4 \text{ s}^{-1}$, respectively. Such fast binding and dissociation will affect the RD curves negligibly. It should be noted that the PCSs are an average of all conformations that exchange faster than determined by the size of PCSs expressed in rad s^{-1} . So, in principle, the observed Δ PCSs could represent the weighted average of the PCSs in the (**ES**)_{open} ground and excited states. We believe that this cannot explain all the Δ PCSs because the excited state is populated for 9%, suggesting that the PCSs for 100% excited state would differ up to 2 ppm from the ground state. Such large differences seem unrealistic.

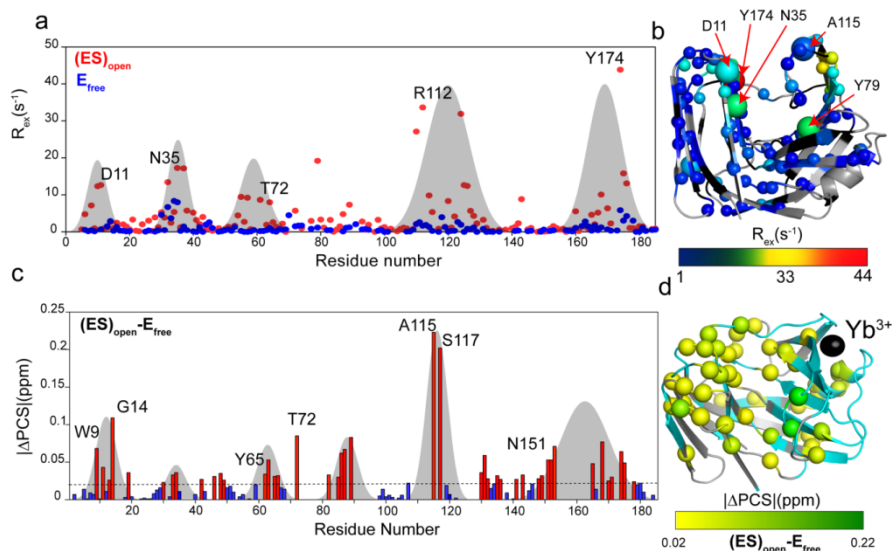


Figure 4.9. $(ES)_{open}$ millisecond time scale dynamics. **(a)** Overlay of the R_{ex} values of $(ES)_{open}$ (red circles) and BCX free states plotted versus the residue numbers. BCX regions that experience R_{ex} enhancements are highlighted with grey shade bell. **(b)** $(ES)_{open}$ complex R_{ex} values (> 1 s⁻¹) mapped on the BCX crystal structure (PDB ID: 1bcx). Backbone amides with moderate R_{ex} enhancement are shown in small spheres. Residues with a large enhancement are labelled and shown in big spheres. The residues are coloured based on their R_{ex} values by a blue/yellow/red gradient. **(c)** $|\Delta PCS|$ between BCX free state and $(ES)_{open}$ states plotted versus the residue numbers to show the correlation between dynamics behaviour and PCSs changes in the $(ES)_{open}$ state. Outliers from the PCSs fit to the BCX crystal structure are shown in red bars. Protein regions with $|\Delta PCS| > 0.02$ ppm are highlighted with a grey shade bell. **(d)** $|\Delta PCS|$ mapped on the BCX crystal structure. Residues with $|\Delta PCS| > 0.02$ are shown in spheres and coloured in yellow/green gradient indicating the strength of the $|\Delta PCS|$. Residues with $|\Delta PCS| < 0.02$ ppm are shown in grey cartoon and residues with non-determined $|\Delta PCS|$ coloured in cyan. The black spheres indicate the position of the lanthanoid (Yb^{3+}).

BCX intermediate state (EI) conformation

Previously, the BCX intermediate state was trapped using a fluorinated substrate 2,4-dinitrophenyl-2-deoxy-2-fluoro-b-xylobioside (DNP-2FXb)^{32,33}. The fluoride at the C2 position of the compound destabilizes the oxocarbenium transition state of the reaction, thus slowing the deglycosylation step and the good 2,4-dinitrophenolate leaving group warrants fast glycosylation of the enzyme. Therefore, the enzyme is trapped into its glycosylated form with a complex half-life of ~ 6 h at 40°C (**Figure 4.10a**). Here, an epoxide-xylobiose (epoxyX2) mechanism based inactivator was used to covalently trap the enzyme in its EI state. The inactivation mechanism involves the attack of the ligand epoxide active center by the enzyme nucleophile, resulting in ring opening and the formation of a covalent bond between the enzyme nucleophile and the inhibitor, which perfectly emulates EI state of the natural substrate hydrolysis reaction. The process is facilitated by protonation of the inactivator reactive center by the general acid/base

residue (**Figure 4.10b**). To generate the covalent complex, BCX was incubated with epoxyX2 at 1:20 ratio at 30°C. The reduction of BCX enzymatic activity was monitored over time using 4MU-xylobiose. After 4h of incubation no residual activity remained and the complex formation was identified by mass spectrometry after discarding the excess ligand by buffer exchange (**Figure 4.11a**). The complex was stable for months at room temperature. To investigate the binding site of the ligand within the protein binding cleft, a ^{15}N uniformly labelled sample of the **EI** was prepared for HSQC spectrum acquisition. By overlaying the **EI** with the protein free state spectrum \mathbf{E}_{free} significant chemical shift perturbations were observed suggesting changes of the chemical environment of the backbone amides, either due to ligand binding or due to conformational changes experienced by the protein upon covalent complex formation (**Figure 4.11b**).

Due to these substantial chemical shift differences, it was difficult to accurately assign the **EI** spectrum only from the free enzyme peak list, so a ^{15}N ^{13}C double labelled **EI** sample was prepared and used for triple resonance experiments for backbone assignment. In the **EI** spectrum three residues were missing, presumably due to peak broadening, including E78, which is supposed to covalently bind to the C1 of the ligand, G70 and S117, which are in contact with the -1 subsite xylobiose sugar unit, according to BCX-2FXb crystal structure (PDB ID: 1bcx)³². The $\Delta\delta_{\text{avg}}$ between the \mathbf{E}_{free} and **EI** states are plotted as function of the residue numbers in **Figure 4.12a**. Several clusters of amides show pronounced chemical shift perturbations between 0.1 and 0.6 ppm. Mapping the $\Delta\delta_{\text{avg}}$ on the protein crystal structure (**Figure 4.12b**) revealed that all of the observed perturbations are located within the protein binding site cleft, in the fingers and the thumb regions. The most significantly shifted residues are Y79, Y80 and V81, in the vicinity of the catalytic nucleophile E78 and also residues G173, Y174 and Q175, close to the catalytic acid/base E172. These observations point toward a correct covalent modification of the protein E78 nucleophile by the ligand and its correct positioning within the enzyme binding site. Although the ligand is supposed to only occupy the -1/ -2 subsites of the enzyme binding cleft, chemical shift perturbations were also observed in the +1/ +2 subsites. The distal chemical shift perturbations suggest changes in the protein conformation upon **EI** complex formation. To establish the presence of conformational changes in BCX upon formation of the **EI** state, diamagnetic and paramagnetic uniformly ^{15}N labelled samples of the **EI** complex were prepared using the procedure described above and 122 PCSs were obtained. To be consistent with the analysis of the $(\mathbf{ES})_{\text{open}}$ state, the observed PCSs of the **EI** were compared to the PCSs predicted from BCX crystal structure (PDB ID:1bcx) using the tensor parameters of the \mathbf{E}_{free} . Multiple outliers were observed suggesting that the crystal structure is not a good representation of the epoxyX2 structure in solution (**Figure 4.12e**). Most of the backbone amides PCSs, especially the ones in the fingers regions, are well correlated with the back-calculated PCSs from the protein crystal structure. Eighteen outliers were observed, mainly located

within the thumb region (**Figure 4.12f**). This suggests a different conformation of the thumb region in the **EI** solution state compared to its crystalline state.

The differences between the observed PCSs of the **EI** complex and E_{free} state ($|\Delta\text{PCSs}|$) indicate also structural changes between the two states of the enzyme in solution (**Figure 4.12c**). The major $|\Delta\text{PCSs}|$ (≥ 0.02 ppm) are located within the enzyme binding cleft, the thumb and the finger regions, in addition to the C-terminal side of the α -helix (**Figure 4.12d**). For instance, residues G70, W71 and T72 and D119 show remarkable ΔPCSs . T72 is next to R73 which is connected to the tip the thumb region through a salt-bridge interaction with residue D119, therefore, it is plausible that any conformational changes experienced by the thumb results in effects on R73 and surrounding residues. Thus, these observations suggest that the thumb in the **EI** state adopts a different conformation than in the free state. W9 shows a ΔPCS of 0.07 which could stem from its different conformational when forming a $\text{CH}-\pi$ stacking interaction with the ligand sugar ring at the -2 subsite, as revealed from the BCX-2FXb crystal structure³². The other residues are in close proximity to E78, which forms a covalent bond with the ligand. Residues T171 and Y174 located in the fingers regions of the +1/ +2 subsites also seem to experience structural changes in the **EI** state, being close to E172 acid/base residue. Correlations between ΔPCSs and $\Delta\delta_{\text{avg}}$ are observed suggesting the simultaneous contributions of ligand binding and its induced conformational changes on the protein structure into the significant differences between the **EI** and the E_{free} HSQCs spectra (**Figure 4.12a,c**).

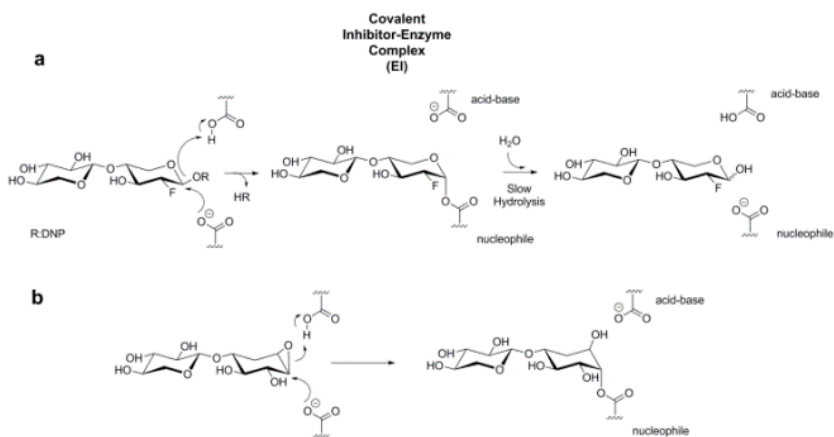


Figure 4.10. **EI** covalent complex formation by the DNP-2FXb (**a**) and the epoxyX2 (**b**).

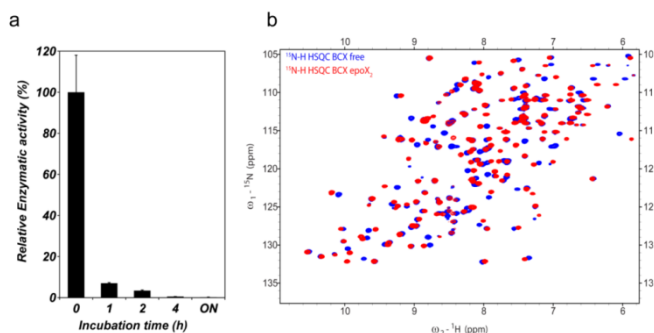


Figure 4.11. BCX-epoxyX2 complex formation. **(a)** Residual BCX activity monitored over course of incubation at 30 °C in the presence of 1:20 (BCX: epoxyX2) ratio. Error bars indicate \pm SD of a duplicate. **(b)** ^1H - ^{15}N HSQC spectra overlay of the \mathbf{E}_{free} and \mathbf{EI} states.

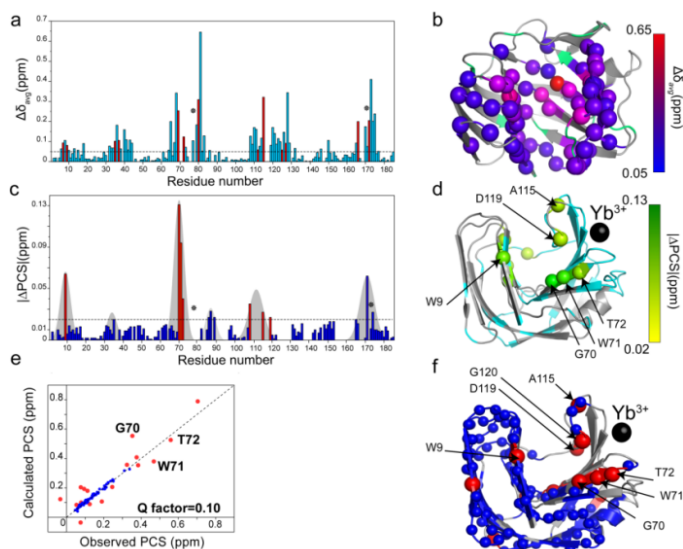


Figure 4.12. The BCX-epoxyX2 complex (\mathbf{EI}). **(a)** $\Delta\delta_{\text{avg}}$ plotted versus BCX residue numbers. Residues that have direct interactions with the ligand (according to BCX crystal structure PDB ID: 1bcx) are shown in red bars. The positions of the E78/E172 catalytic dyad are marked with asterisks. **(b)** Amino acid residues with $\Delta\delta_{\text{avg}} > 0.05$ ppm mapped on the BCX crystal structure (PDB ID: 1bcx) and coloured with a blue/red gradient. Residues with $\Delta\delta_{\text{avg}} < 0.05$ are shown in grey cartoon and the ones with non-determined $\Delta\delta_{\text{avg}}$ in green cartoon. **(c)** $|\Delta\text{PCS}|$ plotted versus the residue numbers. Outliers of the PCSs fit to the BCX crystal structure are shown in red bars. The positions of the catalytic dyad are marked with asterisks. Protein regions with $|\Delta\text{PCS}| > 0.02$ ppm are highlighted with a grey shade bell. **(d)** $|\Delta\text{PCS}|$ mapped on the BCX crystal structure. Residues with $|\Delta\text{PCS}| > 0.02$ are shown in spheres and coloured by a yellow/green gradient based on $|\Delta\text{PCS}|$ strength. Residues with $|\Delta\text{PCS}| < 0.02$ are shown in grey cartoon and the ones with non-observed $|\Delta\text{PCS}|$ in cyan cartoon. The black sphere indicates the position of the lanthanide (Yb^{3+}). **(e)** Plot of the observed \mathbf{EI} PCSs vs. calculated PCSs after fitting to the BCX crystal structure (PDB ID:1bcx) using \mathbf{E}_{free} tensor parameters. Blue circles indicate PCSs with a deviation < 0.02 and red circles indicate PCSs of outliers (PCS deviation > 0.02). **(f)** \mathbf{EI} observed PCSs mapped on the BCX crystal structure. Blue spheres indicate residues with the good correlation between experimental and predicted PCSs and red spheres indicate the outliers. Amides with non-observed PCSs are shown in grey cartoon.

EI dynamics

The previous study of the **EI** dynamics was performed for the ns to ps time scale, revealing no major changes of the dynamics on the probed time scales compared to its free state³³. Here, the ms time scale chemical exchange of **EI** was probed by performing a CPMG RD experiment. Thirty-one residues show dispersion profiles ($R_{\text{ex}} \geq 1 \text{ s}^{-1}$), and these are located within the fingers region at the -1/ -2 subsites of the binding cleft in the proximity of the acid/base catalytic residue and the E78 nucleophile covalently bound to the ligand (**Figure 4.13a,b**). No chemical exchange was observed in the thumb region. The global fit of 15 residues with a $R_{\text{ex}} \geq 1.8 \text{ s}^{-1}$ revealed a $k_{\text{ex}} = 2.05 (\pm 0.08) \times 10^3 \text{ s}^{-1}$ and an excited state fraction p_B of 0.6% (**Figure 4.4c**). A few residues show dynamic enhancement compared to the E_{free} as can be seen from the R_{ex} comparison between the two states (**Figure 4.13a**). The most pronounced changes are for residues I77, R112, T123 and T124, which are located in the vicinity of E78 and for residue G173, located next to E172, the acid base in the -1 subsites. A lesser R_{ex} increase is observed for residues W9, D11, G13 and G14, located in the -2 subsites in direct contact with the non-reducing end sugar ring of the ligand (**Figure 4.13c**). Concomitantly, residues T72, R73 and S74, located in a loop that connects the tip of the thumb to β -strands 6 and 7, show a reduction of their chemical exchanges, presumably as a result of the decrease of the thumb motion by ligand binding. Those residues also experience local conformational changes as concluded from their ΔPCSs (see above). As a conclusion, in the **EI** state the protein does not experience global dynamics changes, but it seems to assume local conformational changes, mainly located in the fingers and the thumb at the aglycon binding site, where the ligand is covalently bound. However, few local chemical exchange enhancements were observed for residues surrounding the nucleophile and acid/base catalytic dyad presumably as a result of the covalent ligand binding. A slight reduction of the thumb and its surrounding loops in the ms time scale motion is noticed compared to E_{free} in solution (**Figure 4.13c**). The ms dynamics and PCSs studies suggest a different **EI** in solution average structure with local changes of the protein dynamics behaviour compared to the free state.

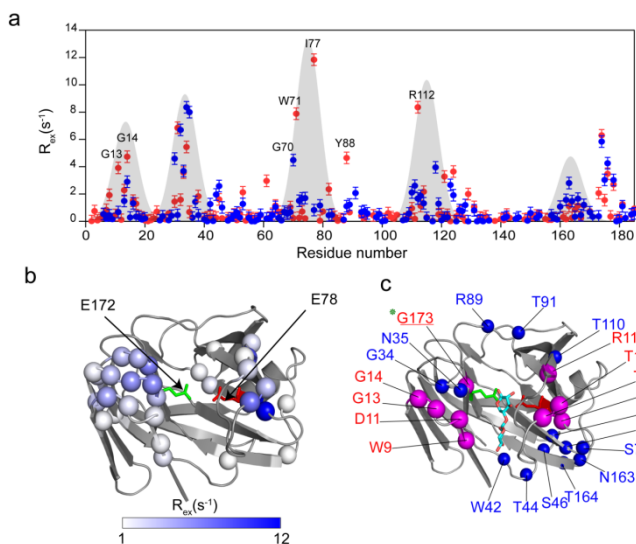


Figure 4.13. EI millisecond time scale dynamics. (a) Overlay between the R_{ex} values of the **EI** complex state (red circles) and **E_{free}** state plotted against the residue numbers. Regions that show differences of R_{ex} between the two states are highlighted with a grey shade bells. (b) **EI** complex R_{ex} values ($> 1 \text{ s}^{-1}$) mapped in spheres on the BCX crystal structure (PDB ID: 1bcx) and coloured in a white/blue gradient. Residues with $R_{ex} < 1 \text{ s}^{-1}$ are shown in grey cartoon. E172 and E78 are shown in sticks and coloured in green and red, respectively. (c) Residues that show an R_{ex} enhancement or reduction in the **EI** state are mapped on BCX crystal structure (PDB ID: 1bcx) and shown in pink and blue spheres, respectively. The catalytic dyad E78 and E172 are displayed in stick and coloured in red and green, respectively. Residues in the proximity of the catalytic dyad are indicated in asterisks. The DNP-2FXb ligand of BCX crystal structure is displayed in sticks³².

BCX product (EP) complex conformation

The last step of xylanases enzymatic reaction is the product release from the -1/-2 /-3 subsites of the enzyme binding cleft. The binding mode of the product X2 in BCX cleft was monitored by an NMR titration using 1.3 mM, 13 mM, 65 mM and 130 mM ligand concentrations. The observed $\Delta\delta_{avg}$ are in the fast exchange regime, exhibiting progressive chemical shift changes. In contrast to the **ES** state, neither line broadening nor the appearance of secondary peaks was observed at high substrate concentration. Residues in the vicinity of the nucleophile and acid/base catalytic dyad at the -1/-2 subsites show significant $\Delta\delta_{avg}$, (**Figure 4.14a**). However, residues of the +1/+2 subsites do not show any chemical shift changes, which suggests differences in the binding affinity between the glycon and aglycon subsites. Substantial chemical shift changes ($> 0.1 \text{ ppm}$) were observed for residues of the thumb regions, for instance S117 and D119 and for residues T69 and V37 located near the E78 and E172 catalytic dyad, respectively (**Figure 4.14b**). In addition, residues V168 and M169 positioned deep in the middle of the hand palm, approximately 10 \AA distant from the catalytic dyad experience also significant $\Delta\delta_{avg}$. The peak shape analysis of the HSQC spectra confirmed the absence of large peak broadening and revealed a dissociation constant of 10 mM and a $k_{off} = 3.1(\pm 0.2) \times 10^3 \text{ s}^{-1}$. Next, the local conformational changes of BCX upon ligand association were

investigated. Using the procedure described above, the changes in PCSs in every titration point were followed. The observed PCSs of the **EP** were compared to the PCSs predicted from BCX crystal structure (PDB ID:2bvv) using the tensor parameters of the \mathbf{E}_{free} state in line with the analysis of the PCSs of the other states. The majority of the 125 PCSs correlate well with the predicted ones ($Q = 0.077$) with a few outliers located in the thumb loop (A115, S117, D119 and R122) (**Figure 4.14c,d**). The $|\Delta\text{PCSs}|$ between the free and **EP** states are plotted in **Figure 4.15C**. $|\Delta\text{PCSs}|$ showed dependence on ligand concentration and the subtle structural changes upon ligand binding occur in the thumb and the α -helix (**Figure 4.15c,d**).

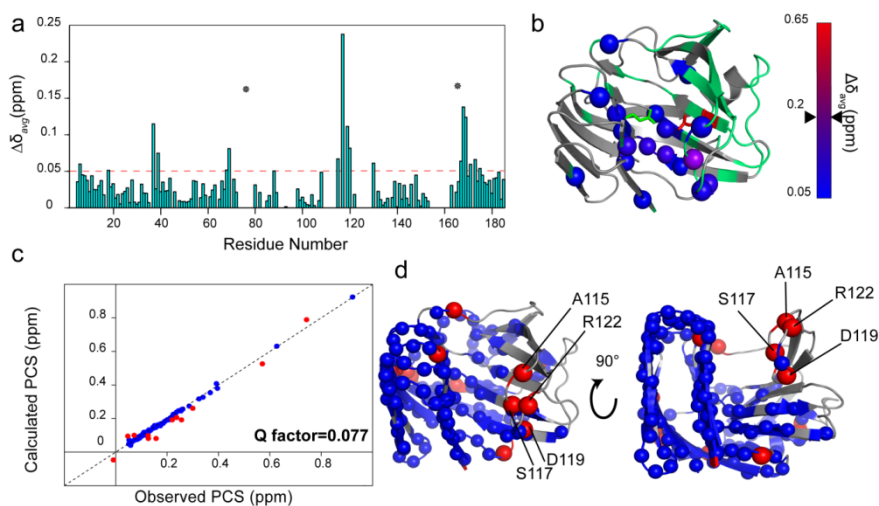


Figure 4.14. The EP complex. (a) $\Delta\delta_{\text{avg}}$ plotted against BCX residues numbers. Positions of the E78/E172 catalytic dyad are indicated with asterisks. (b) Residues with $\Delta\delta_{\text{avg}} > 0.05$ ppm are mapped on the BCX crystal structure (PDB ID:2bvv) in spheres and coloured with a blue/red gradient using the maximum $\Delta\delta_{\text{avg}}$ value observed in the EI state as a colour gradient threshold for comparison. The colour gradient position of the maximum $\Delta\delta_{\text{avg}}$ (0.2 ppm) in the **EP** state is indicated by triangles. Amide residues with $\Delta\delta_{\text{avg}} < 0.05$ ppm are displayed in grey cartoon and the amides with non-determined $\Delta\delta_{\text{avg}}$ in green cartoon. (c) Observed PCSs vs. calculated of the **EP** state after fitting to the BCX crystal structure (PDB ID:2bvv). Blue circles indicate good correlation between the observed PCSs and the back-calculated ones. Red circles indicate outliers (>0.02). (d) **EP** observed PCSs mapped on the BCX crystal structure. Blue spheres indicate the positions of residues with good correlation between their observed PCSs and calculated PCSs. Red spheres indicated the structural positions of the outliers. Only residues of the protein thumb regions are named.

EP dynamics on the millisecond time scale

The paramagnetic NMR analysis suggests that in the **EP** state the protein adopts a slightly different conformation compared to the free form. However, in the presence of 130 mM X2 the protein exhibits a remarkable enhancement of exchange (R_{ex} up to 31 s^{-1}) in regions located within and on both sides of the binding cleft. The R_{ex} of the **E_{free}** and **EP** states are plotted in **Figure 4.15a** for comparison. The most significantly affected regions are clustered approximately between residues N32-F36 ($7\text{ s}^{-1} \leq R_{ex} \leq 31\text{ s}^{-1}$), forming a loop that connects β -strands 3 and 4 in the -1 subsite of the fingers; between residues Y69-Y80 ($7\text{ s}^{-1} \leq R_{ex} \leq 21\text{ s}^{-1}$) in β -strands 7 and 8 of the palm, including the nucleophile E78; between R112-Q127 ($1.5\text{ s}^{-1} \leq R_{ex} \leq 31\text{ s}^{-1}$) that forms the thumb loop and between T171-S176 that accommodates the acid/base E172 (**Figure 4.15b**). Other residues remote from the active site (S140-T143, positioned on the non-catalytic side of the palm) experience smaller exchange effects. A global two-site exchange fit of 36 residues ($R_{ex} \geq 1.8\text{ s}^{-1}$) yielded a $k_{ex} = 1.53 (\pm 18) \times 10^3\text{ s}^{-1}$ and an excited state population of 4% (**Figure 4.4**). The peaks shape analysis of BCX titration with 130 mM X2 ($> 92\%$ saturation) revealed a dissociation rate constant $k_{off} = 3.1 (\pm 0.2) \times 10^3\text{ s}^{-1}$ (see above). At 92% saturation, k_{ex} can be calculated to be $3.9 \times 10^4\text{ s}^{-1}$, which is outside the range of CPMG RD time window. Therefore, it is assumed that the observed enhancement of the protein amide chemical exchange is dominated by structural fluctuations in the **EP** state rather than ligand dissociation. Interestingly, residues like G70 and R112 in the vicinity of E78 and residues N35 and S117 of the fingers and the thumb loop, respectively, show a distinctive increase of their dispersion profiles compared to the free state. N35 and S117 resides on the top of both side of the binding cleft, separated by $\sim 12\text{ \AA}$ distance (**Figure 4.15b**). The tremendous enhancement of their R_{ex} might reflect their involvement in the structural fluctuation of the binding cleft width while the ligand is associated to the protein. Additionally, regions that experience changes of their dynamics properties are also involved in conformational changes in the **EP** state as suggested by $\Delta\delta_{avg}$ and $\Delta PCSs$ (**Figure 4.15c,d**).

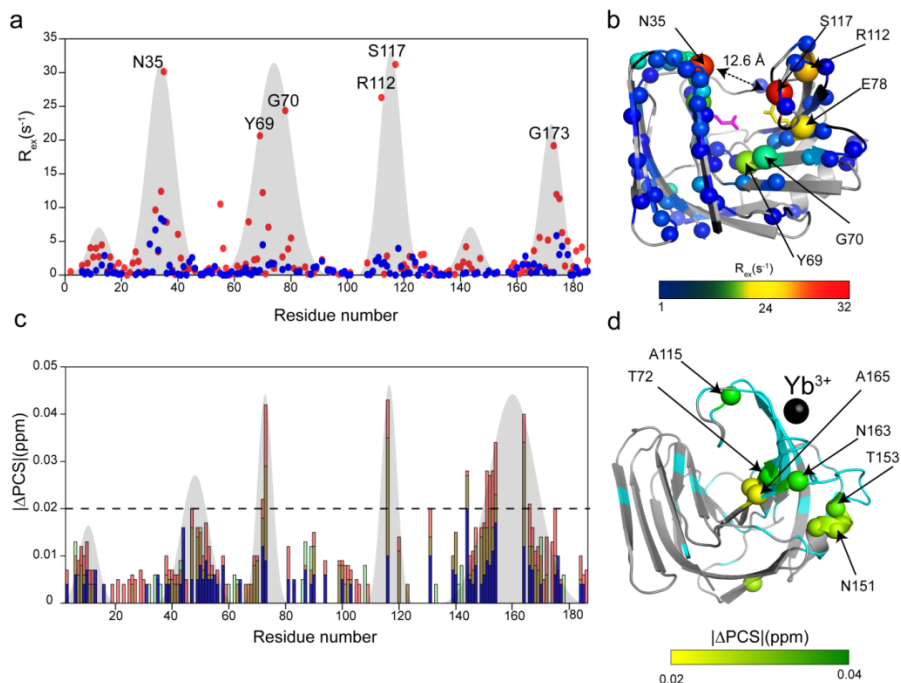


Figure 4.15. EP millisecond time scale dynamics. (a) Overlay between the R_{ex} values of **EP** complex state (red circles) and the **BCX** free state plotted against the residue numbers. **BCX** regions that experience Rex enhancements are highlighted with grey rectangles. (b) **EP** complex R_{ex} values ($> 1 \text{ s}^{-1}$) mapped on the **BCX** crystal structure (PDB ID: 1bcx). Residues with moderate R_{ex} enhancement are shown in small spheres. Residues with a remarkable enhancement are shown in big spheres. The residues are coloured based on their R_{ex} values by a blue/yellow/red gradient. (c) $|\Delta\text{PCSs}|$ between the **EP** and **E_{free}** states plotted against the residue numbers. $|\Delta\text{PCSs}|$ in the presence of 13 mM X2 are displayed in blue bars; the ones in the presence of 65 mM X2 are displayed in green bars and the ones in the presence of 130 mM X2 are in red bars. Protein regions that show ligand dependency of their $|\Delta\text{PCSs}|$ are highlighted in grey shade bell. (d) Amino acid residues with $|\Delta\text{PCSs}| > 0.02 \text{ ppm}$ are shown in spheres on the **BCX** crystal structure (PDB ID: 2bv) and coloured with a yellow/green gradient. Residues with $|\Delta\text{PCSs}| < 0.02$ are displayed in grey cartoon and the ones with non-determined $|\Delta\text{PCSs}|$ are shown in cyan cartoon. The black sphere indicates the position of the lanthanide (Yb^{3+}).

Discussion

BCX substrate binding modes and conformational landscape during catalysis

To investigate **BCX** substrate binding mechanism and follow its conformational changes during catalysis ^1H - ^{15}N HSQC NMR titrations and PCSs were used. Together, these approaches provided detailed information about the substrate binding site location and the binding kinetics in conjunction with indications of conformational changes during the enzyme catalytic pathway.

CHAPTER 4

The fit of the experimental PCSs for free BCX to the protein crystal structure (PDB ID:2bv_v)³² revealed a good agreement between the solution and crystalline ground states. Second, the binding kinetics of BCX to a substrate (X6, **ES** complex) was examined by NMR titration. For this purpose, the E78 nucleophile of the enzyme was substituted for Q, abolishing catalytic activity. During the course of titration, a complex chemical shift perturbation pattern of the backbone amide groups was observed concomitant with general line broadening. This effect was attributed to an increased viscosity caused by the xylose oligosaccharides. Viscosity determine the rotational diffusion time and thus relaxation rates of the protein. Similar observations were made in previous reports³⁴. Chemical shifts changes in the fast exchange regime were noticed for the amides that form the secondary binding site³⁴. Interestingly, at a X6 concentration at which BCX is partially saturated, new secondary peaks emerged for multiple backbone amides located within the binding cleft and its surrounding, indicating the existence of two **ES** bound states. The line shape analysis of the peaks showing this behaviour is suggests an “induced fit” binding mechanism. Therefore, it is hypothesised that in the **ES** state the substrate first binds to the protein in an open form (**ES**)_{open} inducing a global closure of its binding cleft (**ES**)_{closed}. The exchange rate of this process is 20 s⁻¹, which coincides with the hydrolysis rate of BCX artificial substrate PNP-X2, therefore the open and close motion of the protein binding cleft might play a role in substrate turnover³⁶.

To interrogate the different conformations of the **ES** state, the PCSs of the (**ES**)_{open} and (**ES**)_{closed} complexes were measured. The PCSs fit of (**ES**)_{open} to the BCX crystal structure (PDB ID: 2bv_v) shows multiple outliers located within the binding cleft especially for residues that form the thumb, fingers and the α -helix and including also residues in the middle of the hand-palm. The PCSs differences between the free and the (**ES**)_{open} revealed further conformational changes of the protein on both sides of the catalytic cleft, including residues that form the β -strands A and B. Thus, it was concluded that the (**ES**)_{open} conformation is different from the one observed in the free protein. Those pronounce conformational changes of the protein structure might be consequence of simultaneous binding of the substrate in the aglycon and glycon subsites because such large effects are not observed when titrating with X2 (see below). Additionally, the few PCSs measured for residues that exhibit a resonance in the (**ES**)_{closed} state included three amides that do not correlate well with their PCSs in the (**ES**)_{open} state. Those amino acid residues were located in the thumb and deep in the hand palm. Therefore, it is concluded that substrate binding in the **ES** state follows an induced fit mechanism, which provoke two-bound states, none of them resemble the free state conformation of the protein. Previous studies on GH11 xylanases titration with oligosaccharides did not report the same observations^{30, 34}. The structure obtained by co-crystallization of a silenced variant of GH11 xylanase from *Trichoderma reesei* with X6 shows a movement of the thumb region toward the ligand (2 Å compared to the free protein) enabling the formation of close interactions with xylose subunits at the -1/-2/-3 subsites³⁷. This thumb motion might occur in the BCX **ES**

CHAPTER 4

complex in solution, although it is assumed that these local conformational changes in the thumb may not explain the observed global conformational changes of the binding cleft in the (**ES**)_{open} state, as suggested by PCSs.

The next step was to characterize the enzyme in the intermediate state of the reaction (**EI**) by using an epoxy-xylobiose (epoxyX2) compound, which forms an adduct to the enzyme. CSPs were not only observed for residues at the -1/-2, subsites, including the thumb and the fingers, but also for distal residues in the aglycon pocket, suggesting the occurrence of a conformational change upon adduct formation. The **EI** PCSs fits to the **EI** crystal structure (PDB ID: lbcx) revealed multiple outliers for amides located mostly in the thumb region an indication for a different conformation in solution.

The map of $|\Delta\text{PCSs}|$ between the **EI** and **E_{free}** states showed that residues involved in direct interactions with the ligand experience the most significant conformational changes. Therefore, both the thumb and residues at the -1/-2 subsites seem to adopt a new conformation when the protein is covalently bound to the ligand.

In the **EI** complex an outward displacement of thumb was observed in XynII crystallized with epoxyalkyl xylobiosides³⁸ and also a 1.1 Å thumb displacement was observed in the BCX crystal structure when bound to the 2FXb compared to its free form³². Nevertheless, the fit of the **EI** PCSs to the BCX intermediate-state structure did not show a good correlation, suggesting that the **EI** adopts a conformation in solution that differs from the one in the crystal.

The last step of the reaction is the product release from the glycon pocket. Studying the chemical shift perturbations upon protein titration with X2 revealed a ligand binding in the fast exchange regime with $k_{\text{off}} = 3.1 (\pm 0.2) \times 10^3 \text{ s}^{-1}$. No minor peaks were observed at high product concentration, contrary to the titration with X6. The ligand seems to occupy only the -1/-2 subsites not the +1/+2 subsites. This suggests a difference in the binding sites affinities between the glycon and aglycon sites towards the product. These differences in affinity might be an adopted mechanism by the enzyme to facilitate the dissociation of the leaving group from the aglycon site. The paramagnetic NMR experiments on the **EP** complex revealed that the **EP** complex structure exhibits only small deviations from the **E_{free}** crystalline state, localized in the glycon site, in the thumb (-1/-2 subsite) and the α -helix.

The **EP** complex has been trapped by co-crystallizing a GH11 xylanase from *Trichoderma reesei* with X6 due to the substantial reduction of its catalytic activity by single point mutation. The only significant conformational changes of the protein in the **EP** complex were observed in the thumb region where the atoms move closer to the product compared to their position in the ligand free structure of the mutant³⁷.

Therefore, based on crystallography studies of GH11 xylanases in complex with covalent and non-covalent ligands, the thumb region of the β -jelly roll fold might experience two types of movement: a movement that brings the thumb closer to the substrate in the case of non-covalent ligands, while in the **EI** complex the thumb experiences a backward

movement, which seems to assist the accommodation of the covalent ligands into the -1/-2 subsites. It is speculated that the modulation of the thumb region conformations by the covalent and the non-covalent forms might play a role in positioning the substrate into the correct configuration to facilitate the glycosidic link hydrolysis and also to assist the product release from binding cleft in the final step of the catalytic reaction.

This study of BCX covalently and non-covalently bound to its ligands revealed conformational changes not only of the thumb region but also within the α -helix and its binding cleft. The conformational changes depend also on the length of the bound substrate and on the occupancy of the protein glycon and aglycon sites.

BCX dynamics during catalysis

After studying the different average conformations of the protein in each step of its catalytic cycle, it was aimed to follow the ms time scale motions to investigate if there is an interconnection through their sampled excited states. The enzyme in the free state shows small chemical exchange effects for residues located mainly within the finger and the thumb regions. A two-site exchange model fit of the dispersion data revealed a $k_{ex} = 2.5 \times 10^3 \text{ s}^{-1}$ and a population of the excited state p_B of 0.7%. The global rate of xylanase B2 (XlnB2) from *Streptomyces lividans* conformational exchange is equal to $k_{ex} = 1.2 \times 10^3 \text{ s}^{-1}$ for several residues in the fingers, yet no chemical exchange was observed in the thumb³⁰.

Next, the dynamics behaviour of the enzyme in the $(\mathbf{ES})_{open}$ state was examined by using a silenced version of the enzyme in the presence of X6 as a substrate. A global ms time motion enhancement was observed with a prominent increase of the R_{ex} (up to 50 s^{-1}). Amino acid residues that sculpture the binding cleft in addition to residues remote from the binding site experienced exchange.

Residues with enhanced R_{ex} exchange were also identified to experience conformational changes in the $(\mathbf{ES})_{open}$ upon ligand binding. The calculated k_{ex} of the substrate binding in the binding cleft and secondary binding site are 1.3 and $5.7 \times 10^4 \text{ s}^{-1}$ respectively, which falls outside the time scale window of the CPMG RD experiment. Therefore, the contributions of the dissociation process to the RD are considered negligible and the observed ms motion enhancement seems to be dominated by the intrinsic structural fluctuations of the protein in the $(\mathbf{ES})_{open}$ state.

The enhancement of the ms time scale dynamics was also observed in the case of XlnB2 in the presence of xylopentaose with an increase in its global k_{ex} from $1.2 \times 10^3 \text{ s}^{-1}$ to $3 \times 10^3 \text{ s}^{-1}$. Residues of the fingers region, hand palm and thumb showed significant conformational exchanges leading to the conclusion that the substrate triggers the ms motion of the protein especially in the thumb, which was observed to be rigid in the free state³⁰. However, in BCX, substrate binding reduces the k_{ex} from $2.5 \times 10^3 \text{ s}^{-1}$ in the free state to 740 s^{-1} in the $(\mathbf{ES})_{open}$ complex. The explanation for the different substrate effects

between the two homologues (40% primary sequence identity) of GH11 xylanases is unclear.

The **EI** complex experiences subtle dynamics changes compared to the free protein with $k_{\text{ex}} = 2 (\pm 0.08) \times 10^3 \text{ s}^{-1}$ and $p_{\text{B}} = 0.6 \%$, when fitted to a global two-site exchange model. Nonetheless, local chemical exchange enhancement of residues in the vicinity of the catalytic dyad were observed, concomitant with a reduction of the thumb region dynamics and its surrounding loops, presumably due to the covalent ligand binding.

The last step of the reaction is the product dissociation from the enzyme binding site. By following the dynamic of the **EP** state, a pronounced enhancement of the ms time scale chemical exchange was observed although to a lesser degree than in the ES complex. Significant R_{ex} increases were noticed for amides of the thumb and the fingers at the -1/-2 subsites. The global fit of the dispersion profile to a two-site exchange model revealed a $k_{\text{ex}} = 1.5 \times 10^3 \text{ s}^{-1}$ and 4% of the protein in the excited state. The observed increase of the protein dynamics is not related to $\Delta\delta_{\text{avg}}$ caused by ligand binding ($k_{\text{ex}} = 3.9 \times 10^4 \text{ s}^{-1}$).

All of the mentioned observations indicate a diversity in the protein dynamics behaviour in each step of the catalytic cycle, which depends on the substrate mode of binding (covalent or non-covalent) and also on its length (number of sugars units). To unravel the conformational connections between the BCX ground states, a comparison between the $\Delta\delta_{\text{N}}$ and the $\Delta\omega_{\text{N}}$ from the global CPMG RD data fits was performed. No correlations between the $\Delta\omega_{\text{N}}$ values of the **E_{free}** and **EI** excited states with the $\Delta\delta_{\text{N}}$ of the (**ES**)_{open} and the **EP** were observed, suggesting that those excited states are not interconnected (**Figure 4.16a,b**). A correlation was observed, however, between $\Delta\omega_{\text{N}}$ values of (**ES**)_{open} excited state and the $\Delta\delta_{\text{N}}$ of the **EI** ground state (**Figure 4.17a**). For instance, residues N114, F125, T126, Q127 and Y128, clustered in the thumb region, show a remarkable correlation with a $R^2=0.8$ (**Figure 4.17c**). Additionally, Y79, located next to E78 that form a covalent bond with the ligand in the **EI** state, show also a strong correlation. These observations suggest that the conformation of the thumb and residues proximal to the nucleophile in the (**ES**)_{open} excited state resemble the adopted conformation in the **EI** ground state. Similarly, a correlation between the **EP** excited and **EI** ground states is observed, for residues I77, Y79 and Y80 in close proximity of the E78 nucleophile in conjunction to N114 and T126 of the thumb region (**Figure 4.17b,d**). This suggests that also the **EP** complex visits the **EI** conformation. Based on these observations, it is proposed that the (**ES**)_{open} and **EP** ground states are connected through an excited state conformation in which the thumb and the proximal residues of the nucleophile adopt a conformation that resembles the one observed in the **EI** ground state.

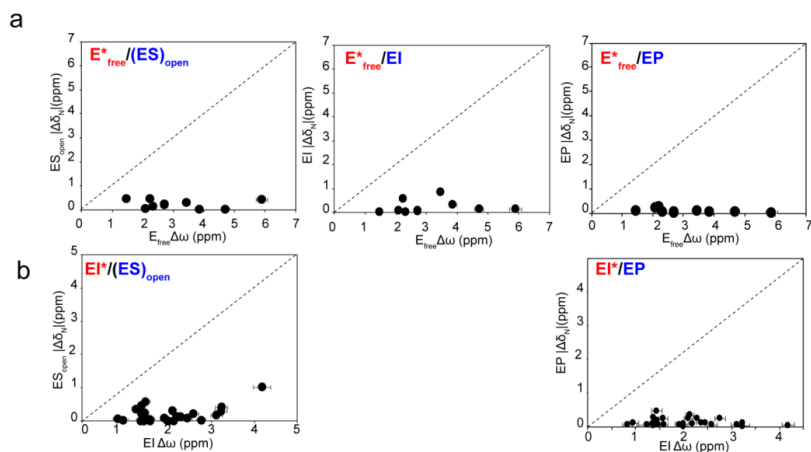


Figure 4.16. Correlation between the $\Delta\omega$ from global residues fits of the CPMG RD data with the $\Delta\delta_N$ of the NMR titration data. **(a)** The $\Delta\omega$ of the E_{free} excited state plotted against the $\Delta\delta_N$ of the $(ES)_{\text{open}}$, EI and EP ground states. **(b)** The $\Delta\omega$ of the EI excited state plotted against the $\Delta\delta_N$ of the $(ES)_{\text{open}}$ and EP ground states. Excited states are indicated in red and marked with asterisks and ground states in blue.

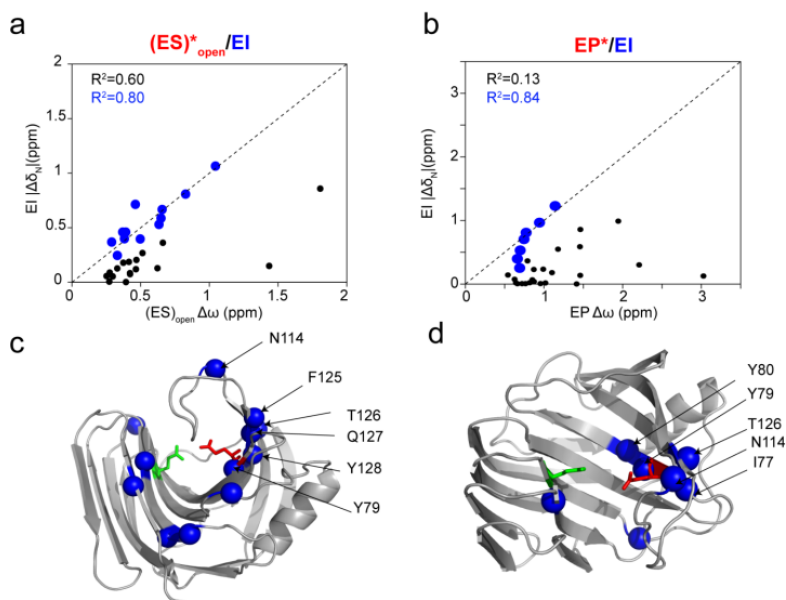


Figure 4.17. Correlation between excited states and the EI ground state. **(a, b)** Correlation of $\Delta\omega$ of the $(ES)_{\text{open}}$ excited state **(a)** and the EP excited state **(b)** with the $\Delta\delta_N$ of EI state. Good correlations are shown in blue circles and the poor ones in black dots. The correlation factor (R^2) is indicated using the same colour code. **(c, d)** Backbone amides that show a good correlation for $(ES)_{\text{open}}$ **(c)** and EP **(d)** excited state chemical shifts with EI ground state chemical shifts are mapped on the BCX crystal structure (PDB ID:2bv) in blue spheres. Some residues are labelled. Acid/base and nucleophilic catalytic residues are shown in green and red, respectively.

Conclusions

The aim of this study was to follow the conformational changes and dynamics of GH11 xylanase during their catalytic pathway, using BCX as a model. The titration and paramagnetic NMR experiments identified different binding modes of the enzymes to its substrate and product, which seems to be concomitant with changes of the protein conformation. The conformational changes are dependent on the mode of the ligand interactions (non-covalent versus covalent) and also on the glycon and aglycon binding sites occupancy.

MD simulations by Muilu et al. on XYNII from *Trichoderma reesei*, captured in different crystalline states, suggested that the protein samples three sequential substates during its catalytic reaction. First, the protein adopts an open state to accommodate the substrate in the cleft. Substrate binding induces a closed conformation necessary for positioning the substrate into the correct configuration for glycosidic bond hydrolysis. The last state is a loose structure from which the product is released³⁷. The results of MD simulations are in agreement with the present study in the solution state. Nevertheless, BCX seems to display more diverse conformational and dynamics behaviour during its catalytic pathway. Therefore, a new model is proposed for the GH11 xylanase conformational landscape changes and the contribution of dynamics to catalysis.

PCSs analysis showed that the protein adopts at least five distinctive average structures where approximately five regions, including the fingers, the hand palm, the thumb, the cord and the α -helix contribute to this conformer diversity. The protein in the free state (\mathbf{E}_{free}) is in an open structure. The NMR titration of BCX with substrate point toward an induced fit binding mechanism, suggesting that the protein indeed experiences conformational changes necessary for the formation of the Michaelis complex. Based on the chemical shifts and the PCSs, it was concluded that the two \mathbf{ES} bound states conformations differ from each other as well as from that of the free state. The induced state seems to be similar to the $(\mathbf{ES})_{\text{closed}}$ state, yet is formed slowly, indicating a high activation barrier for its formation. It may be the dual occupancy of the glycon and the aglycon sites that induces this rearrangement. The slow conversion could limit catalysis, as the rate of formation is of a similar size as the turnover rate. The observed ms enhancement of the $(\mathbf{ES})_{\text{open}}$ motion in residues that sculpture the binding cleft, including the thumb and the fingers, could be an indication of structural fluctuations necessary for substrate positioning, deformation or even sliding, a process that was observed in other biomass degrading enzymes like cellulases³⁹. Through the $(\mathbf{ES})_{\text{closed}}$ state, the glycosylation step occurs and the protein is locked into a closed conformation $(\mathbf{EI})_{\text{closed}}$ * that differs from the \mathbf{E}_{free} , $(\mathbf{ES})_{\text{open}}$ and $(\mathbf{ES})_{\text{closed}}$ ground state conformations. The covalent bond formation restricts the protein dynamics in the thumb region concomitant with an observed enhancement of the ms motion for residues surrounding the nucleophile. Those subtle

Material and Methods

Mutagenesis

BCX E78Q, BCX T109C/T111C and BCX E78Q T109/T111C mutants were prepared by site-directed mutagenesis using Quik-Change protocol. The presence of the mutations was confirmed by sequencing.

BCX overexpression and NMR samples preparation

The gene of BCX with a sequence optimized for expression in *E. coli* was purchased from life technologies, including a N-terminus 6-His-Tag followed by a TEV protease recognition site. The gene was subcloned into plasmid pET28a using NcoI/XhoI restriction sites. *E. coli* BL21DE Rosetta cells were transformed with the obtained vector and cultured in 2 ml lysogeny broth media containing 100 µg/mL kanamycin for 6 hours at 37°C. 100 µl of the miniprep culture were used to inoculate 50 mL minimum medium supplemented with ¹⁵N labeled ammonium chloride (¹⁵NH₄Cl) or in combination with ¹³C-glucose. The next day, 0.5 L of the same medium was inoculated with the overnight preinoculation culture and incubated for 8 hours at 37°C with shaking until the OD₆₀₀ reached 0.6. BCX gene expression was induced with 0.5 mM IPTG and the culture was incubated overnight at 20°C with shaking. The cells were harvested by centrifugation and the pellet was resuspended in an extraction buffer (50 mM phosphate buffer solution (PBS), 40 mM imidazole, pH 7.5) and sonicated. The resulting 6His-BCX supernatant was purified by Ni(II) affinity chromatography. Subsequently, the eluted BCX fractions were collected and the protein was brought into a solution of 50 mM PBS using PD10 column. The 6-His-BCX protein was incubated with TEV protease overnight at 4°C. Next, the cleaved 6-His-Tag and the TEV protease were separated from BCX using Ni(II) affinity chromatography. The unbound protein fraction, that included BCX, was collected and buffer exchanged to 25 mM sodium acetate buffer pH= 5.8 using PD10 column. The protein was concentrated using Amicon® Ultra-Centrifugal Filters with 10 kDa cutoff and its purity was checked by SDS page. The BCX concentration was determined by UV absorbance using the theoretical extinction coefficient of 84,3 M⁻¹ cm⁻¹.

EI covalent complex formation

The epoxyX2 was synthesized by Schroder S.P. et al.⁴⁰. The protein was incubated with 20 times molar equivalent of BCX sample at 30 °C. The reduction of the enzyme activity was monitored over the course of incubation using 4MU-xylobiose as a substrate (Megazyme). The reaction rates were monitored by measuring the fluorescence of the released 4MU at its emission wavelength of 445 nm on a Cary Eclipse Fluorescence Spectrophotometer (Agilent). After an overnight incubation, the excess of epoxyX2 was removed using PD10 column and complex formation was checked by electrospray mass spectrometry (Waters). The same procedure was applied to prepare a ¹⁵N ¹³C BCX-epoxyX2 sample (for assignment), ¹⁵N BCX-epoxyX2 sample (for ¹⁵N CPMG RD) and ¹⁵N BCX T109C/T111C-LaNP-5-(Lu³⁺/Yb³⁺)-epoxyX2 samples for PCSs calculations.

NMR spectroscopy

Sequential assignment of the BCX WT at 20 °C was performed by recording triple resonance HNCACB and CBCAcoNH spectra on a ^{15}N ^{13}C BCX NMR sample (0.6 mM)²². The obtained peak list was used to assign the BCX E78Q, BCX T109C/111C and BCX E78Q T109C/111C mutants backbone amides. The assignments of these later were curated using PCSs. The same assignment procedure as for the BCX WT was applied for the assignment of the BCX-epoxyX2 (**EI** complex). The NMR spectra were acquired on Bruker Avance III (HD) 600 or 850 MHz spectrometers, equipped with TCI cryoprobes, processed by TopSpin 3.5 (Bruker Biospin) and analysed with Sparky Software⁴¹.

NMR titration with oligosaccharides and peak shape analysis

The NMR titration of ^{15}N BCX E78Q (123 μM) with an increasing X6 concentration (123 μM -20 mM) was performed in 25 mM sodium acetate (pH=5.8) and 6% D_2O at 20 °C. The ^1H - ^{15}N HSQC spectrum of every titration point was recorded and the average chemical shift perturbation values ($\Delta\delta_{\text{avg}}$) relative to the free protein were calculated according to the equation:

$$\Delta\delta_{\text{avg}} = \sqrt{\Delta\delta_{\text{H}}^2 + \frac{\Delta\delta_{\text{N}}^2}{25}}$$

An iterative least-squares procedure for 2D peak shape analysis of the HSQC titration spectra was performed using TITAN software³⁵ and the titration data were fitted to either a two-state or an induced fit binding model. The fit yielded the K_d and k_{off} values and also the R_2 relaxation, in addition to the k_{open} and k_{closed} for the induced fit binding model.

Paramagnetic NMR spectroscopy

Uniformly labelled ^{15}N BCX T109C/T111C was incubated with 10 mM DTT in 50 mM PBS (pH=7.2) and 150 mM NaCl for 1 h on ice to reduce the disulphide bridges between the protein dimers. DTT was removed by using a PD10 column. The protein was mixed with 10 molar equivalents of CLaNP-5- Lu^{3+} (diamagnetic sample) or CLaNP-5- Yb^{3+} (paramagnetic sample) and left stirring for 2 h at room temperature. The samples were concentrated to 0.5 mL using a 10 kDa Amicon® Ultra-Centrifugal Filter and injected into a Superdex G75 analytical gel filtration column to remove unreacted tag and protein dimers. To verify the labelling efficiency, the protein samples were analyzed on 15 % SDS-PAGE in the presence and absence of a reducing reagent (β -mercaptoethanol) and checked by acquiring ^1H - ^{15}N HSQC spectra. weak peaks of untagged BCX were observed for both samples (<5% unlabeled). The obtained PCSs were fitted to the BCX crystal structures (PDB ID:2bv v or 1bcx) to optimize the location of the lathanoid and the tensor position and orientation using Numbat software⁴². The Q factor score of the experimental PCSs fit to the BCX crystal structure was calculated using the equation⁴³.

$$Q = \sqrt{\frac{\sum (\text{obs} - \text{calc})^2}{\sum (\text{obs} + \text{calc})^2}}$$

A jackknife error analysis of the obtained tensors is part of the Numbat software and was used to enable $\Delta\chi$ tensor comparison for different BCX states. The differences between the experimental PCSs of each BCX ligand-complex and the free protein were also calculated to monitor the conformational changes that occur upon ligand binding.

NMR relaxation dispersion and CPMG data analysis

^{15}N CPMG RD data sets were recorded at 20 °C using a ^{15}N TROSY-CPMG pulse scheme⁴⁴. Data sets were recorded at field strengths of 11.7 T (600 MHz) and at 19.9 T (850 MHz). The constant time relaxation delay, τ_{CPMG} , was set to 50 ms. Dispersion profiles comprised ~ 20 different ν_{CPMG} frequencies, recorded in an interleaved manner, with values ranging from the minimum possible value ($1/\tau_{\text{CPMG}}$) to a maximum of 1000 Hz. Errors were estimated on the basis of repeat measurements at two or three different ν_{CPMG} frequencies. Each CPMG dataset required approximately 14 hours of measurement time. All experiments were performed on Bruker spectrometers equipped with a TCI-Z-GRAD triple resonance cryoprobe. The peak shape fit of the 3D-pseudo plans was performed using FuDa⁴⁵. The $R_{2,\text{eff}}(\nu_{\text{CPMG}})$ were obtained via the relation:

$$R_{2,\text{eff}}(\nu_{\text{CPMG}}) = \frac{1}{T_{\text{relax}} \times \ln\left(\frac{I_{\nu_{\text{CPMG}}}}{I_0}\right)}$$

Where $I(\nu_{\text{CPMG}})$ and I_0 are peak intensities with and without the 50 ms τ_{CPMG} , respectively. Values of the exchange parameters were extracted from a global fit of $R_{2,\text{eff}}(\nu_{\text{CPMG}})$ profiles to a two-site exchange model using CATIA (<http://www.biochem.ucl.ac.uk/hansen/catia>). The experimental R_{ex} were calculated using the formula $R_{\text{ex}} = R_{2,\text{eff}}(20 \text{ Hz}) - R_{2,\text{eff}}(1000 \text{ Hz})$ and plotted versus the residue numbers.

References

1. Wolynes, P. G. (2005) Recent successes of the energy landscape theory of protein folding and function, *Q. Rev. Biophys.* 38, 405-410.
2. Hegler, J. A., Weinkam, P., and Wolynes, P. G. (2008) The spectrum of biomolecular states and motions, *HFSP journal* 2, 307-313.
3. Mulder, F. A., Mittermaier, A., Hon, B., Dahlquist, F. W., and Kay, L. E. (2001) Studying excited states of proteins by NMR spectroscopy, *Nat. Struct. Mol. Biol.* 8, 932-935.
4. Söderberg, O., Gullberg, M., Jarvius, M., Ridderstråle, K., Leuchowius, K.-J., Jarvius, J., Wester, K., Hydbring, P., Bahram, F., and Larsson, L.-G. (2006) Direct observation of individual endogenous protein complexes in situ by proximity ligation, *Nat. Methods* 3, 995-1000.
5. Petersen, F. N. R., and Bohr, H. (2010) The mechanisms of excited states in enzymes, *Theor. Chem. Acc.* 125, 345-352.
6. Eisenmesser, E. Z., Bosco, D. A., Akke, M., and Kern, D. (2002) Enzyme dynamics during catalysis, *Science* 295, 1520-1523.
7. Nitsche, C., and Otting, G. (2016) Pseudocontact shifts in biomolecular NMR using paramagnetic metal tags, *Prog. Nucl. Magn. Reson. Spectrosc.*
8. Gaponenko, V., Sarna, S. P., Altieri, A. S., Horita, D. A., Li, J., and Byrd, R. A. (2004) Improving the accuracy of NMR structures of large proteins using pseudocontact shifts as long-range restraints, *J. Biomol. NMR* 28, 205-212.
9. Chen, J. L., Wang, X., Yang, F., Cao, C., Otting, G., and Su, X. C. (2016) 3D structure determination of an unstable transient enzyme intermediate by paramagnetic NMR spectroscopy, *Angew. Chem. Int. Ed.* 55, 13744-13748.
10. Keizers, P. H., Saragliadis, A., Hiruma, Y., Overhand, M., and Ubbink, M. (2008) Design, synthesis, and evaluation of a lanthanide chelating protein probe: CLaNP-5 yields predictable paramagnetic effects independent of environment, *J. Am. Chem. Soc.* 130, 14802-14812.
11. Meiboom, S., and Gill, D. (1958) Modified spin-echo method for measuring nuclear relaxation times, *Rev. Sci. Instrum.* 29, 688-691.
12. Carr, H. Y., and Purcell, E. M. (1954) Effects of diffusion on free precession in nuclear magnetic resonance experiments, *Phys. Rev.* 94, 630.
13. Henzler-Wildman, K. A., Thai, V., Lei, M., Ott, M., Wolf-Watz, M., Fenn, T., Pozharski, E., Wilson, M. A., Petsko, G. A., and Karplus, M. (2007) Intrinsic motions along an enzymatic reaction trajectory, *Nature* 450, 838-844.
14. Santoso, Y., Joyce, C. M., Potapova, O., Le Reste, L., Hohlbein, J., Torella, J. P., Grindley, N. D., and Kapanidis, A. N. (2010) Conformational transitions in DNA polymerase I revealed by single-molecule FRET, *Proc. Natl. Acad. of Sci. U.S.A.* 107, 715-720.
15. Bohr, D. D., McElheny, D., Dyson, H. J., and Wright, P. E. (2006) The dynamic energy landscape of dihydrofolate reductase catalysis, *Science* 313, 1638-1642.
16. Henrissat, B. (1991) A classification of glycosyl hydrolases based on amino-acid-sequence similarities, *Biochem. J.* 280, 309-316.
17. Saha, B. C. (2003) Hemicellulose bioconversion, *J. Ind. Microbiol. Biotechnol.* 30, 279-291.
18. Polizeli, M., Rizzatti, A., Monti, R., Terenzi, H., Jorge, J. A., and Amorim, D. (2005) Xylanases from fungi: properties and industrial applications, *Appl. Microbiol. Biotechnol.* 67, 577-591.
19. Paës, G., Berrin, J.-G., and Beaugrand, J. (2012) GH11 xylanases: structure/function/properties relationships and applications, *Biotechnol. Adv.* 30, 564-592.
20. Paës, G., Tran, V., Takahashi, M., Boukari, I., and O'donohue, M. J. (2007) New insights into the role of the thumb-like loop in GH-11 xylanases, *Protein Eng. Des. Sel.* 20, 15-23.
21. Wakarchuk, W. W., Campbell, R. L., Sung, W. L., Davoodi, J., and Yaguchi, M. (1994) Mutational and crystallographic analyses of the active site residues of the *Bacillus circulans* xylanase, *Protein Sci.* 3, 467-475.
22. Plesniak, L. A., McIntosh, L. P., and Wakarchuk, W. W. (1996) Secondary structure and NMR assignments of *Bacillus circulans* xylanase, *Protein Sci.* 5, 1118-1135.
23. Davies, G. J., Wilson, K. S., and Henrissat, B. (1997) Nomenclature for sugar-binding subsites in glycosyl hydrolases, *Biochem. J.* 321, 557.
24. Rye, C. S., and Withers, S. G. (2000) Glycosidase mechanisms, *Curr. Opin. Chem. Biol.* 4, 573-580.
25. Mhlongo, N. N., Ebrahim, M., Skelton, A. A., Kruger, H. G., Williams, I. H., and Soliman, M. E. S. (2015) Dynamics of the thumb-finger regions in a GH11 xylanase *Bacillus circulans*: comparison between the Michaelis and covalent intermediate, *RSC Advances* 5, 82381-82394.

CHAPTER 4

26. Paës, G., Cortés, J., Siméon, T., O'Donohue, M. J., and Tran, V. (2012) Thumb-loops up for catalysis: a structure/function investigation of a functional loop movement in a GH11 xylanase, *Comput. Struct. Biotechnol. J.* 1, e201207001.
27. Murakami, M. T., Arni, R. K., Vieira, D. S., Degrève, L., Ruller, R., and Ward, R. J. (2005) Correlation of temperature induced conformation change with optimum catalytic activity in the recombinant G/11 xylanase A from *Bacillus subtilis* strain 168 (1A1), *FEBS Lett.* 579, 6505-6510.
28. Paës, G., Cortés, J., Siméon, T., O'Donohue, M. J., and Tran, V. (2012) Thumb-loops up for catalysis: a structure/function investigation of a functional loop movement in a GH11 xylanase, *Comput. Struct. Biotechnol. J.* 1, 1-10.
29. Pollet, A., Vandermarliere, E., Lammertyn, J., Strelkov, S. V., Delcour, J. A., and Courtin, C. M. (2009) Crystallographic and activity-based evidence for thumb flexibility and its relevance in glycoside hydrolase family 11 xylanases, *Proteins* 77, 395-403.
30. Gagné, D., Narayanan, C., Nguyen-Thi, N., Roux, L. D., Bernard, D. N., Brunzelle, J. S., Couture, J.-F., Agarwal, P. K., and Doucet, N. (2016) Ligand binding enhances millisecond conformational exchange in xylanase B2 from *Streptomyces lividans*, *Biochemistry* 55, 4184-4196.
31. Muilu, J., Törrönen, A., Peräkylä, M., and Rouvinen, J. (1998) Functional conformational changes of endo-1, 4-xylanase II from *Trichoderma reesei*: A molecular dynamics study, *Proteins* 31, 434-444.
32. Sidhu, G., Withers, S. G., Nguyen, N. T., McIntosh, L. P., Ziser, L., and Brayer, G. D. (1999) Sugar ring distortion in the glycosyl-enzyme intermediate of a family G/11 xylanase, *Biochemistry* 38, 5346-5354.
33. Connelly, G. P., Withers, S. G., and McIntosh, L. P. (2000) Analysis of the dynamic properties of *Bacillus circulans* xylanase upon formation of a covalent glycosyl-enzyme intermediate, *Protein Sci.* 9, 512-524.
34. Ludwiczek, M. L., Heller, M., Kantner, T., and McIntosh, L. P. (2007) A secondary xylan-binding site enhances the catalytic activity of a single-domain family 11 glycoside hydrolase, *J. Mol. Biol.* 373, 337-354.
35. Waudby, C. A., Ramos, A., Cabrita, L. D., and Christodoulou, J. (2016) Two-dimensional NMR lineshape analysis, *Sci. Rep.* 6, 24826.
36. Zechel, D. L., Konermann, L., Withers, S. G., and Douglas, D. (1998) Pre-steady state kinetic analysis of an enzymatic reaction monitored by time-resolved electrospray ionization mass spectrometry, *Biochemistry* 37, 7664-7669.
37. Wan, Q., Zhang, Q., Hamilton-Brehm, S., Weiss, K., Mustyakimov, M., Coates, L., Langan, P., Graham, D., and Kovalevsky, A. (2014) X-ray crystallographic studies of family 11 xylanase Michaelis and product complexes: implications for the catalytic mechanism, *Acta Crystallogr. Sect. D. Biol. Crystallogr.* 70, 11-23.
38. Havukainen, R., Törrönen, A., Laitinen, T., and Rouvinen, J. (1996) Covalent binding of three epoxyalkyl xylosides to the active site of endo-1, 4-xylanase II from *Trichoderma reesei*, *Biochemistry* 35, 9617-9624.
39. Igarashi, K., Koivuola, A., Wada, M., Kimura, S., Penttilä, M., and Samejima, M. (2009) High speed atomic force microscopy visualizes processive movement of *Trichoderma reesei* cellobiohydrolase I on crystalline cellulose, *J. Biol. Chem.* 284, 36186-36190.
40. Schröder, S. P., Petracca, R., Minnee, H., Artola, M., Aerts, J. M., Codée, J. D., Van Der Marel, G. A., and Overkleef, H. S. (2016) A Divergent Synthesis of l-arabino- and d-xylo-Configured Cyclophellitol Epoxides and Aziridines, *Eur. J. Org. Chem.* 2016, 4787-4794.
41. Lee, W., Tonelli, M., and Markley, J. L. (2014) NMRFAM-SPARKY: enhanced software for biomolecular NMR spectroscopy, *Bioinformatics* 31, 1325-1327.
42. Schmitz, C., Stanton-Cook, M. J., Su, X.-C., Otting, G., and Huber, T. (2008) Numbat: an interactive software tool for fitting $\Delta\chi$ -tensors to molecular coordinates using pseudocontact shifts, *J. Biomol. NMR* 41, 179.
43. Bashir, Q., Volkov, A. N., Ullmann, G. M., and Ubbink, M. (2009) Visualization of the encounter ensemble of the transient electron transfer complex of cytochrome c and cytochrome c peroxidase, *J. Am. Chem. Soc.* 132, 241-247.
44. Loria, J. P., Rance, M., and Palmer, A. G. (1999) A relaxation-compensated Carr-Purcell-Meiboom-Gill sequence for characterizing chemical exchange by NMR spectroscopy, *J. Am. Chem. Soc.* 121, 2331-2332.
45. Hansen, D. F., Yang, D., Feng, H., Zhou, Z., Wiesner, S., Bai, Y., and Kay, L. E. (2007) An exchange-free measure of ^{15}N transverse relaxation: an NMR spectroscopy application to the study of a folding intermediate with pervasive chemical exchange, *J. Am. Chem. Soc.* 129, 11468-11479.

CHAPTER 5

General Conclusion & Perspectives

Due to their central physiological roles in living organisms, retaining β -glycosidases have been the subject of tremendous research efforts to examine their structure/function relation using numerous biophysical and biochemical approaches. Since the proposition of the hydrolysis mechanism in the late fifties by Koshland¹, the fundamental research on retaining β -glycosidases has been revolutionized by the discovery of multiple reversible and irreversible inhibitors²⁻⁵. One of the most successful class of inhibitors are mechanism based inactivators, which were extensively used to identify the nucleophilic catalytic residues and to comprehend the catalytic mechanism and substrate itinerary^{2, 6, 7}. Subsequently, covalent inhibitors were used as warheads to synthesize chromogenic activity based probes (ABPs), which were widely used to selectively label and discover new retaining β -glycosidases in complex biological samples^{8, 9}. For instance, Overkleeft and co-workers have developed ultrasensitive ABPs against human β -glucosidase (GBA)¹⁰. These ABPs were successfully utilized by Aerts and co-workers to deepen our understanding of the physiopathology underlying Gaucher disease^{11, 12}. The organic synthesis and biological applications of these ABPs has become routine¹³. Nevertheless, their binding mechanism and influences on protein conformation and dynamics remained unexplored. Therefore, this work is aimed to establish a bridge between the two research disciplines, using ABP technology to understand functional dynamics and conformational stability of retaining β -glycosidases *in solution* and *in vivo*. The research relied on standard biochemistry and advanced NMR spectroscopy research approaches.

The deficiency of GBA activity in Gaucher patients¹⁴ leads to the accumulation of glucocerebrosides in lysosomes¹⁵ and GM3 gangliosides in plasma¹⁶. Such accumulations are the cause of the clinical manifestations of the disease^{17, 18}. Continuous intravenous administration of exogenous GBA (rGBA) is, so far, the most efficient treatment for Gaucher disease¹⁹⁻²⁴. It remains costly²⁵ and non-affordable for many patients around the world, especially in countries with low health care quality. Thus, finding an inexpensive therapeutic alternative is imperative.

The endo-glycosylceramidase II from *Rhodococcus* sp. is a bacterial homologue of GBA able to endo-hydrolyse the glycosidic link in complex glycosylceramidases. The enzyme was first discovered in 1980s by Ito et al. and found multiple applications in gangliosides analysis²⁶. The crystal structure of EGCII was solved in 2007 by Strynadka and co-workers in the free and GM3 ganglioside-bound forms.²⁷ In theory, this protein holds promise as a potential drug against Gaucher disease and other glycosphingolipidose disorders, *via* administration once in a lifetime for clearance of the accumulated gangliosides. Hence, ABPs were used to gain insight into factors that influence the conformational stability of EGCII as a preliminary step toward its design as a therapeutic agent. The study revealed that the protein is thermolabile and highly flexible in its free state. The inherent flexibility of EGCII is postulated to be requested for its peripheral

CHAPTER 5

interaction with the cell membrane to exert its function against its amphiphilic substrates. This hypothesis was supported by the highly exposed hydrophobic surface to the solvent probed by ANSA. Flexibility could also play a role in the interaction between EGCII and its activator, a protein partner that enhances its activity against gangliosides in the absence of detergents²⁸. Upon complex formation with hydrophilic, activity-based inhibitors, a minor increase in thermostability and rigidity were observed, concomitant with a preserved high hydrophobic surface exposed to the solvent. However, the interactions with activity-based inhibitors with high lipophilic potential increased the protein thermostability and rigidity, and reduced its exposed hydrophobic surface. The stabilization of EGCII conformation correlates with the shape and hydrophobicity of the substituents of the ABPs. It was concluded that amphiphilic active site binders that mimic the natural substrate are superior stabilizers, compared to their small hydrophilic counterpart. By virtue of ABPs technology, the characteristics of the enzyme-inhibitors complex were investigated and helped to elucidate which parts of the inhibitors are important for efficient stabilization activity. This information could be further exploited in the design of more specific ABPs and inhibitors against other β -glycosidases. EGCII thermostability and flexibility might hamper its therapeutic use, and, therefore, one strategy to overcome these disadvantages is to re-engineer the protein by including glycosylation sites on its surface²⁹. This approach might enhance EGCII stability and also assist its uptake by macrophages receptors through those glycosylation sites²⁰. Additionally, an endoglycoceramidase activity towards gangliosides has been reported for human cancer cells³⁰, but the protein responsible for such activity has not been characterized yet. The development of endo-glycosidases activity-based probes (endo-ABPs) could help in uncovering the enzyme behind the endo-hydrolysis of gangliosides in cancer cells and their role in cancer pathology. If the endoglycoceramidase is a marker for cancer cells phenotype, ultrasensitive endo-ABPs might be also be used for diagnosis purposes in the initial stage of cancer development.

In addition to enzyme replacement therapy in Gaucher disease, new therapeutic approaches are under intense investigation, based on identifying small chemical molecules that rescue GBA proteostasis in Gaucher patients³¹⁻³⁴. Those small molecules called “pharmacological chaperones” are supposed to stabilize GBA mutants fold in the ER compartment of the cells, thus escaping the quality control machinery in the ER compartment, so that they can reach their final lysosomal destination^{31, 35}. Several GBA active site binders have validated this proof of principle *in vivo* and *in vitro*³⁶⁻³⁹. However, their stabilization mechanism on GBA and their effects on the enzyme conformation in solution remained unclear. Therefore, reversible, semi-reversible (time dependent) and irreversible (ABPs) inhibitors with different chemical characteristics were used to investigate the stabilization mechanism of those active site binders on GBA fold *in vitro* and *in vivo*.

CHAPTER 5

The outcomes of the study revealed that small active site binders, which only occupy the glycon pocket of the active site, provoke minor changes of the biophysical properties of the protein. When interacting with amphiphilic ABPs, which are thought to occupy simultaneously the glycon and aglycon sites, a remarkable increase of the protein thermal stability was observed (up to 21°C) in conjunction to its resistance against trypsin digestion, suggesting rigidification. Additionally, ABPs induced a shift of the GBA fluorescence spectrum toward the blue region, again suggesting a more compact conformation upon complex formation. Serendipitously, an iFRET mechanism between the BODIPY fluorescence reporter of the ABPs and the protein tryptophan residues was observed. This phenomenon could potentially be exploited as a method for cell imaging. By exciting the indole rings of GBA tryptophans and recording the BODIPY emission spectrum of the ABPs, the background signals originating from free ABPs might be bypassed and clearer images could be obtained⁴⁰.

The *in vitro* findings were validated *in vivo* by observing a correlation between the binding site occupancy of GBA by ABPs and the intracellular increase of the protein level.

The studies on EGCII and GBA lead to the conclusion that both proteins share a similar stabilizing mechanism by active site binders. Therefore, evidence is provided about the increase in cellular levels of GBA by ABPs and reversible inhibitor is in part caused by their ability to stabilize GBA folding, which increases its resistance against breakdown by lysosomal proteases. Those finding provided extra information that could be considered when designing new pharmacological chaperones for Gaucher disease.

Despite the devoted efforts to discover an optimal candidate for pharmacological chaperone treatment, none of the available compounds has reached the clinic. Isofagomine was the most successful compound but failed to pass the clinical trials, presumably due to its poor biodistribution, ascribed to its hydrophilicity⁴¹. Therefore, a hybrid therapy between pharmacological chaperones and enzyme administration represent a therapeutic alternative, which is under investigations. Continuous administration of rGBA to Gaucher patients is required because of the short half-life in the blood⁴². Providing a cocktail of rGBA and isofagomine might increase the half-life of the protein under physiological conditions, thus lowering the frequency of the enzyme transfusion and the cost of the treatment. However, this approach might require a high dose of isofagomine to warrant an effective rGBA stabilisation that could induce unwanted side-effects.

An alternative in this hybrid therapy is the use of a fluorinated glucoside inhibitor, instead of isofagomine. This class of inhibitors is supposed to bind rGBA in a time dependent manner^{43, 44}. The fluoride in the C2 position of the pyranose ring ensures slow dissociation of the enzyme-inhibitor complex, providing sufficient time for rGBA to reach its destination without being degraded in the blood circulation. The one to one ratio between the enzyme-inhibitor cocktail could reduce the possible side effects, compared to isofagomine.

CHAPTER 5

The use of GBA active site binders as pharmacological chaperones appears promising, however, their potential inhibition of the enzyme activity at high dose represents a potential problem. Therefore, attention should also be paid to allosteric pharmacological chaperone because they bind remote from the active site, avoiding such inhibitory effects.

Like EGCII, GBA also has an activator called saposin C⁴⁵. Saposin C is an 80-amino acid protein and its structure was determined by NMR spectroscopy and X-ray crystallography under different condition⁴⁶⁻⁴⁸. Saposin C binding to GBA induces significant changes of its fluorescence spectrum, suggesting changes in the GBA conformational state upon protein-protein complex formation⁴⁹. Attempts to characterize the GBA-saposin C complex using X-ray crystallography was unsuccessful. The complex was modelled by molecular docking though⁵⁰. Uncovering the saposin C binding site on GBA experimentally might give an idea about which structural location should be targeted to design allosteric pharmacological chaperones. The binding site could be studied by paramagnetic NMR spectroscopy. A new type of activity-based probes against GBA could be developed for this purpose, using epoxide as a warhead linked to lanthanoid paramagnetic NMR tag (PABP) instead of BODIPY. The covalent complex between GBA and the PABP might be used to obtain experimental restraints (PREs, PCSs and RDCs) of the GBA-Saposin C complex⁵¹⁻⁵⁴. The experimental restraints can be used to direct the docking between the two proteins, providing realistic model of their complex⁵⁵. Uncovering the saposin C binding site on GBA surface will assist the design of allosteric pharmacological chaperone.

The characteristic shared between the different families of retaining β -glycosidase is their conserved and well understood catalytic mechanism. This has somehow limited the research devoted to understand the contribution of the enzyme dynamics and conformational changes in the different steps of the catalytic reaction. In the present work, this question was addressed using BCX as a model. the choice was based on the suitable biophysical characteristics of BCX for NMR spectroscopy studies. Moreover, this protein has been extensively investigated by NMR spectroscopy and X-ray crystallography in combination with other biochemistry techniques⁵⁶⁻⁶². This knowledge provided a solid starting point that facilitated the task in exploring the conformational landscape and dynamics of this protein during its catalytic pathway. By incubating the protein with different non-covalent ligands and a covalent active based inhibitor, a novel compound that was specifically made for this study⁶³, the enzyme-ligand complexes were systematically characterized in every step of the catalytic reaction using paramagnetic NMR spectroscopy and CPMG RD techniques. In its free state, the protein populates a ground state similar to its crystalline state as concluded from PCS data. The protein displays subtle millisecond dynamics in the thumb and fingers regions with an excited state population = 0.7%. The Michaels complex displays an induced fit

CHAPTER 5

mechanism as shown by CSP analysis. This observation has not been reported before for a GH11 xylanase. Both states of the enzyme appear to have different conformations compared to the free protein, as concluded from the paramagnetic NMR data. The exchange rate between the initial and induced states is low, on the order of the turn-over rate of the enzyme, suggesting that the formation of the induced state may contribute to the rate limiting step of catalysis. In the ES state, the millisecond dynamics is strongly enhanced with a population of the excited state(s) of 9%. This finding is in accordance with a previous report on another GH11 xylanase family member. No major changes of the protein dynamics behaviour were observed in the case of the EI state compared to the free protein, despite the occurrence of conformational changes upon its covalent modification by epoxyX2. In the EP state the protein displays minor conformational changes upon ligand binding, again concomitant with enhancement of the millisecond dynamics, similar to the ES state. The ES and the EP ground states are connected *via* excited states to the EI ground state conformation. Based on those findings, a description of BCX conformational landscape and dynamics during catalysis is proposed, providing evidence for involvement of enzyme motions in the catalytic mechanism.

References

1. Koshland, D. E. (1953) Stereochemistry and the mechanism of enzymatic reactions, *Biological Reviews* 28, 416-436.
2. Rempel, B. P., and Withers, S. G. (2008) Covalent inhibitors of glycosidases and their applications in biochemistry and biology, *Glycobiology* 18, 570-586.
3. Asano, N., Nash, R. J., Molyneux, R. J., and Fleet, G. W. J. (2000) Sugar-mimic glycosidase inhibitors: natural occurrence, biological activity and prospects for therapeutic application, *Tetrahedron-Asymmetry* 11, 1645-1680.
4. de Melo, E. B., da Silveira Gomes, A., and Carvalho, I. (2006) α - and β -Glucosidase inhibitors: chemical structure and biological activity, *Tetrahedron* 62, 10277-10302.
5. Caron, G., and Withers, S. (1989) Conduritol aziridine: a new mechanism-based glucosidase inactivator, *Biochem. Biophys. Res. Commun.* 163, 495-499.
6. Davies, G. J., Planas, A., and Rovira, C. (2011) Conformational analyses of the reaction coordinate of glycosidases, *Acc. Chem. Res.* 45, 308-316.
7. Withers, S. G., and Aebersold, R. (1995) Approaches to labeling and identification of active site residues in glycosidases, *Protein Sci.* 4, 361-372.
8. Willems, L. I., Jiang, J., Li, K. Y., Witte, M. D., Kallemeijn, W. W., Beenakker, T. J., Schröder, S. P., Aerts, J. M., van der Marel, G. A., and Codée, J. D. (2014) From Covalent Glycosidase Inhibitors to Activity-Based Glycosidase Probes, *Chem. Eur. J.* 20, 10864-10872.
9. Vocadlo, D. J., and Bertozzi, C. R. (2004) A strategy for functional proteomic analysis of glycosidase activity from cell lysates, *Angew. Chem. Int. Ed.* 43, 5338-5342.
10. Kallemeijn, W. W., Li, K. Y., Witte, M. D., Marques, A. R., Aten, J., Scheij, S., Jiang, J., Willems, L. I., Voorn-Brouwer, T. M., and van Roomen, C. P. (2012) Novel Activity-Based Probes for Broad-Spectrum Profiling of Retaining β -Exoglucosidases *in situ* and *in vivo*, *Angew. Chem. Int. Ed.* 51, 12529-12533.
11. Witte, M. D., Kallemeijn, W. W., Aten, J., Li, K.-Y., Strijland, A., Donker-Koopman, W. E., van den Nieuwendijk, A. M. C. H., Bleijlevens, B., Kramer, G., Florea, B. I., Hooibrink, B., Hollak, C. E. M., Ottenhoff, R., Boot, R. G., van der Marel, G. A., Overkleeft, H. S., and Aerts, J. M. F. G. (2010) Ultrasensitive *in situ* visualization of active glucocerebrosidase molecules, *Nat. Chem. Biol.* 6, 907.
12. Dekker, N., van Dussen, L., Hollak, C. E., Overkleeft, H., Scheij, S., Ghauharali, K., van Breemen, M. J., Ferraz, M. J., Groener, J. E., and Maas, M. (2011) Elevated plasma glucosylsphingosine in Gaucher disease: relation to phenotype, storage cell markers, and therapeutic response, *Blood* 118, e118-e127.
13. Li, K. Y., Jiang, J., Witte, M. D., Kallemeijn, W. W., van den Elst, H., Wong, C. S., Chander, S. D., Hoogendoorn, S., Beenakker, T. J., and Codée, J. D. (2014) Synthesis of cyclophellitol, cyclophellitol aziridine, and their tagged derivatives, *Eur. J. Org. Chem.* 2014, 6030-6043.
14. Brady, R., Kanfer, J., Bradley, R., and Shapiro, D. (1966) Demonstration of a deficiency of glucocerebrosidase-cleaving enzyme in Gaucher's disease, *J. Clin. Invest.* 45, 1112.
15. Brady, R. O., Kanfer, J. N., and Shapiro, D. (1965) Metabolism of glucocerebrosides II. Evidence of an enzymatic deficiency in Gaucher's disease, *Biochem. Biophys. Res. Commun.* 18, 221-225.
16. Ghauharali-van der Vlugt, K., Langeveld, M., Poppema, A., Kuiper, S., Hollak, C. E., Aerts, J. M., and Groener, J. E. (2008) Prominent increase in plasma ganglioside GM3 is associated with clinical manifestations of type I Gaucher disease, *Clin. Chim. Acta* 389, 109-113.
17. Kaye, E. M., Ullman, M. D., Wilson, E. R., and Barranger, J. A. (1986) Type 2 and type 3 Gaucher disease: a morphological and biochemical study, *Ann. Neurol.* 20, 223-230.
18. Orvisky, E., Park, J. K., LaMarca, M. E., Ginns, E. I., Martin, B. M., Tayebi, N., and Sidransky, E. (2002) Glucosylsphingosine accumulation in tissues from patients with Gaucher disease: correlation with phenotype and genotype, *Mol. Genet. Metab.* 76, 262-270.
19. Barton, N. W., Furbish, F. S., Murray, G. J., Garfield, M., and Brady, R. O. (1990) Therapeutic response to intravenous infusions of glucocerebrosidase in a patient with Gaucher disease, *Proc. Natl. Acad. Sci. U.S.A.* 87, 1913-1916.
20. Grabowski, G. A., Barton, N. W., Pastores, G., Dambrosia, J. M., Banerjee, T. K., McKee, M. A., Parker, C., Schifmann, R., Hill, S. C., and Brady, R. O. (1995) Enzyme therapy in type 1 Gaucher disease: comparative efficacy of mannose-terminated glucocerebrosidase from natural and recombinant sources, *Ann. Intern. Med.* 122, 33-39.
21. Brady, R. O., Pentchev, P. G., Gal, A. E., Hibbert, S. R., and Dekaban, A. S. (1974) Replacement therapy for inherited enzyme deficiency: use of purified glucocerebrosidase in Gaucher's disease, *New Engl. J. Med.* 291, 989-993.

CHAPTER 5

22. Beutler, E., Dale, G., Guinto, D., and Kuhl, W. (1977) Enzyme replacement therapy in Gaucher's disease: Preliminary clinical trial of a new enzyme preparation, *Proc. Natl. Acad. Sci. U.S.A.* 74, 4620-4623.
23. Altarescu, G., Hill, S., Wiggs, E., Jeffries, N., Kreps, C., Parker, C. C., Brady, R. O., Barton, N. W., and Schiffmann, R. (2001) The efficacy of enzyme replacement therapy in patients with chronic neuronopathic Gaucher's disease, *J. Pediatr.* 138, 539-547.
24. Barton, N. W., Brady, R. O., Dambrosia, J. M., Di Bisceglie, A. M., Doppelt, S. H., Hill, S. C., Mankin, H. J., Murray, G. J., Parker, R. I., and Argoff, C. E. (1991) Replacement therapy for inherited enzyme deficiency-macrophage-targeted glucocerebrosidase for Gaucher's disease, *New Engl. J. Med.* 324, 1464-1470.
25. Connock, M., Burls, A., Frew, E., Fry-Smith, A., Juarez-Garcia, A., McCabe, C., Wailoo, A. J., Abrams, K. R., Cooper, N., and Sutton, A. J. (2006) The clinical effectiveness and cost-effectiveness of enzyme replacement therapy for Gaucher's disease: a systematic review.
26. Ito, M., and Yamagata, T. (1986) A novel glycosphingolipid-degrading enzyme cleaves the linkage between the oligosaccharide and ceramide of neutral and acidic glycosphingolipids, *J. Biol. Chem.* 261, 14278-14282.
27. Caines, M. E., Vaughan, M. D., Tarling, C. A., Hancock, S. M., Warren, R. A. J., Withers, S. G., and Strynadka, N. C. (2007) Structural and mechanistic analyses of endo-glycoceramidase II, a membrane-associated family 5 glycosidase in the Apo and GM3 ganglioside-bound forms, *J. Biol. Chem.* 282, 14300-14308.
28. Ito, M., Ikegami, Y., and Yamagata, T. (1991) Activator proteins for glycosphingolipid hydrolysis by endoglycoceramidas. Elucidation of biological functions of cell-surface glycosphingolipids in situ by endoglycoceramidas made possible using these activator proteins, *J. Biol. Chem.* 266, 7919-7926.
29. Solá, R. J., and Griebenow, K. (2009) Effects of glycosylation on the stability of protein pharmaceuticals, *J. Pharm. Sci.* 98, 1223-1245.
30. Basu, M., Kelly, P., Girzadas, M., Li, Z., and Basu, S. (2000) Properties of animal ceramide glycanases, *Methods Enzymol.* 311, 287-297.
31. Benito, J. M., García Fernández, J. M., and Mellet, C. O. (2011) Pharmacological chaperone therapy for Gaucher disease: a patent review, *Expert Opin. Ther. Pat.* 21, 885-903.
32. Jung, O., Patnaik, S., Marugan, J., Sidransky, E., and Westbrock, W. (2016) Progress and potential of non-inhibitory small molecule chaperones for the treatment of Gaucher disease and its implications for Parkinson disease, *Expert. Rev. Proteomics.* 13, 471-479.
33. Pastores, G. M., and Sathe, S. (2006) A chaperone-mediated approach to enzyme enhancement as a therapeutic option for the lysosomal storage disorders, *Drugs in R & D* 7, 339-348.
34. Fan, J.-Q. (2008) A counterintuitive approach to treat enzyme deficiencies: use of enzyme inhibitors for restoring mutant enzyme activity, *Biol. Chem.* 389, 1-11.
35. Yu, Z., Sawkar, A. R., and Kelly, J. W. (2007) Pharmacologic chaperoning as a strategy to treat Gaucher disease, *The FEBS journal* 274, 4944-4950.
36. Zechel, D. L., Boraston, A. B., Gloster, T., Boraston, C. M., Macdonald, J. M., Tilbrook, D. M. G., Stick, R. V., and Davies, G. J. (2003) Iminosugar glycosidase inhibitors: structural and thermodynamic dissection of the binding of isofagomine and 1-deoxynojirimycin to β -glucosidases, *J. Am. Chem. Soc.* 125, 14313-14323.
37. Khanna, R., Benjamin, E. R., Pellegrino, L., Schilling, A., Rigat, B. A., Soska, R., Nafar, H., Ranes, B. E., Feng, J., and Lun, Y. (2010) The pharmacological chaperone isofagomine increases the activity of the Gaucher disease L444P mutant form of β -glucosidase, *The FEBS journal* 277, 1618-1638.
38. Abian, O., Alfonso, P., Velazquez-Campoy, A., Giraldo, P., Pocovi, M., and Sancho, J. (2011) Therapeutic strategies for Gaucher disease: miglustat (NB-DNJ) as a pharmacological chaperone for glucocerebrosidase and the different thermostability of velaglucerase alfa and imiglucerase, *Mol. Pharm.* 8, 2390-2397.
39. Steet, R., Chung, S., Lee, W.-S., Pine, C. W., Do, H., and Kornfeld, S. (2007) Selective action of the iminosugar isofagomine, a pharmacological chaperone for mutant forms of acid- β -glucosidase, *Biochem. Pharmacol.* 73, 1376-1383.
40. Ghisaidoobe, A. B., and Chung, S. J. (2014) Intrinsic tryptophan fluorescence in the detection and analysis of proteins: a focus on Förster resonance energy transfer techniques, *Int. J. Mol. Sci.* 15, 22518-22538.
41. Kaul, R., Mceachern, E. J., Sun, J., Vocadlo, D. J., Zhou, Y., and Zhu, Y. (2015) Glucocerebrosidase modulators and uses thereof, Google Patents.
42. Friedman, B., Vaddi, K., Preston, C., Mahon, E., Cataldo, J. R., and McPherson, J. M. (1999) A comparison of the pharmacological properties of carbohydrate remodeled recombinant and placental-derived β -

CHAPTER 5

- glucocerebrosidase: implications for clinical efficacy in treatment of Gaucher disease, *Blood* 93, 2807-2816.
43. Walvoort, M. T., Kallemeijn, W. W., Willems, L. I., Witte, M. D., Aerts, J. M., van der Marel, G. A., Codée, J. D., and Overkleeft, H. S. (2012) Tuning the leaving group in 2-deoxy-2-fluoroglucoside results in improved activity-based retaining β -glucosidase probes, *Chem. Commun.* 48, 10386-10388.
 44. Wicki, J., Rose, D. R., and Withers, S. G. (2002) Trapping covalent intermediates on β -glycosidases, *Methods Enzymol.* 354, 84-105.
 45. Tamargo, R.J., Velayati, A., Goldin, E., and Sidransky, E. (2012) The role of saposin C in Gaucher disease, *Mol. Genet. Metab.* 106, 257-263.
 46. Hawkins, C. A., de Alba, E., and Tjandra, N. (2005) Solution structure of human saposin C in a detergent environment, *J. Mol. Biol.* 346, 1381-1392.
 47. de Alba, E., Weiler, S., and Tjandra, N. (2003) Solution structure of human saposin C: pH-dependent interaction with phospholipid vesicles, *Biochemistry* 42, 14729-14740.
 48. Rossmann, M., Schultz-Heienbrok, R., Behlke, J., Remmel, N., Alings, C., Sandhoff, K., Saenger, W., and Maier, T. (2008) Crystal structures of human saposins C and D: implications for lipid recognition and membrane interactions, *Structure* 16, 809-817.
 49. Qi, X., and Grabowski, G. A. (1998) Acid β -glucosidase: intrinsic fluorescence and conformational changes induced by phospholipids and saposin C, *Biochemistry* 37, 11544-11554.
 50. Atrian, S., López-Viñas, E., Gómez-Puertas, P., Chabás, A., Vilageliu, L., and Grinberg, D. (2008) An evolutionary and structure-based docking model for glucocerebrosidase-saposin C and glucocerebrosidase-substrate interactions-Relevance for Gaucher disease, *Proteins* 70, 882-891.
 51. Volkov, A. N., Worrall, J. A., Holtzmann, E., and Ubbink, M. (2006) Solution structure and dynamics of the complex between cytochrome c and cytochrome c peroxidase determined by paramagnetic NMR, *Proc. Natl. Acad. Sci. U.S.A.* 103, 18945-18950.
 52. Ubbink, M., Ejdebäck, M., Karlsson, B. G., and Bendall, D. S. (1998) The structure of the complex of plastocyanin and cytochrome f, determined by paramagnetic NMR and restrained rigid-body molecular dynamics, *Structure* 6, 323-335.
 53. Hass, M. A., and Ubbink, M. (2014) Structure determination of protein-protein complexes with long-range anisotropic paramagnetic NMR restraints, *Curr. Opin. Struct. Biol.* 24, 45-53.
 54. Volkov, A. N., Ubbink, M., and van Nuland, N. A. (2010) Mapping the encounter state of a transient protein complex by PRE NMR spectroscopy, *J. Biomol. NMR* 48, 225-236.
 55. Dominguez, C., Boelens, R., and Bonvin, A. M. (2003) HADDOCK: a protein-protein docking approach based on biochemical or biophysical information, *J. Am. Chem. Soc.* 125, 1731-1737.
 56. Wakarchuk, W. W., Campbell, R. L., Sung, W. L., Davoodi, J., and Yaguchi, M. (1994) Mutational and crystallographic analyses of the active site residues of the *Bacillus circulans* xylanase, *Protein Sci.* 3, 467-475.
 57. Plesniak, L. A., McIntosh, L. P., and Wakarchuk, W. W. (1996) Secondary structure and NMR assignments of *Bacillus circulans* xylanase, *Protein Sci.* 5, 1118-1135.
 58. Sidhu, G., Withers, S. G., Nguyen, N. T., McIntosh, L. P., Ziser, L., and Brayer, G. D. (1999) Sugar ring distortion in the glycosyl-enzyme intermediate of a family GH11 xylanase, *Biochemistry* 38, 5346-5354.
 59. Paes, G., Berrin, J. G., and Beaugrand, J. (2012) GH11 xylanases: Structure/function/properties relationships and applications, *Biotechnol. Adv.* 30, 564-592.
 60. Wan, Q., Zhang, Q., Hamilton-Brehm, S., Weiss, K., Mustyakimov, M., Coates, L., Langan, P., Graham, D., and Kovalevsky, A. (2014) X-ray crystallographic studies of family 11 xylanase Michaelis and product complexes: implications for the catalytic mechanism, *Acta Crystallogr. Sect. D. Biol. Crystallogr.* 70, 11-23.
 61. Connelly, G. P., Withers, S. G., and McIntosh, L. P. (2000) Analysis of the dynamic properties of *Bacillus circulans* xylanase upon formation of a covalent glycosyl-enzyme intermediate, *Protein Sci.* 9, 512-524.
 62. Ludwiczek, M. L., Heller, M., Kantner, T., and McIntosh, L. P. (2007) A secondary xylan-binding site enhances the catalytic activity of a single-domain family 11 glycoside hydrolase, *J. Mol. Biol.* 373, 337-354.
 63. Schröder, S. P., Petracca, R., Minnee, H., Artola, M., Aerts, J. M., Codée, J. D., Van Der Marel, G. A., and Overkleeft, H. S. (2016) A Divergent Synthesis of l-arabino- and d-xylo-Configured Cyclophellitol Epoxides and Aziridines, *Eur. J. Org. Chem.* 2016, 4787-4794.

Appendix I

Length: 602
 # Identity: 88/602 (14.6%)
 # Similarity: 161/602 (26.7%)
 # Gaps: 238/602 (39.5%)

```

EGCII 1 -----MSG
GBA 1 EFARPCIPKSFYSSVVCVNATYCDSEFPPTFPALGTFSTRYSRSTRSGRRMELSMGPTQA

EGCII 4 SCSGSGTALTPSYLKDDGCRSLILRGENTASAKSAPDGPOFTEADLAREYADMGTNFV
GBA 61 NHGIGLLLT-----QPQONFQWKGFEGGAMDAALNIAL-----

EGCII 64 RFLISWRSVEPAPGYDQOQLDRVEDRGNVAERGYKVMDDMHQDVYCGAITPEGNS---
GBA 99 -----SPPAQNILLKSYFS--EEGLGYNIIIRVPMASCDFSIRTYIADTPDDFQLHN

EGCII 121 -----GNGACAINGAPAWAT
GBA 149 FSLPEEDTKLKIPLIHRALQLAQRVSVLLASPWTSPTWLKTNGAVNCKGSI-----

EGCII 137 YMDGLEVEEP-QPRWELYIYIOPGVMRAFDNFWNTTGKHPELVEHYAKANRAVADRFDNDA
GBA 200 --KQPCDIHQTWARYFYKF-----LDAY-----AEHKLQFW-----

EGCII 196 VVAIDLMNEEFGCSLQCPAIEAGPLAAMYQRTD-----AIFQDODITWVC
GBA 231 --AVTARNEEBSAGLISGYPFQCLGFTPEHQRFIARDLGPTLANSTHNVRLMLDDQRL

EGCII 242 VAFQAIQVNGQLPSGLTKLDDPRACQORIA-----YCPHYELPLDYGEGHEGLARIT-
GBA 289 LLEHWAKV-----VLTDPAAKYVHGIAVHWMLDFLAPAKATIGETHRLFPNIMLE

EGCII 296 -----DVTIDAWRANTA-----HTARVL
GBA 340 ASEACVSGSKFWEQSVRIGSMDRGMQYSHSIITNLLYHVVGWTDWNLALNPEGGPNVVRNF

EGCII 314 GQVPIIIGEFGLDITLPGARDYIERVYGTAREMGAGVSYWSSDPGPGYLPPIGICQLLV
GBA 400 VDSPIIV-DITKDTFYKQPMF-----YHLGHSKFIPEGSQRVGI

EGCII 374 DTLNKPYPRVAGTPTWSSSTSDRLQLTIEPDAAITAPTEHYLPEAGPGDVHVE-GADV
GBA 439 VASQKNDLDAVALMHPDGSVAVVVVL-----NRSSKDVPLTIKDFAVGLETSFGYSIHT

EGCII 433 VGWDRQSRLLVWRTPADSGNVTVVTPAA
GBA 494 YLWHRQLLVDTM-----

```

Figure A1.1: EGCII and GBA primary sequences alignment using Needleman-Wunsch algorithm from EMBOSS Needle server (emboss.open-bio.org). Identical residues are highlighted on black background, conservative changes are highlighted in grey. The acid /base and nucleophile catalytic residues are marked with stars.

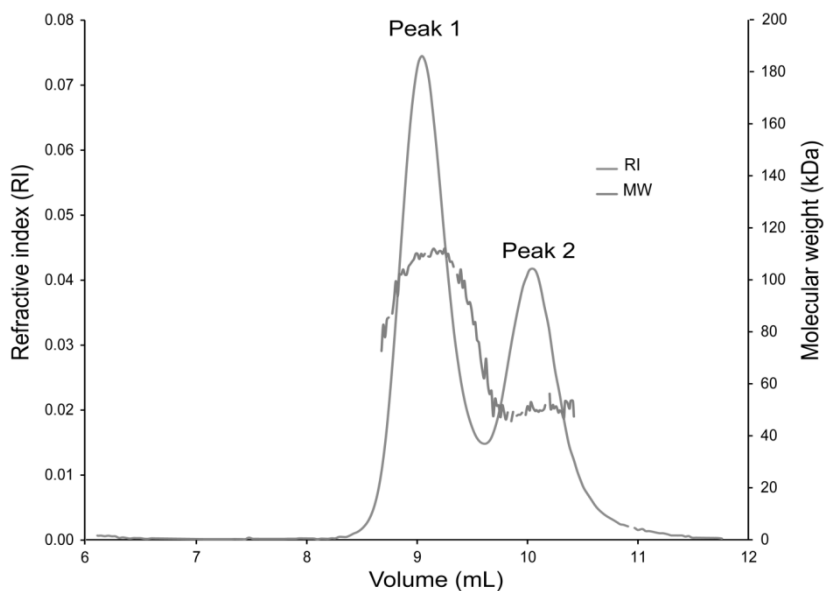
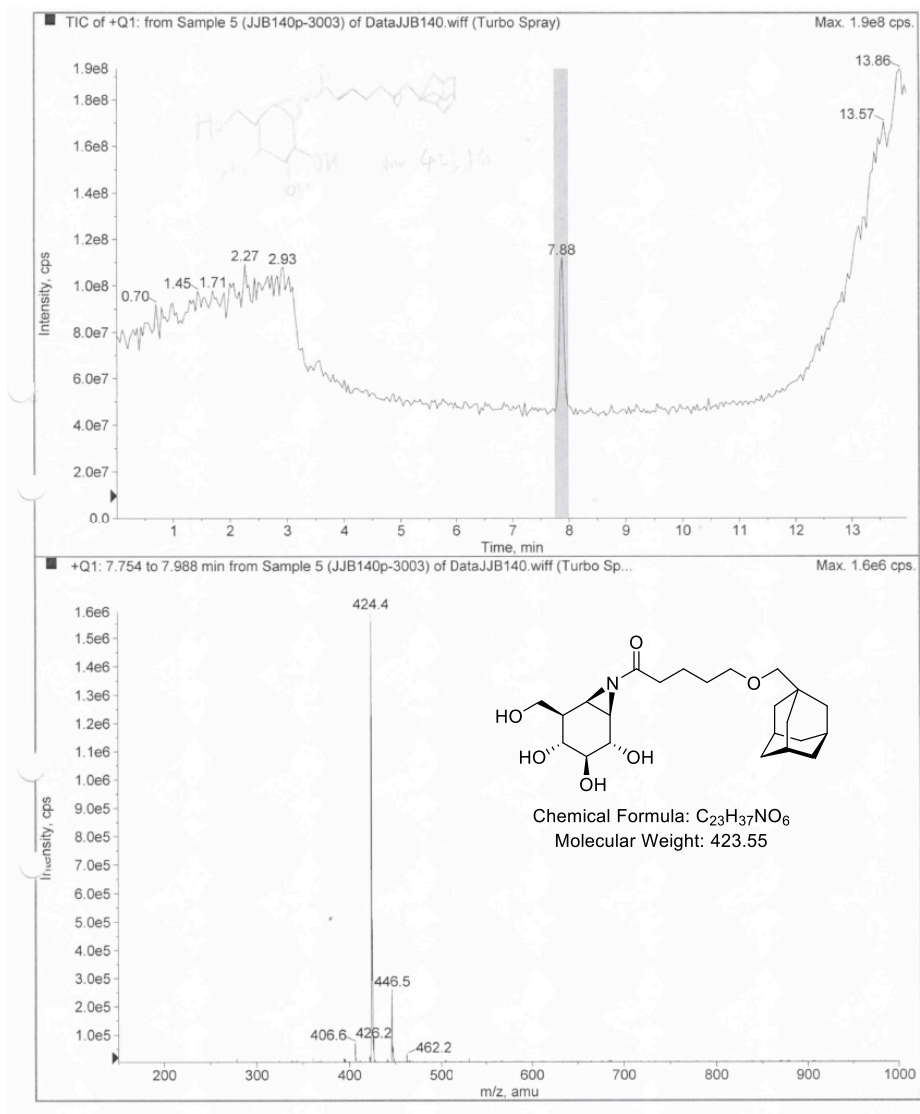


Figure A1.2. EGCII size exclusion chromatogram analyzed by Multi Angle Laser Light Scattering.

Results

	Peak 1	Peak 2
Volume (mL)	8.75-9.42	9.64-10.42
Injection Mass (g)	$1.0 \cdot 10^{-4}$	$1.0 \cdot 10^{-4}$
Calc. Mass (g)	$3.82 \cdot 10^{-5}$	$2.47 \cdot 10^{-5}$
dn/dc (mL/g)	0.186	0.186
Polydispersity (Mw/Mn)	1.003 ± 0.033	1.002 ± 0.086
Molar Mass Moments (g/mol)	$1.062 \cdot 10^{+5}$	$5.0 \cdot 10^{+4}$

LC/MS spectra of compound **8**

Appendix II

Table A2.1: LC-MS identification of peptides in Band 1

Start-End	m/z (exp)	z	ppm	Score	Peptide sequence
117-145	9.655.467	3	3	30	VKGFGGAMTDAALNINLALSPPAQNLLLK
119-145	13.422.294	2	1	80	GFGGAMTDAALNINLALSPPAQNLLLK*
146-159	8.244.048	2	1	81	SYFSEEGIGYNIIR
160-170	6.417.996	2	0	53	VPMASCDFSIR
195-202	3.305.582	3	-2	48	LKIPLIHR
197-202	3.747.444	2	-2	48	IPLIHR
203-225	8.551.525	3	1	22	ALQLAQRPVSLASPWTSPITWLK
234-250	6.386.585	3	0	36	GSLKGGQPGDIYHQTWAR
238-250	7.648.692	2	1	54	GQPGDIYHQTWAR
251-263	5.442.807	3	1	44	YFVKFLDAYAEHK
255-263	3.651.819	3	0	43	FLDAYAEHK
264-296	12.509.374	3	-1	138	LQFWAVTAENEPSAGLLSGYPFQCLGFTPEHQ
297-301	3.111.708	2	-2	22	DFIAR
317-324	5.022.659	2	0	63	LLMLDDQR
325-332	4.893.011	2	2	31	LLLPHWAK
325-342	6.677.226	3	0	38	LLLPHWAKVVLTDPEAAK
333-342	5.217.918	2	-2	10	VVLTDPEAAK
333-360	7.816.724	4	0	37	VVLTDPEAAKYVHGIAVHWYLDFLAPAK
343-360	10.505.557	2	-1	86	YVHGIAVHWYLDFLAPAK
343-368	7.421.416	4	-1	28	YVHGIAVHWYLDFLAPAKATLGETHR
369-385	9.364.572	2	2	85	LFPNTMLFAEACVGSK
386-392	4.762.372	2	-1	39	FWEQSVR
393-398	3.671.845	2	-1	40	LGSWDR
399-434	13.853.512	3	1	116	GMQYSHSITNLLYHVVGWTDWNLALNPEGGPNWVR*
435-447	7.309.018	2	-2	89	NFVDSPIIVDITK
435-452	7.057.049	3	0	24	NFVDSPIIVDITKDTFYK
448-452	3.371.629	2	-1	15	DTFYK
453-464	4.979.123	3	1	24	QPMFYHLGHFSK
465-472	4.672.421	2	-2	15	FIPEGSQR
473-480	4.012.456	2	1	51	VGLVASQK
481-502	7.744.033	3	2	84	NDLDAVALMHPDGSAVVVVLR*
503-512	3.632.164	3	-1	16	SSKDVPLTIK
506-512	3.932.421	2	0	14	DVPLTIK

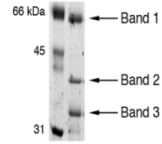


Table A2.2: LC-MS identification of peptides in Band 3

Start-End	m/z (exp)	z	ppm	Score	Peptide sequence
234-250	6.386.578	3	-1	42	GSLKGGQPGDIYHQTWAR
238-250	7.648.693	2	1	64	GQPGDIYHQTWAR
238-250	7.648.694	2	2	69	GQPGDIYHQTWAR
251-263	5.442.804	3	0	45	YFVKFLDAYAEHK
255-263	5.472.696	2	1	49	FLDAYAEHK
264-296	12.509.392	3	1	92	LQFWAVTAENEPSAGLLSGYPFQCLGFTPEHQ
302-316	5.446.115	3	-3	41	DLGPTLANSTHINVR
317-324	5.022.657	2	0	63	LLMLDDQR
325-332	4.893.012	2	2	48	LLLPHWAK
325-342	6.677.218	3	-1	56	LLLPHWAKVVLTDPEAAK
343-360	10.505.557	2	-1	97	YVHGIAVHWYLDFLAPAK
343-368	7.421.419	4	-1	56	YVHGIAVHWYLDFLAPAKATLGETHR
369-385	9.364.542	2	-1	105	LFPNTMLFAEACVGSK
386-392	4.762.373	2	-1	52	FWEQSVR
399-434	13.800.196	3	1	117	GMQYSHSITNLLYHVVGWTDWNLALNPEGGPNWVR
435-447	7.309.021	2	-2	92	NFVDSPIIVDITK
453-464	7.463.647	2	1	63	QPMFYHLGHFSK
473-480	4.012.456	2	1	60	VGLVASQK
473-502	7.726.692	4	-2	46	VGLVASQKNDLDAVALMHPDGSAVVVVLR
473-505	8.482.103	4	0	60	VGLVASQKNDLDAVALMHPDGSAVVVVLRSSK
481-502	11.611.033	2	3	90	NDLDAVALMHPDGSAVVVVLR*

G noting the N-terminus residue of Band 3; asterisk * (Asterisk) noting Methionine oxidation

ENGLISH SUMMARY

B-glycosidases play fundamental roles in maintaining the cellular homeostasis in living organisms. In the last decades, this widespread enzyme family has found multiple industrial applications. Given the importance of these enzymes, characterization of the biophysical properties of β -glycosidases is a necessity for deepening our understanding of their structure/function relationship. **Chapter 1** is a general introduction describing the biophysical and structural characteristics of β -glycosidases that belong to the GH5, GH11 and GH30 families, as well as the commonly used inhibitors that modulate their activities.

In humans, ganglioside catabolism comprises consecutive hydrolysis of the oligosaccharide moieties by different exo β -glycosidases. Deficiency in ganglioside processing enzymes leads to a range of metabolic disorders collectively classified as glycosphingolipidoses. In bacteria, ganglioside metabolism follows a different path, in which the entire oligosaccharide chain is removed from the ceramide moiety in a single step. One of the first enzymes identified to be able to perform this reaction is endoglycoceramidase II (EGCII) from *Rhodococcus* sp. In theory, this enzyme could be applied to treat human glycosphingolipidoses, and insight into factors that influence EGCII conformational stability is an important prerequisite for its application as a therapeutic agent. **Chapter 2** describes the characterization of EGCII using activity-based probes (ABPs) initially developed against the human β -glucocerebrosidase (GBA.) The protein is heat labile and its stability is markedly enhanced by formation of covalent complexes with ABPs based on cyclophellitol linked to hydrophobic substituents. This is evidenced by an increased melting temperature, resistance against tryptic digestion, changes in ^{15}N - ^1H NMR spectra of the enzyme, and changes in the degree of exposed hydrophobic surface area, as determined by 8-anilino-1-naphthalenesulfonic acid fluorescence.

Deficiency of GBA function leads to the accumulation of its glucocerebroside substrate in the lysosomal compartment of the cell, thus causing a syndrome called Gaucher disease. The application of small chemical compounds that rescue the activity of GBA mutants in Gaucher patients is under intense investigation. This new therapeutic approach represents a promising avenue for treatment of Gaucher patients with symptoms that also include neural manifestation of the disease. However, the effects of those compounds on the protein conformation in solution remain unclear. Therefore, **Chapter 3** describes the utilization of a variety of active site binders to dissect their stabilization mechanisms on the GBA fold. Amphiphilic ABPs, which are supposed to simultaneously occupy the glycon and aglycon pockets of GBA binding site, exert superior stabilization effects presumably by promoting a further structural compactness of GBA through hydrophobic interactions.

ENGLISH SUMMARY

Despite the differences in folds and in substrate specificities between the β -glycosidases, these enzymes share a common catalytic mechanism, in which two catalytic residues act in a synchronized manner on the glycosidic link, causing its hydrolysis. The chemistry that governs this mechanism became widely accepted, which somehow limited the study of the contribution of the conformational changes of the enzyme and the dynamics in the catalytic reaction. In **chapter 4** this topic is addressed by following the dynamics of *Bacillus circulans* xylanase during its catalytic pathway using standard and advanced NMR spectroscopy techniques. In its resting state, the protein shows minor millisecond time scale dynamics. The Michaelis complex formation seems to follow an induced fit mechanism and the exchange between the two bound forms of the enzyme is revealed to be in the slow exchange regime. It is hypothesised that this step with a high activation barrier is a change in the protein conformation that is necessary for substrate positioning and distortion, which could represent a rate limiting step of the reaction. In the covalent intermediate state of the reaction, the protein preserves its free state dynamics behaviour although it assumes a different conformational state. A drastic enhancement of the millisecond motion of the protein in the last step of the catalytic reaction (product dissociation) suggests a role of such dynamics in assisting the product dissociation from the enzyme binding site. The study provided evidence for the involvement of β -glycosidases motions in their paradigmatic hydrolysis mechanism.

Chapter 5 discusses and suggests future perspectives for the insights generated in this thesis.

NEDERLANDSE SAMENVATTING

B-glycosidasen spelen een fundamentele rol bij het handhaven van de cellulaire homeostase in levende organismen. Bovendien heeft deze wijdverspreide groep van enzymen de afgelopen decennia meerdere industriële toepassingen gevonden. Het belang van deze enzymfamilie maakt het karakteriseren van de biofysische eigenschappen van β -glycosidasen zeer relevant. Daarmee kunnen we een beter begrip krijgen van hun structuur/functie relatie. **Hoofdstuk 1** is een algemene inleiding waarin de biofysische en structurele kenmerken van β -glycosidasen die tot de GH5, GH11 en GH30 families behoren, worden beschreven, alsmede de vaak gebruikte remmers die hun activiteiten moduleren.

In de mens bestaat het katabolisme van gangliosiden uit de sequentiële hydrolyse van hun oligosaccharidegroep door verschillende exo β -glycosidasen. Het ontbreken van de activiteit van één van de ganglioside verwerkende enzymen vormt de oorzaak van een reeks metabole aandoeningen die collectief worden geclassificeerd als glycosfingolipidosen. In bacteriën volgt het metabolisme van gangliosiden een ander pad, waarbij de gehele oligosaccharideketen in een enkele stap van het ceramidedeel wordt verwijderd. Een van de eerst ontdekte enzymen die deze reactie kunnen uitvoeren, is endoglycoceramidase II (EGCII) van *Rhodococcus* sp. In theorie zou dit enzym kunnen worden toegepast om menselijke glycosfingolipidosen te behandelen. Inzicht in factoren die de stabiliteit van EGCII beïnvloeden, is een belangrijke voorwaarde voor eventuele toepassing ervan als therapeuticum. **Hoofdstuk 2** beschrijft de karakterisering van EGCII met behulp van *activity based probes* (ABPs) die aanvankelijk waren ontwikkeld voor humaan glucocerosidase GBA. EGCII is warmtelabiel en de stabiliteit wordt aanzienlijk verbeterd door de vorming van covalente complexen met ABPs op basis van cyclofellitol, gesubstitueerd met hydrofobe groepen, zoals blijkt uit een verhoogde smeltemperatuur, resistentie tegen tryptische digestie, veranderingen in ^{15}N - ^1H NMR-spectra van het enzym en in de hoeveelheid hydrofoob eiwitoppervlak, zoals bepaald door 8-anilino-1-naftaleensulfonzuurfluorescentie.

Een verlaagde of afwezige activiteit van GBA leidt bij de mens tot accumulatie van het glucocerosidesubstraat in het lysosomale compartiment van de cel, waardoor een syndroom ontstaat dat de ziekte van Gaucher wordt genoemd. De toepassing van kleine chemische verbindingen die de activiteit van GBA-mutanten bij Gaucherpatiënten kunnen verhogen, wordt intensief onderzocht. Deze nieuwe therapeutische aanpak vertegenwoordigt een veelbelovend vorm van behandeling van Gaucher-symptomen, in het bijzonder voor de neurale manifestatie ervan. De effecten van die verbindingen op de eiwitconformatie in oplossing zijn echter nog onduidelijk. Daarom beschrijft **hoofdstuk 3** de karakterisatie van de effecten van een serie verbindingen op de stabiliteit van GBA. De experimenten laten zien dat de toename in cellulaire niveaus van GBA door ABPs en

NEDERLANDSE SAMENVATTING

door de reversibele remmers ten dele wordt veroorzaakt door hun vermogen om de gevouwen vorm van GBA te stabiliseren, waardoor de weerstand tegen afbraak door lysosomale proteasen toeneemt. Deze effecten zijn het duidelijkst voor de amfifiele ABPs, vermoedelijk vanwege hun hoge lipofiele karakter, die compactheid van GBA kan bevorderen door middel van hydrofobe interacties.

Ondanks de verschillen in vouwing en in substraatspecificiteiten tussen de β -glycosidasen, delen deze enzymen een gemeenschappelijk katalytisch mechanisme, waarbij twee katalytische residuen samenwerken om de glycosidische binding te hydrolyseren. Het mechanisme van deze reactie is algemeen geaccepteerd, wat op de een of andere manier de studie naar de rol van conformatieveranderingen en dynamiek van het enzym in de katalyse heeft beperkt. In **hoofdstuk 4** wordt dit onderwerp bestudeerd door de dynamiek van *Bacillus circulans* xylanase te karakteriseren voor de opeenvolgende stappen van de katalyse, met behulp van standaard en geavanceerde NMR spectroscopische technieken. In de rusttoestand vertoont het enzym een geringe dynamiek op de milliseconde tijdschaal. De Michaelis-complexvorming lijkt een geïnduceerde fit-mechanisme te volgen en de uitwisseling tussen de twee gebonden vormen van het enzym blijkt langzaam te zijn. Er wordt voorgesteld dat deze conformatieverandering met een hoge activeringsenergie nodig is voor substraatpositionering en -vervorming. Dit zou de snelheidsbeperkende stap van de reactie zou kunnen zijn. In de toestand van de covalente intermediair laat het enzym hetzelfde dynamisch gedrag zien als in de rusttoestand, hoewel het een andere conformatie heeft. Een drastische verhoging van de dynamiek op de millisecondetijdschaal van het enzym in de laatste stap van de reactie suggereert dat het enzym een actieve rol speelt bij de productdissociatie. Deze studie leverde het eerste bewijs voor dynamiek en conformationele veranderingen bij β -glycosidasen en impliceert betrokkenheid van de enzymmatrix bij het paradigmatische hydrolysemechanisme.

Hoofdstuk 5 bespreekt de nieuwe inzichten beschreven in dit proefschrift en schetst enkele toekomstperspectieven voor onderzoek en toepassing.

List of Publications

PhD-related publications:

Ben Bdira, F., Jiang, J., Kallemeijn, W., de Haan, A., Florea, B. I., Bleijlevens, B., Boot, R., Overkleef, H. S., Aerts, J. M., and Ubbink, M. (2016) Hydrophobic Interactions Contribute to Conformational Stabilization of Endoglycoceramidase II by Mechanism-Based Probes, *Biochemistry* 55, 4823-4835.

Ben Bdira, F., Kallemeijn, W., Oussoren, S., Scheij, S., Bleijlevens, B., Florea, B. I., van Roomen, C., Ottenhoff, R., van Kooten, M., Walvoort, M., Witte M.D, Boot, R., Ubbink M., Overkleef, H. S., and Aerts, J. M. (2017) Stabilization of Glucocerebrosidase by Active-site Occupancy, *ACS Chemical Biology* 12, 1830-1841.

Ben Bdira F., Volkov N. A., Eiso AB., Schroder, S., Codee, J., Overkleef, H. S., Aerts, J. M., van Ingen, H., Ubbink, M. Exploring the Conformational Landscape and the Dynamics of GH11 xylanases During Catalysis. *To be submitted*

Ben Bdira, F., Artola M., Overkleef, H. S., Ubbink, M., Aerts, J. M., Retaining β -glycocylceramidases: Fold, Dynamics, Modulation and Applications. Review *to be submitted*

Ben Bdira, F., Marneth, K., Codee, J., Overkleef, H. S., Aerts, J. M., Ubbink, M., Modulation by Single Point Mutation of the GH11 xylanases Transglycosylation Reaction. *In preparation.*

Publication from previous research work:

Ben Bdira, F., Gonzalez, E., Pluta, P., Lain, A., Sanz-Parra, A., Falcon-Perez, J. M., and Millet, O. (2014) Tuning Intracellular Homeostasis of Human Uroporphyrinogen III Synthase by Enzyme Engineering at a Single Hotspot of Congenital Erythropoietic Porphyria, *Hum. Mol. Genet.* 23, 5805-5813.

Curriculum Vitae

Fredj Ben Bdira was born on March 31st 1982 in Sousse, Tunisia. After high school graduation he first studied medicine at the University of Sousse, Tunisia in order to become a physician. During that time, he became more interested in understanding the physiopathology of a disease rather than its diagnosis, therefore he changed his study discipline to Medicinal Biotechnology and obtained a master degree from the University of Monastir, Tunisia. To deepen his knowledge about the chemistry of life he also obtained a master degree in Biochemistry at the University of Science ElManar Tunis, Tunisia. He moved to Spain in 2011 as research visitor to work at CICBiogune research center where he investigated the molecular basis of Porphyrria with the aim to develop innovative therapeutic approaches.



To pursue his goal in becoming a scientist, he joined the research group of Professor Marcellus Ubbink at the Leiden Institute of Chemistry in December 2013, to work on a multidisciplinary project in collaboration with Professor Hans Aerts and Professor Hermen Overkleeft as a PhD. candidate. His research project was aimed at comprehending the functional dynamics and conformational stability of the ubiquitous enzyme family of β -glycosidases, including the human glucocereamidase GBA, deficient in patients suffering from Gaucher disease.